COLLECTIVE STRUCTURES IN TWO-DIMENSIONAL STRONGLY COUPLED DUSTY PLASMAS

By

Sandeep Kumar

PHYS06201304004

Institute for Plasma Research, Gandhinagar

A thesis submitted to the
Board of Studies in Physical Sciences

In partial fulfillment of the requirements

For the Degree of

DOCTOR OF PHILOSOPHY

of

HOMI BHABHA NATIONAL INSTITUTE

April 2019

Homi Bhabha National Institute

Recommendations of the Viva Voce Committee

As members of the Viva Voce Committee, we certify that we have read the dissertation prepared by **Sandeep Kumar** entitled "**Collective structures in two-dimensional strongly coupled dusty plasmas**" and recommend that it may be accepted as fulfilling the thesis requirement for the award of Degree of Doctor of Philosophy.

Chairman - Prof. Sudip Sengupta		Date: 22/04/2019
Guide/ Convener – Prof. Amita Das	Amita Das	Date: 22-4-19
Examiner – Prof. H. Bailung		Date: 22/04/19
Member 1- Prof. Abhijit Sen	Abhijit	Date: 22/04/19
Member 2- Dr. Devendra Sharma	Devendra Sharma	Date: 22/4/19
Member 3- Dr. Sarveshwar Sharma		Date: 22/04/19

Final approval and acceptance of this thesis is contingent upon the candidate's submission of the final copies of the thesis to HBNI.

I/We hereby certify that I/we have read this thesis prepared under my/our direction and recommend that it may be accepted as fulfilling the thesis requirement.

Date: 22nd April 2019

Place: Gandhinagar

Amita Das

Prof. Amita Das

Guide

STATEMENT BY AUTHOR

This dissertation has been submitted in partial fulfillment of requirements for an advanced degree at Homi Bhabha National Institute (HBNI) and is deposited in the Library to be made available to borrowers under rules of the HBNI.

Brief quotations from this dissertation are allowable without special permission, provided that accurate acknowledgement of source is made. Requests for permission for extended quotation from or reproduction of this manuscript in whole or in part may be granted by the Competent Authority of HBNI when in his or her judgment the proposed use of the material is in the interests of scholarship. In all other instances, however, permission must be obtained from the author.

Sandeep Kumar

Sandeep Kumar

DECLARATION

I, hereby declare that the investigation presented in the thesis has been carried out by me. The work is original and the work has not been submitted earlier as a whole or in part for a degree/diploma at this or any other Institution or University.

Sandeep Kumar

Sandeep Kumar

List of Publications arising from the thesis

Journals:

- **Observation of the Korteweg-de Vries soliton in molecular dynamics simulations of a dusty plasma medium**,
  Sandeep Kumar, Sanat Kumar Tiwari, and Amita Das
  Physics of Plasmas (24), 033711 (2017)

- **Spiral waves in driven dusty plasma medium: Generalized hydrodynamic fluid description**,
  Sandeep Kumar, Bhavesh Patel, and Amita Das
  Physics of Plasmas (25), 043701 (2018)

- **Spiral waves in driven strongly coupled Yukawa systems**,
  Sandeep Kumar, and Amita Das
  Physical Review E (97), 063202 (2018)

Other publications:

- **Interplay of single particle and collective response in molecular dynamics simulation of dusty plasma system**,
  Srimanta Miaty, Amita Das, Sandeep Kumar, and Sanat Kumar Tiwari
  Physics of Plasmas (25), 043705 (2018)

- **Simulation of Rayleigh-Taylor instability in strongly coupled dusty plasma medium**,
  Sandeep Kumar, Vikram Singh Dharodi, Amita Das, Predhiman Kaw, and Sanat Kumar Tiwari.
  To be submitted

Conferences:

International Participation

- Molecular Dynamics Simulation of Dust Particle Levitation in the Presence of Sheath. (**Poster presentation**)
  Sandeep Kumar, Amita Das, Sanat Kumar Tiwari, and P. K. Kaw
  Asia Plasma And Fusion Association (APFA), 14th-18th December 2015, Gandhinagar, India.

- Observation of the Korteweg-de Vries soliton in molecular dynamics simulations of a dusty plasma medium. (**Poster presentation**)
  Sandeep Kumar, Amita Das, Sanat Kumar Tiwari
  8th International Conference on Physics of Dusty Plasmas (ICPDP), Prague, Czech Republic, 20th - 25th May, 2017.

- Spiral Waves in the Driven Two-dimensional Dusty Plasmas. (**Poster Presentation**)
  Sandeep Kumar, Bhavesh Patel, and Amita Das
  Hands-On Research in Complex Systems School, 16 - 27 July, 2018, Abdus Salam International Centre for Theoretical Physics (ICTP), Trieste, Italy.

- Excitation and evolution of spiral structures in two-dimensional dusty plasmas. (**Oral Presentation**)
  Sandeep Kumar, Srimanta Maity, Bhavesh Patel, and Amita Das
  American Physical Society-Division of Plasma Physics (APS-DPP) meeting, Portland, Oregon, USA, 5th - 9th November, 2018.

National Participation

- Molecular Dynamics Simulation of Rayleigh - Taylor Instability in Dusty Plasmas. (**Poster Presentation**)
  Sandeep Kumar, Amita Das, P. K. Kaw, and Sanat Kumar Tiwari
  30th National Symposium on Plasma Science and Technology, 1 - 4 Dec, 2015, Kolkata, India.

- Spiral Waves in Driven Dusty Plasmas. (**Oral Presentation**)
  Sandeep Kumar, Bhavesh Patel, and Amita Das
  32th National Symposium On Plasma Science and Technology, 7 - 10 Nov, 2017, Gandhinagar, India.

- Excitation and dynamics of spiral structures (wave) in strongly coupled dusty plasmas. (**Oral Presentation**)
  Sandeep Kumar, Bhavesh Patel, and Amita Das
  33th National Symposium On Plasma Science and Technology, 4 - 9 Dec, 2018, New Delhi, India.

- Staggering transverse shear waves in strongly coupled dust fluid. (**Poster Presentation**)
  Sandeep Kumar, Srimanta Maity, Bhavesh Patel, and Amita Das
  33th National Symposium On Plasma Science and Technology, 4 - 9 Dec, 2018, New Delhi, India.

Schools:

- International School on Ultra - Intense Lasers at National Research Nuclear University, MEPhI, Moscow, Russia, 4th - 10th October, 2015.

- Hands-On Research in Complex Systems School, Abdus Salam International Centre for Theoretical Physics (ICTP), Trieste, Italy, 16 - 27 July, 2018.

Sandeep Kumar

Sandeep Kumar

Dedicated to

my family and friends

ACKNOWLEDGEMENTS

First and foremost, I would like to express my great gratitude to my thesis supervisor Prof. Amita Das for guiding me all the way in my research. I would really like to acknowledge her for always has been available for listening to me and discussions on my research work very patiently. I am very grateful for the freedom she gave me in choosing research topics. I have always received a constant encouragement and motivation to pursue my work implementing new, independent thoughts and ideas. Their deep insight into research problems, approach to tackle the problems, marvelous skills in computational physics, and awesome writing skill, have always been a great source of inspiration to me. I could not have imagined having better mentor for my Ph.D.

I would like to express my sincere regards to my doctoral committee members late Predhiman Kaw, Prof. Abhijit Sen, Prof. Sudip Sengupta, Prof. Subrata Pradhan, Dr. Devendra Sharma, and Dr. Sarveshwar Sharma for their careful monitoring of my progress during the Ph.D. tenure and giving their comments and helpful discussions on the work during my doctoral reviews. Their appreciations and suggestions have always encouraged me to give my best in the work.

I am also indebted to late Predhiman Kaw, Prof. Abhijit Sen, Dr. S. K. Mattoo, Dr. Y. C. Saxena, Dr. Prabal Chattopadyay, Prof. Sudip Sengupta, Dr. Joydeep Ghosh, Dr. Subrato Mukharji, Dr. Mrityunjay Kundu, Dr. R. Ganesh, Dr. Devendra Sharma, Dr. N. Ramasubramanian, Dr. G. Ravi, Dr. V. P. Anitha, Dr. S. K. Pathak, Dr. Mainak Bandyoadhaya and Dr. Rajiv Goswami for their excellent teaching and support during my first-year course-work at IPR.

I would also like acknowledge the computer center staff, library staff and the administration staff at the IPR for always being cooperative. I would also like to thank all my seniors Vikram, Ujjwal, Sanat, Sushil, Rameshwar, Pravesh, Sayak, Soumen, Manjit, Kshitish, Deepak, Sanat, Sushil, Aditya, Vikram, Rana, Akanksha, Vidhi, Vara, Neeraj, Roopendra, Bibhu, Mangilal, Harish, Megharaj, Sameer, Chandrasekhar, Bibhu, Deepa, Veda, Dushyant, Ratan, Umesh, Surabhi, Debraj, Arghya, Bhumika, Modhu, Sonu, Amit, Narayan for their wonderful company in the hostel and their co-operation whenever I needed. I would also like to convey my best wishes to my younger friends Shivam, Rupak, Avanish, Subrato Jana, Arun Pandey, Dipshikha, Arnab, Priti, Garima, Neeraj Wakde, Srimanta, Prince, jagganath, Pawandeep, Vijay Shankar, Kaushal, Anjan, Sukriti and other IPR scholars and colleagues for providing friendly atmosphere to me in the IPR.

I would like to greatly acknowledge my classmates Atul, Sagar, Jervis, Alam, Prabhakar, Meenakshi, Pallavi, Harshita, Deepak, Chetan, and Lavkesh for their unconditional support throughout my Ph.D. tenure. My sincere thanks to Dr. Bhavesh Patel, Dr. Sanat Kumar Tiwari, and Dr. Vikram Singh Dharodi for teaching numerical and computational knowledge to me. I also wish a special thank to Dr. Chandrasekhar Shukla, Dr. Deepa Verma, Dr. Ratan Kumar Vera, Atul Kumar, Srimanta Maity, Devshree, Ayushi, and Prince Kumar for their support while discussing, teaching, and debating on various research problems, numerical techniques, and on social issues too. I am also thankful to Mr. Avadesh Maurya for his technical and official support and having a wonderful office roommate throughout my Ph.D. tenure.

I would also like to acknowledge HBNI, Strong Field Science (SFS), IPR, ICPDP, ICTP, APS-DPP for proving fund to me to participate and present my work in international schools and conferences/meetings.

I would also like to convey my heartiest thank to my family members, whose love and confidence in me, took a great load off my shoulder. Among my family members, I would like to express my special heartiest regards to my parents for their unconditional love and believe in me that helped me a lot achieving my goal. This thesis is dedicated to my brothers Pradeep Shukla and Sunil Shukla for their love, unconditional, and selfless support that encourage me to come out of all sort of odds in my life and inspired me to achieve better.

Contents

Synopsis . . . iii
List of Figures . . . xii
List of Tables . . . xx

1 Introduction **3**
1.1 Introduction . . . 3
1.2 Introduction to complex plasma or dusty plasma . . . 6
1.2.1 Dusty plasma . . . 6
1.2.2 Strong coupling . . . 7
1.3 Models to study dusty plasmas . . . 10
1.3.1 Generalized Hydrodynamic (GHD) model . . . 10
1.3.2 Quasi-localized charge approximation (QLCA) . . . 11
1.3.3 Particle-in-cell (PIC) simulations . . . 12
1.3.4 Molecular-dynamics simulation . . . 12
1.3.5 Vlasov approach . . . 13
1.4 Review of earlier work on collective structures in the dusty plasmas and the motivation . . . 14
1.5 Structure of the Thesis . . . 19

2 Molecular dynamics and computational fluid dynamics **23**
2.1 Molecular dynamics simulations of dusty plasmas . . . 24
2.1.1 Interaction potential for MD simulations of dusty plasmas: . . . 24
2.1.2 Trajectory evolution: . . . 25
2.1.3 Addition of neutral force on the dust grains due to the background gas: . . . 29
2.1.4 Details of a typical MD simulation: . . . 31
2.1.5 Diagnostic tools to extract Physics from the MD data: . . . 33
2.2 Fluid simulation of dusty plasma . . . 39

3 Korteweg-de Vries (KdV) solitons in molecular dynamics simulations of a dusty plasma medium **45**
3.1 Introduction . . . 46
3.2 Description of MD simulations . . . 48

3.3 Excitation of solitons and dispersive waves 49
3.4 Interaction between solitons 54
3.4.1 Head-on collision of same amplitude solitons: 54
3.4.2 Head-on collision of different amplitude solitons: 55
3.4.3 Overtaking collision amidst different amplitude solitons: . . 58
3.5 Excitation of Multi-solitons, effect of the coupling parameter and neutral drag: 59
3.6 Summary 62

4 Spiral wave (structure) in driven dusty plasmas: Fluid (continuum) simulations 65
4.1 Introduction 65
4.2 Numerical observations 71
4.2.1 Weak coupling: Fluid regime 71
4.2.2 Strong coupling: GHD regime 77
4.3 Summary and conclusion 86

5 Spiral waves in strongly coupled Yukawa Systems: A molecular dynamics study 89
5.1 Introduction 90
5.2 Simulation details 92
5.3 Numerical Observations 95
5.4 Conclusion 106

6 Conclusion and future scope 109
6.1 Salient features of this thesis 109
6.2 Future scope 113

Bibliography 114

SYNOPSIS

Dusty plasma is a four-component plasma consists of electrons, ions, neutrals and embedded solid (dust) particles. These solid particles could be conductor, dielectric or made of ice particulates. In vast amount of natural [1] (star forming regions, interstellar clouds, Zodiacal light, planetary rings, Comet tails, Earth's ionosphere) and laboratory [2] (fusion devices [3], rocket exhaust, thin film deposition, production of solar cell by nanometer size dust, direct current (DC) and radio frequency (RF) discharges) scenario macroscopic solid particles (dust particles) are inadvertently present in plasma. Therefore, the study on dusty plasmas help to understand the various types of natural and laboratory phenomena. Often these have important implications for industrial applications viz. thin film deposition[4, 5] in which presence of dust deteriorate/destroy the quality of the chips and production of solar cell by nanometer size dust[6]. These macroscopic particles are much heavier than ions and their typical mass ranges from 10^{-18} - 10^{-12} Kg. The lighter mobile electron species strike the dust particles and sticks on their surface. In this fashion the solid particles acquire high negative charge. The total charge on the dust particles increases with the size/radius (r_d) of the particles. The typical size of the solid particles ranges from nanometer to micrometer for which accordingly the net acquired charge on them ranges from -100e to -10,000e, where e is elementary charge. Shielding to these charged dust particles are provided by background electrons and ions. When the condition $a > \lambda_D >> r_d$ is satisfied for such a medium, then the medium behaves like an ordinary plasma with isolated dust particles, termed as "dust in plasma". Here, a is average inter particle distance between dust grains, and λ_D is the Debye length of ambient plasma. On the other hand, if $\lambda_D > a >> r_d$, then the medium is referred as "dusty plasma". In the later case, dust particles participate in the collective phenomena. The inclusion of dust to the plasma increases the complexity of the medium as new physical processes get introduced, viz. effects associated with dissipation, plasma recombination on the particle surface and variation of particle charge as a function of time. Often these phenomena concerning dusty plasma involve the energy influx in the medium making it a non-Hamiltonian system [7]. Thus presence of dust component in plasma introduces a rich class of collective phenomena in the medium and it is often referred to as a "complex plasma".

The time scale associated with the dynamics of dust species (for micron size particles) are 10 to 100's of milliseconds (1 - 100 Hz). Therefore, they can be tracked by bare eyes and can easily be diagnosed (eg. by CCD camera) in the experiments, which is impractical to do the atoms and molecules of the liquids and solids. Due to longer time and length scales (100's of micrometer) strongly coupled dusty plasmas offer a model system to study generic phenomena such as self-organization, transport, phase transitions, waves, structures and instabilities at individual particle level which is of relevance in regular liquids, charged colloids, polymers, electrolytes and condensed matter system[7].

The properties of the dusty plasma medium can be characterized by two dimensionless parameters $\Gamma = Q^2/4\pi\epsilon_0 a k_b T_d$ (known as the coupling parameter) and $\kappa = a/\lambda_D$ (known as the screening parameter). Here T_d and a are the dust temperature and the Wigner-Seitz (WS) radius, respectively. For 2-D and 3-D systems, Wigner-Seitz (WS) radius is $(n_{2d}\pi)^{-1/2}$ and $(3/4\pi n_{3d})^{1/3}$, respectively. Due to high charge on the dust grains ($\approx -10,000$e), the dusty plasmas can be easily found in the strongly coupled state (i.e. their electrostatic average potential energy can be made comparable to or higher than the average kinetic energy of particles easily and does not require extreme conditions of temperature and/or density). Such a plasma can, therefore, have traits of a gas, a liquid and a solid depending upon where medium lies in the (Γ, κ) plane [8]. For a given κ, dusty plasma imbricate to crystalline state when the coupling parameter $\Gamma > \Gamma_c$, where Γ_c is the critical value for crystallization. At intermediate value of Γ ($1 < \Gamma < \Gamma_c$) the system behaves like a complex fluid with both fluid and solid like traits. Fluid nature of complex fluid gives viscosity and solid nature provides the elasticity in the medium. Hence, both longitudinal and transverse wave modes can be excited in strongly coupled dusty plasmas. Different phases (phase transitions) in typical dusty plasma experiments are achieved by either varying RF power or by changing neutral gas pressure [9]. Increasing RF power leads to increase in the ion density, resulting decrement in the Debye length (or increment in κ) occurs so that the dust crystal melts down. On the other hand, increasing neutral gas pressure leads to a decrease in the dust temperature which results increment in the coupling parameter Γ and liquid phase converts into crystalline phase. In addition to dusty plasmas many other system viz. Inertial confinement fusion (ICF) plasmas, colloidal suspensions, ultracold-neutral plasmas, and warm dense matter also show strong coupling behavior and phase transitions. Dusty plasma offers a model system to study the strong correlations related phenomena which is difficult to study in previously mentioned systems [10]. Strongly coupled dusty plasma also provides a direct analogy to liquid and solid phase of matter. Here, individual particle level dynamics of these phase can also be traced.

Collective phenomena have great prominence in the dynamics and evolution of complex plasma. Therefore, studies on collective dynamics in dusty plasma have been carried out [2, 11–13]. In this thesis, we have studied the characteristic properties of the KdV soliton and multisoliton using molecular dynamics (MD) simulations. We have also studied soliton collisions (head-on and overtaking) and associated phase shift. Comparison of simulation finding with experimental observations has also provided.

The spiral waves are ubiquitous and can be found in a wide range of natural and laboratory scenario [14–25]. We have looked into the possibility of exciting such structures in the context of the dusty plasma medium in both weak and strong coupling limits. We have employed both MD and fluid simulations for the depiction of the dusty plasma medium. In the MD simulations, dust are considered as point particles and they interact electrostatically with each other via Yukawa pair potential. The Yukawa interaction mimics the screening due to the presence of free electrons and ions between dust species. For fluid simulations, we have considered dusty plasma as a visco-elastic fluid using Generalized Hydrodynamic model (GHD) [26, 27] equations. In the GHD model, strong coupling is incorporated through the non-local visco-elastic operator. The non-local visco-elastic operator contains the memory effects and the short range order that develops in the system with increased correlation. In strong coupling regime dust fluid retain the memory of its past configurations. The memory function has often been modeled as exponentially decaying in time i.e as $\exp(-t/\tau_m)$ [28, 29]. Here, τ_m is a time constant representing the relaxation time. A finite τ_m represents the time for which the fluid retains the memory of its past configurations arising due to elastic behavior of strongly coupled dusty plasma.

The thesis comprises of six chapters. A brief summary of the content of these chapters is provided below.

- **Chapter - I:** In chapter 1, we provide an introduction to the field of dusty plasma medium. The various model depictions for the medium have been discussed and a summary of earlier works in the context of observing collective structures in this medium has also been provided.

- **Chapter - II:** In chapter 2, the details of simulation techniques (molecular dynamics and computational fluid dynamics) has been discussed. We also describe the various diagnostic tool that have been employed to extract the physics from the simulation data to investigate physical phenomena responsible for the collective structures. Benchmarking of the code with well known features of the dusty plasma medium such as dispersion relation, radial distribution function (RDF), diffusion and velocity auto-correlation function (VACF), and phase space distribution etc., are also shown in this chapter.

- **Chapter - III:** In chapter 3, we have studied the KdV solitons in complex plasmas using Molecular-dynamics simulations. Solitons are robust and stable non-linear localized structures which have been observed in myriad different contexts such as optical fibers [30, 31], semiconductors [32], oceanography [33], and plasmas [34–36]. In our MD simulations studies, we have applied electric field perturbations of the experimental situation [37–39] to excite the solitonic structures. The collective response of the dust particles to such an applied electric field impulse gives an excitation of a perturbed dust density pulse (compression) propagating in one direction along with a train of negative perturbed rarefactive density oscillations in the opposite direction. We have also shown that by increasing the strength of electric field impulse, the amplitude of the solitonic structure increases and above a threshold, it split in the form of multiple solitons. Further, we have shown that by increasing the coupling parameter of the medium, the amplitude of the solitonic structures increases while their width decreases. We have also found that with an increase in the neutral drag on the dust particles the amplitude of the solitonic structures decreases and its width increases. We have carried out collisional interaction of these solitonic structures in many different configurations. As expected, we find that phase shift is more in overtaking collision compared to head-on collisions. Furthermore, we have observed that the phase shifts in the collisional interaction decreases with the increasing amplitude of the colliding solitonic structures. Though this is contrary to some experimental observation [38], our observations can be understood from physical arguments.

- **Chapter - IV:** In Chapter 4, we have studied a novel non-linear two dimensional structure in dusty plasma using fluid simulations. This is essentially the observation of spiral wave excitation in dusty plasma medium. Spiral waves are ubiquitous structures found in a wide range of natural and laboratory scenario. In this chapter, the spatiotemporal development of spiral waves in the context of weak and strong coupling limits has been shown. While the weakly coupled medium has been represented by a simple charged fluid description, for strong coupling, a generalized hydrodynamic visco-elastic fluid [26] description has been employed. The medium has been driven by an external force in the form of a rotating electric field. It is shown that when the amplitude of force is small, the density perturbations in the medium are also small. In this case, the excitations do not develop as a spiral wave. Only when the amplitude of force is high so as to drive the density perturbations to nonlinear amplitudes does the spiral density wave formation occurs. We have found that the number of rings in the spiral at a given time is proportional to the number of rotations made by the external forcing. Thus, if frequency of the driver is high then number of rings is also high. The radial propagation speed of the spiral is equal to the acoustic speed of the medium. The interplay between the acoustic speed of medium and frequency of forcing decides the spiral structure. With increasing shear viscosity (η) the source of vorticity diffuses out. On the other hand in visco-elastic fluids, an additional traverse shear wave (TSW) generated from the forcing region. Thus, in our studies the expansion of this wave increases with an increase in the strong coupling (the ratio of η and τ_m) of the medium because its velocity is equal to ($\sqrt{\eta/\tau_m}$).

- **Chapter - V:** In chapter 5, the excitation of spiral waves in the context of driven two-dimensional dusty plasma (Yukawa system) has been demonstrated at particle level using molecular-dynamics (MD) simulations. The interaction amidst dust particles is modeled by the Yukawa potential to take account of the shielding of dust charges by the lighter electron and ion species. The spatiotemporal evolution of these spiral waves has been characterized as a function of the frequency and amplitude of the driving force and dust neutral collisions. The radial propagation of the spiral waves is governed by the dust lattice speed and the rotation gets decided by the forcing period. The interplay between the two decides the spiral wave structure. For distinctly clear spiral to form a proper combination of the two is essential. The parametric dependence is consistent with the continuum study carried out in Chapter 4 wherein the dusty plasma was considered as a visco-elastic fluid.

  Further, we have shown that there are additional features which emerge when the discrete particle effects are taken into account using MD simulations. For instance, when the amplitude of forcing is high the particles at the center get heated by acquiring random thermal velocity. This in turn effects the spacing of subsequent rings and collective spiral structure. Furthermore, a large amplitude forcing throws the particle out of the external forcing regime. The restoring force to bring the particles back at the center would, however, depends on the interparticle interaction. When κ is chosen high, the shielding range is small and this restoring effect reduces. Thus for high amplitude and high κ the central region where external forcing has been chosen to be finite becomes devoid of particles. The spiral then fails to form adequately. Another interesting feature that has been observed when the dust medium is in two-dimensional hexagonal crystalline symmetry (triangular lattice) state. In this case, for high values of κ (for which the interparticle potential gets very weak) only a few neighboring particles participate in the interactions. The spiral waveform in such cases has a hexagonal front. This can be understood by realizing that for a hexagonal lattice the nearest neighbors separation along different directions are different. Therefore, there is an anisotropy in the radial propagation speed along lattice axis and lattice diagonal directions and which leads to the formation of hexagonal waveform.

- **Chapter - VI:** In Chapter 6, summary and conclusion of the thesis along with future directions has been provided.

  This thesis comprises series of studies on the collective structures in the two-dimensional strongly coupled dusty plasma using both hydrodynamic and particle simulations approach. These studies contribute significantly to the field of dusty (complex) plasma and also to the multidisciplinary fields of physics.

[1] Goertz C. K. Dusty plasmas in the solar system. *Reviews of Geophysics*, 27(2):271–292.

[2] P.K. Shukla and A.A. Mamun. *Introduction to Dusty Plasma Physics*. Series in Plasma Physics. CRC Press, 2015.

[3] J Winter. Dust in fusion devices - experimental evidence, possible sources and consequences. *Plasma Physics and Controlled Fusion*, 40(6):1201, 1998.

[4] G. S. Selwyn, J. Singh, and R. S. Bennett. In situ laser diagnostic studies of plasmagenerated particulate contamination. *Journal of Vacuum Science & Technology A*, 7(4):2758–2765, 1989.

[5] Pere Roca i Cabarrocas, Patrick Gay, and Aomar Hadjadj. Experimental evidence for nanoparticle deposition in continuous argonsilane plasmas: Effects of silicon nanoparticles on film properties. *Journal of Vacuum Science & Technology A*, 14(2):655–659, 1996.

[6] L Boufendi, M Ch Jouanny, E Kovacevic, J Berndt, and M Mikikian. Dusty plasma for nanotechnology. *Journal of Physics D: Applied Physics*, 44(17):174035, 2011.

[7] Gregor E. Morfill and Alexei V. Ivlev. Complex plasmas: An interdisciplinary research field. *Rev. Mod. Phys.*, 81:1353–1404, Oct 2009.

[8] P. Hartmann, G. J. Kalman, Z. Donkó, and K. Kutasi. Equilibrium properties and phase diagram of two-dimensional yukawa systems. *Phys. Rev. E*, 72:026409, Aug 2005.

[9] A. Melzer, A. Homann, and A. Piel. Experimental investigation of the melting transition of the plasma crystal. *Phys. Rev. E*, 53:2757–2766, Mar 1996.

[10] M Bonitz, C Henning, and D Block. Complex plasmas: a laboratory for strong correlations. *Reports on Progress in Physics*, 73(6):066501, 2010.

[11] P K Shukla and A A Mamun. Solitons, shocks and vortices in dusty plasmas. *New Journal of Physics*, 5(1):17, 2003.

[12] Vikram Singh Dharodi, Sanat Kumar Tiwari, and Amita Das. Visco-elastic fluid simulations of coherent structures in strongly coupled dusty plasma medium. *Physics of Plasmas*, 21(7), 2014.

[13] Sanat Kumar Tiwari, Amita Das, Predhiman Kaw, and Abhijit Sen. Observation of sharply peaked solitons in dusty plasma simulations. *New Journal of Physics*, 14(6):063008, 2012.

[14] John J. Tyson and James P. Keener. Singular perturbation theory of traveling

waves in excitable media (a review). *Physica D: Nonlinear Phenomena*, 32(3):327 – 361, 1988.

[15] A. V. Holden, M. Markus, and Hans G. Othmer, editors. *Nonlinear Wave Processes in Excitable Media*, volume 244 of *NATO ASI series, Series B, Physics*, 1991.

[16] Vladimir S. Zykov and Eberhard Bodenschatz. Wave propagation in inhomogeneous excitable media. *Annual Review of Condensed Matter Physics*, 9(1):435–461, 2018.

[17] Alain Karma. Electrical alternans and spiral wave breakup in cardiac tissue. *Chaos: An Interdisciplinary Journal of Nonlinear Science*, 4(3):461–472, 1994.

[18] Jorge M. Davidenko, Arcady V. Pertsov, Remy Salomonsz, William Baxter, and Jose Jalife. Stationary and drifting spiral waves of excitation in isolated cardiac muscle. *Nature*, 355(6358):349–351, Jan 1992.

[19] T. Frisch, S. Rica, P. Coullet, and J. M. Gilli. Spiral waves in liquid crystal. *Phys. Rev. Lett.*, 72:1471–1474, Mar 1994.

[20] D. M. Elmegreen. A near-infrared atlas of spiral galaxies. *The Astrophysical Journal Supplement Series*, 47:229–233, nov 1981.

[21] Volker Springel and Lars Hernquist. Formation of a spiral galaxy in a major merger. *The Astrophysical Journal Letters*, 622(1):L9, 2005.

[22] Erik A. Martens, Carlo R. Laing, and Steven H. Strogatz. Solvable model of spiral wave chimeras. *Phys. Rev. Lett.*, 104:044101, Jan 2010.

[23] Shin-ichiro Shima and Yoshiki Kuramoto. Rotating spiral waves with phase-randomized core in nonlocally coupled oscillators. *Phys. Rev. E*, 69:036213, Mar 2004.

[24] Gui-Quan Sun, Zhen Jin, Quan-Xing Liu, and Li Li. Chaos induced by breakup of waves in a spatial epidemic model with nonlinear incidence rate. *Journal of Statistical Mechanics: Theory and Experiment*, 2008(08):P08011, 2008.

[25] Ligang Li, Xinhao Liao, Kit H. Chan, and Keke Zhang. On nonlinear multiarmed spiral waves in slowly rotating fluid systems. *Physics of Fluids*, 22(1):011701, 2010.

[26] P. K. Kaw and A. Sen. Low frequency modes in strongly coupled dusty plasmas. *Physics of Plasmas*, 5(10):3552–3559, 1998.

[27] P. K. Kaw. Collective modes in a strongly coupled dusty plasma. *Physics of Plasmas*, 8(5):1870–1878, 2001.

[28] M. S. Murillo. Critical wave vectors for transverse modes in strongly coupled dusty plasmas. *Phys. Rev. Lett.*, 85:2514–2517, Sep 2000.

[29] B. M. Veeresha, S. K. Tiwari, A. Sen, P. K. Kaw, and A. Das. Nonlinear wave propagation in strongly coupled dusty plasmas. *Phys. Rev. E*, 81:036407, Mar

2010.

[30] M. Gedalin, T. C. Scott, and Y. B. Band. Optical solitary waves in the higher order nonlinear schrödinger equation. *Phys. Rev. Lett.*, 78:448–451, Jan 1997.

[31] Hermann A. Haus and William S. Wong. Solitons in optical communications. *Rev. Mod. Phys.*, 68:423–444, Apr 1996.

[32] Stephane Barland, Jorge R. Tredicce, Massimo Brambilla, Luigi A. Lugiato, Salvador Balle, Massimo Giudici, Tommaso Maggipinto, Lorenzo Spinelli, Giovanna Tissoni, Thomas Knodl, Michael Miller, and Roland Jager. Cavity solitons as pixels in semiconductor microcavities. *Nature*, 419(6908):699–702, Oct 2002.

[33] A.L. New and R.D. Pingree. Large-amplitude internal soliton packets in the central bay of biscay. *Deep Sea Research Part A. Oceanographic Research Papers*, 37(3):513 – 524, 1990.

[34] N. J. Zabusky and M. D. Kruskal. Interaction of "solitons" in a collisionless plasma and the recurrence of initial states. *Phys. Rev. Lett.*, 15:240–243, Aug 1965.

[35] M Q Tran. Ion acoustic solitons in a plasma: A review of their experimental properties and related theories. *Physica Scripta*, 20(3-4):317, 1979.

[36] P. K. Shukla and B. Eliasson. Nonlinear dynamics of large-amplitude dust acoustic shocks and solitary pulses in dusty plasmas. *Phys. Rev. E*, 86:046402, Oct 2012.

[37] P. Bandyopadhyay, G. Prasad, A. Sen, and P. K. Kaw. Experimental study of nonlinear dust acoustic solitary waves in a dusty plasma. *Phys. Rev. Lett.*, 101:065006, Aug 2008.

[38] S. K. Sharma, A. Boruah, and H. Bailung. Head-on collision of dust-acoustic solitons in a strongly coupled dusty plasma. *Phys. Rev. E*, 89:013110, Jan 2014.

[39] T. E. Sheridan, V. Nosenko, and J. Goree. Experimental study of nonlinear solitary waves in two-dimensional dusty plasma. *Physics of Plasmas*, 15(7):073703, 2008.

List of Figures

1.1 Spokes in the Saturn's ring. These spokes are the radial fingers of charged dust particles that is levitated by the Saturn's strong magnetic field (Credit: NASA/JPL-Caltech/Space Science Institute). 5

1.2 Comet Hale-Bopp featuring two distinct tails, a dust tail of white color and an ion tail of blue color (Credit: Tiverton and Mid Devon Astronomy Society). 5

1.3 (Γ, κ) plane for 2-d Yukawa systems. Figure credit: Hartman et al., Phys. Rev. E. **72**, 026409 (2005) [1] 9

1.4 (Γ, κ) plane for 3-d Yukawa systems. Figure credit: Hamaguchi et al., Phys. Rev. E. **56**, 4671 (1997) [2] 10

2.1 Particle trajectories for $\Gamma = 1$ and $\kappa = 0.5$. Trajectories are shown for a time interval $\omega_{pd}t = 2.86$. From the figure it is clear that particle trajectories are diffusive due to the weak coupling. 27

2.2 Particle trajectories for $\Gamma = 10$ and $\kappa = 0.5$. Trajectories are shown for a time interval $\omega_{pd}t = 2.86$. 28

2.3 Particle trajectories for $\Gamma = 50$ and $\kappa = 0.5$. Trajectories are shown for a time interval $\omega_{pd}t = 2.86$. 28

2.4 Particle trajectories for $\Gamma = 200$ and $\kappa = 0.5$. Trajectories are shown for a time interval $\omega_{pd}t = 2.86$. In this case particle trajectories are localized because average value of inter-particle electrostatic potential energy is much higher than average thermal energy of particles. 29

2.5 Mean square displacement (MSD) with varying Γ. Particles motion is ballistic at initial time with a slope of 2 but it becomes diffusive with a slope of 1 on later time. From the figure it is clear that motion is diffusive for $\Gamma = 1$, 50, 100, and 200 but non-diffusive for $\Gamma = 10$. [3] 30

2.6 Velocity auto-correlation function (VACF) of the strongly coupled dusty plasmas. From the oscillations it is clear that velocities are less correlated in the weak coupled regime. 31

2.7 Radial distribution function (RDF) with varying Γ. Shielding parameter κ for all the Γ's are 0.5. With increasing Γ, peaks appear in g(r) which shows that now medium have not homogeneous distribution of particles. Splitting of second peak (peak lies just after sharp peak) at $\Gamma = 200$ shows that medium obtains crystalline phase and inter-particle distance is different along different directions. 32

2.8 Evolution of the kinetic energy (KE) of the system during the equilibration of the 2D medium. 33

2.9 Evolution of the potential energy (PE) of the system during the equilibration of the 2D medium. 34

2.10 Evolution of the temperature (T_d) of the system during the equilibration of the 2D medium. 34

2.11 Evolution of the total energy (TE) of the system during the equilibration of the 2D medium. 35

2.12 Equilibrium x-component velocity distribution $f(v_x)$ of the particles. 35

2.13 Equilibrium y-component velocity distribution $f(v_y)$ of the particles. 36

2.14 Dispersion relation for DLW in the two-dimensional dusty (Yukawa) plasmas. Γ and κ value of the medium for this plot is 100 and 0.5, respectively. At higher ka, $\partial\omega/\partial ka$ is < 0 means phase reversal occurs due to the strong coupling nature of the medium. 38

2.15 Dispersion relation for TSW in the two-dimensional dusty (Yukawa) plasmas. Γ and κ value of the medium for this plot is 100 and 0.5, respectively. 38

3.1 Schematic representation of the two-dimensional simulation system used for the KdV soliton study. Here, width "d" represents the region on which electric field perturbation is applied for the KdV excitation. 51

3.2 Time evolution of a solitary pulse (moving $+\hat{y}$ direction) and a dispersive mode (moving $-\hat{y}$ direction) excited through the electric field perturbation ($E = 25.40$) in the medium. 52

3.3 Comparison of theoretical and simulation results of amplitude ($\frac{\delta n}{n_{d0}}$) damping for rarefactive dispersive wave. 52

3.4 Time evolution of a Gaussian form of density perturbation in the medium. The Gaussian pulse splits in two A ($+\hat{y}$) and B ($-\hat{y}$) oppositely propagating symmetric pulses due to the left and right symmetry in the medium [4]. 53

3.5 Collision of two same amplitude counter propagating solitons. Oppositely moving solitons (A and B) were excited with same amplitude electric field ($E = 25.40$) in $+\hat{y}$ and $-\hat{y}$ directions respectively. 55

3.6 Phase shift during same amplitude soliton collision. An initial electric field to excite them is $E = 25.40$. 55

3.7 Phase shift during same amplitude soliton collision. An initial electric field to excite them is $E = 12.70$. 56

3.8 Head-on collision of different amplitude solitons A ($E = 25.40$) and B ($E = 15.24$) moving in opposite direction. 57

3.9 Phase shift for head-on collision of different amplitude solitons A ($E = 25.40$) and B ($E = 15.24$). 57

3.10 Density evolution for overtaking collision of A ($E = 25.40$) and B ($E = 15.24$) amplitude solitons. 58

3.11 Formation of multi-soliton due to the increase in electric field strength (E). Density of medium for all E is taken at time $263.78\omega_{pd}^{-1}$. In all three cases perturbation width (d) is 10. 60

3.12 Formation of multi-soliton due to the increase in perturbation width (d). Density of medium for all d is taken at time $242.28\omega_{pd}^{-1}$. In all three cases perturbation strength of electric field (E) is 25.40. . . . 60

3.13 Density of medium for three $\Gamma = 10$, 50 and 100 is taken at time $235.11\omega_{pd}^{-1}$. For all three cases magnitude and width of electric field perturbation is 50.81 and 10 respectively. 61

3.14 Density of medium for three neutral drag parameter $\nu/\omega_{pd} = 0.00$, 0.0139 and 0.0279 is taken at time $101.78\omega_{pd}^{-1}$. For all three cases magnitude and width of electric field perturbation is 25.40 and 10 respectively. 61

4.1 Patterns in the Belousov-Zhabotinsky (BZ) reaction image. Image credit: Michael C. Rogers and Stephen Morris, University of Toronto. 67

4.2 Rotating spiral waves of electrical activity on a heart surface. Image credit: A. V. Holden, Nature 392, 20 (1998) 68
4.3 Spiral galaxy NGC 6814 is captured by NASA/ESA Hubble Space Telescope. Image credit: ESA/Hubble and NASA 69
4.4 Recently NASA's Cassini spacecraft shows this figure which is taken from the Saturn's ring and concluded that it is a spiral density wave structure in the Saturn's ring. Image credit: NASA/JPL-Caltech/Space Science Institute 69
4.5 Schematic representation of the circularly rotating force ($\mathrm{F_{rot}}$). Here, $\mathrm{F_{rot}} = \mathrm{A}\sin(\omega_f t)\hat{x} + \mathrm{A}\cos(\omega_f t)\hat{y}$ which is only acting within the circular region on each grid point. The Absolute value of the $\mathrm{F_{rot}}$ is constant but direction rotating clockwise with leading time. The solid large arrow depicts the direction of $\mathrm{F_{rot}}$ and small dotted arrows direction of rotation. This force creates perturbation in the density ($\vec{\nabla} n_d$) and potential ($\vec{\nabla}\phi$) of the medium. 70
4.6 Schematic representation of the circularly rotating force ($\mathrm{F_{rot}}$) at different times. The direction of REF shown in the subplots of this Fig. is obtained by putting t $= 0, T_f/4, T_f/2, T_f$, respectively in Eq. 2.17. 70
4.7 Time evolution of I_1 and I_2 (Eq. 4.3) for compressible HD fluids with different values of η. Simulation parameters for this plot are $A = 10$, $\alpha = 5$ and $\omega_f = 10$. Here, applied force switched off after $\omega_{pd}t = 0.55$ time. In the plot I_1 and I_2 for different η are represented by different line styles. There is perfect matching of I_1 and I_2 (dash and solid line, respectively) for the value of $\eta = 0$. 74
4.8 Time evolution of the density for HD fluid. Here, $\mathrm{F_{rot}}$ applied for whole duration of simulation. For simulation, we have taken $A = 10$, $\omega_f = 10$, $\alpha = 5$ and $\eta = 0.1$. Small circle in the figure represent the region where REF applied. Color bar in the figure represents the density of the medium: equal to 1.00 shows equilibrium density, greater than 1.0 is density compression, and less than 1.0 is density rarefaction. The Density evolution of the medium show the formation of spiral wave. 75

4.9 Spiral wave for different frequency of forcing. In this case rotating external forcing applied for whole duration of simulation. Simulation parameters for this plot are $A = 10$, $\eta = 0.1$, and $\alpha = 5$. Density for all subplots are taken at time $\omega_{pd}t = 1.60$. First subplot elucidate that when driver frequency is high then radial velocity cannot pace with it resulting spiral becomes smeared out. 76

4.10 Dynamics of spiral wave for different value of sound velocity of medium ($\sqrt{\alpha}$). Simulation parameters for this plot are $A = 10$, $\omega_f = 10$, and $\eta = 0.1$. In this case rotating external forcing applied for whole duration of simulation. Density for all subplots are taken at time $\omega_{pd}t = 1.84$. Here by increasing α inner part of spiral wave breakup avoided. For higher value of α, radial expansion is larger than azimuthal expansion. 77

4.11 Spiral wave with varying amplitude of forcing. In this case rotating external forcing applied for whole duration of simulation. Simulation parameters are $\omega_f = 10$, $\alpha = 5$ and $\eta = 0.1$. Density plots for all amplitudes are taken at time $\omega_{pd}t = 1.97$. 78

4.12 Density plot of spiral wave for different values of η in HD fluid. Simulation parameters in this plot are $A = 10$, $\alpha = 5$ and $\omega_f = 10$. Density plots for all values of η are taken at time $\omega_{pd}t = 2.45$. . . . 79

4.13 Ω/n_d (vorticity) of the HD fluid medium for different values of η. Simulation parameters in this plot are $A = 10$, $\alpha = 5$ and $\omega_f = 10$. Vorticity plots for all values of η are taken at time $\omega_{pd}t = 2.45$. From the figure it is clear that diffusion of source of vorticity increases with increase in the coefficient of viscosity of the medium. 80

4.14 Time evolution of the density for strongly coupled visco-elastic fluid. Here F_{rot} applied for whole duration of simulation. For simulation, We have taken $A = 10$, $\omega_f = 10$, $\alpha = 5$, $\eta = 5$ and $\tau_m = 20$. Small circle in the figure represent the region where REF applied. 81

4.15 Spiral wave for different frequency of forcing. In this case too rotating external forcing applied for whole duration of simulation. Simulation parameters in this plot are $A = 10$, $\alpha = 5$, $\eta = 5$ and $\tau_m = 20$. Density for all subplots are taken at time $\omega_{pd}t = 1.55$. At higher ω_f (first subplot), angular velocity is not in pace with the radial velocity resulting spiral becomes smeared and broken out. 82
4.16 characteristic of spiral wave with varying sound velocity of the visco-elastic medium ($\sqrt{\alpha}$). Simulation parameters in this plot are $A = 10$, $\omega_f = 10$, $\eta = 5$ and $\tau_m = 20$. In this case rotating external forcing applied for whole duration of simulation. Density for all subplots are taken at time $\omega_{pd}t = 2.13$. Here by increasing α inner part of spiral wave breakup avoided. For higher value of α, radial velocity is larger than angular velocity. 83
4.17 Spiral wave behavior in GHD fluid with varying amplitude of forcing. In this case rotating external forcing applied for whole duration of simulation. Simulation parameters are $\omega_f = 10$, $\alpha = 5$, $\eta = 5$ and $\tau_m = 20$. Density plots for all amplitudes are taken at time $\omega_{pd}t = 1.76$. 84
4.18 Density plot of spiral wave with increasing strong coupling. Simulation parameters in this plot are $A = 10$, $\alpha = 5$ and $\omega_f = 10$. In this case too external REF applied for the whole duration of simulation. Density plots for all ratio of η and τ_m are taken at time $\omega_{pd}t = 2.8068$. 85
4.19 Ω/n_d (vorticity) of the GHD fluid medium with increasing ratio of η and τ_m. Simulation parameters in this plot are $A = 10$, $\alpha = 5$ and $\omega_f = 10$. Vorticity plots for all ratio of η and τ_m are taken at time $\omega_{pd}t = 2.8068$. From the figure it is clear that expansion of source of vorticity increases with increase in the ratio of η and τ_m. 85
4.20 Ω/n_d (vorticity) of the visco - elastic fluid for the same ratio of η and τ_m. Simulation parameters for this plot are $A = 10$, $\alpha = 5$ and $\omega_f = 10$. Vorticity plots for all ratio of η and τ_m are taken at time $\omega_{pd}t = 2.8068$. Small circle in the figure represent the region where REF applied. From the figure it is clear that expansion of source of vorticity depends only upon the ratio of η and τ_m, not upon the individual values. 87

5.1 Schematic representation of the circularly rotating electric field. Here, REF is only acting within the circular region on each dust particle. The Absolute value of the REF is constant but direction rotating anti-clockwise with leading time. The solid large arrow depicts the direction of REF and small dotted arrows direction of rotation. 96
5.2 Time evolution of the medium for REF of amplitude $A = 0.203$, $\omega_{pd}T_f = 26.88$, $\Gamma = 100$, and $\kappa = 0.5$. Particle snapshots taken at time (a) $\omega_{pd}t = 17.92$, (b) $\omega_{pd}t = 35.84$, (c) $\omega_{pd}t = 53.76$, and (d) $\omega_{pd}t = 71.68$ are clearly showing the formation of spiral wave. Circle at the center represents the region of forcing. 97
5.3 Spiral waves for different value of driver frequency (a) $\omega_{pd}T_f = 12.54$, (b) $\omega_{pd}T_f = 16.12$, (c) $\omega_{pd}T_f = 26.88$, and (d) $\omega_{pd}T_f = 35.84$ at $A = 0.203$, $\Gamma = 100$, and $\kappa = 0.5$. Snapshot of particles for all frequencies are taken at time $\omega_{pd}t = 71.68$. 98
5.4 One-dimensional density of the medium for the different frequencies of driver at $A = 0.203$, $\Gamma = 100$, and $\kappa = 0.5$. Density plot for all frequencies are taken at time $\omega_{pd}t = 71.68$. From the plot it is clear that with decrease in the frequency of external driver, density compression, rarefaction and distance between two consecutive rings increases. 99
5.5 Characteristics of spiral waves with varying amplitude of REF (a) $A = 0.101$, (b) $A = 0.203$, (c) $A = 0.406$, and (d) $A = 1.27$. Coupling parameter, screening parameter, and time period of REF for all amplitudes are $\Gamma = 100$, $\kappa = 0.5$, and $\omega_{pd}T_f = 26.88$, respectively. Snapshot of particles for all amplitudes are taken at time $\omega_{pd}t = 50.17$. From the figure, it is clear that an undistorted (tip) spiral wave can be excited when the amplitude of REF is smaller than inter-dust unscreened electric field (E_0). 100
5.6 Effect of neutral damping (a) $\nu/\omega_{pd} = 0.0$, (b) $\nu/\omega_{pd} = 0.014$, (c) $\nu/\omega_{pd} = 0.0279$, and (d) $\nu/\omega_{pd} = 0.0558$ on the spiral wave are shown here. For all the plots, $A = 0.203$, $\omega_{pd}T_f = 26.88$, $\Gamma = 100$, and $\kappa = 0.5$. Snapshot of particles for all damping parameters are taken at time $\omega_{pd}t = 71.68$. 101

5.7 Characteristics of spiral wave with varying coupling parameter (a) $\Gamma = 10$, (b) $\Gamma = 50$, (c) $\Gamma = 100$, and (d) $\Gamma = 800$. Strength of REF, period of REF, and screening parameter for all the Γ are $A = 0.203$, $\omega_{pd}T_f = 26.88$, and $\kappa = 0.5$, respectively. Snapshot of particles for all Γ are taken at time $\omega_{pd}t = 71.68$. 102

5.8 Dynamics of spiral waves for different values of screening parameter (a) $\kappa = 0.25$, (b) $\kappa = 0.50$, (c) $\kappa = 1.0$, and (d) $\kappa = 2.0$. Amplitude of driver, period of driver, and coupling parameter for all the plots are $A = 0.203$, $\omega_{pd}T_f = 26.88$, and $\Gamma = 100$, respectively. Snapshot of particles for all the κ are taken at time $\omega_{pd}t = 71.68$. 103

5.9 Effect of screening parameter (a) $\kappa = 0.5$, (b) $\kappa = 1.0$, (c) $\kappa = 1.5$, and (d) $\kappa = 2.0$ on the spiral structure when dust medium is in crystalline state. Amplitude of driver, period of driver, and coupling parameter for all the plots are $A = 0.203$, $\omega_{pd}T_f = 26.88$, and $\Gamma = 2000$, respectively. Snapshot of particles for all κ are taken at time $\omega_{pd}t = 53.76$. 104

5.10 Schematic representation of interparticle distance asymmetry when dusty plasma is in crystalline phase. This is the equilibrium snapshot of particles for $\Gamma = 2000$ and $\kappa = 1.5$. Solid and dotted arrows depict the lattice axial and diagonal directions, respectively in the crystal. Asymmetry in the dust crystal spacing have also shown experimentally by J. H. Chu and Lin I [5]. 105

5.11 Radial distribution function (RDF) for three $\Gamma = 100, 400, 2000$ are shown here. Screening parameter (κ) for all Γ are 1.5. At $\Gamma = 2000$, appearance of one more peak near the second peak (peak comes just after sharp first peak) confirms the anisotropy in the interparticle distance of hexagonal crystal. 105

5.12 Schematic representation of the suggested experimental system. Rectangular black regions on circumference of the circle represents the two prongs of the fork and arrows depicts the direction of electric field. Plots (a), (b), (c), and (d) shows the spatial location of the fork at time 0.0, $T_f/4$, $T_f/2$ and T_f, respectively. where, T_f is the time period of rotation of the fork. 107

List of Tables

3.1 Soliton Parameter with varying amplitude of perturbation (E). Parameters are taken at the time $55.91\omega_{pd}^{-1}$. 53

1

Introduction

1.1 Introduction

In general, matter can exist in any of the solid, liquid or gaseous phase. Heating or providing energy by other means to the gaseous atoms decompose them into electrons and ions (a fraction or whole depending on the amount of energy supplied) leading to a quasi-neutral ionized gas of charged particles. This quasi-neutral gas is called the plasma state of matter. Approximately 99 % observable matter (excluding the dark matter) of the universe is in the plasma state. Plasma show various type of single particle and collective response to the externally applied electric and magnetic fields. It can be used in various type of applications such as etching in microelectronics, plasma spraying (coating), metal cutting, designing energy storage devices, medical science, agriculture, producing fusion energy, and also in particle acceleration etc.

In the vast amount of natural and laboratory scenario dust is inadvertently present in plasma. For instance, star forming regions, interstellar clouds, Zodiacal light, planetary rings (Fig. 1.1), Comet tails (Fig. 1.2), Earth's ionosphere are some of the examples of natural [6] scenario and fusion devices [7], rocket exhaust, thin film deposition, production of the solar cell by nanometer size dust, direct current (DC) and radio frequency (RF) discharges are few examples from laboratory [8] scenario. These solid particles become negatively charged (can also become positively charged depends upon the plasma environment) due to the high mobility of electrons and becomes an extra component of the plasma medium. This extra component adds new types of individual particle and collective response in the plasma medium. Therefore, the study on dusty plasma helps to understand the various types of natural and laboratory phenomena. Often these have important implications for industrial applications viz. thin film deposition [9, 10] in which presence of dust deteriorate/destroy the quality of the chips and production of solar cell by nanometer size dust [11].

This thesis is devoted to the studies of collective structures in the dusty plasmas. The collective structures hold great prominence in the dusty plasma medium. The rest part of this chapter is organized as follows. Section 1.2 provides the basic concepts and characteristics of dusty plasmas. Section 1.3 presents the various models used to study dusty plasmas with outlining their advantages and disadvantages. In section 1.4, review of earlier works carried out on collective structures in dusty plasmas are provided and motivation for this thesis is also presented. Last section 1.5 contains the outline of the thesis.

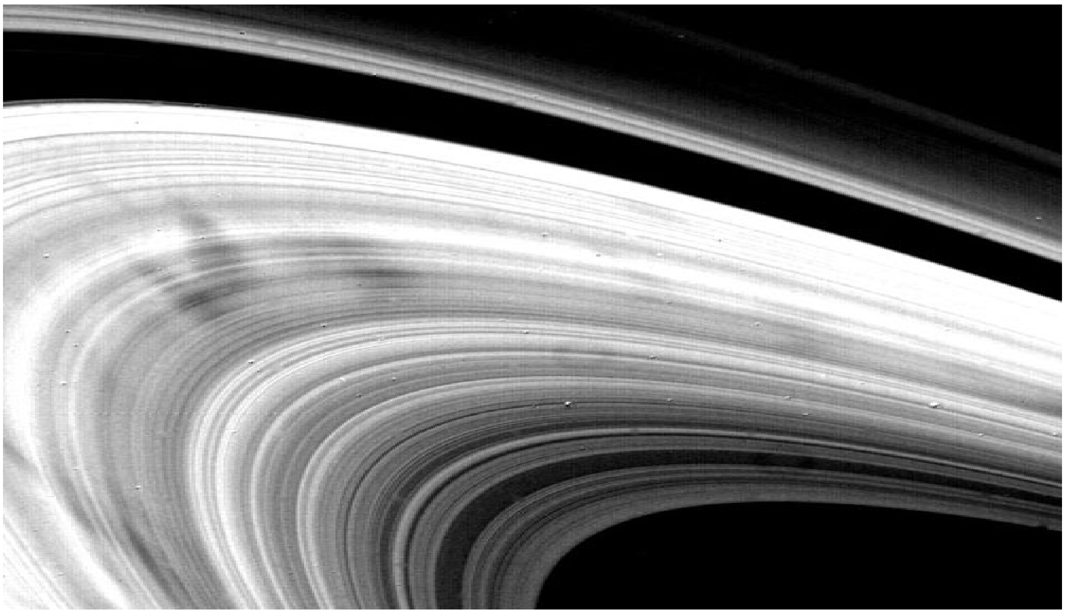

Figure 1.1: Spokes in the Saturn's ring. These spokes are the radial fingers of charged dust particles that is levitated by the Saturn's strong magnetic field (Credit: NASA/JPL-Caltech/Space Science Institute).

Figure 1.2: Comet Hale-Bopp featuring two distinct tails, a dust tail of white color and an ion tail of blue color (Credit: Tiverton and Mid Devon Astronomy Society).

1.2 Introduction to complex plasma or dusty plasma

1.2.1 Dusty plasma

Dusty plasma is a four-component plasma consists of electrons, ions, neutrals and embedded solid (dust) particles. These solid particles could be conductor, dielectric or made of ice particulates [8]. They are much heavier than ions and their typical mass ranges from 10^{-18} - 10^{-12} Kg. Due to light mass, electrons acquire high thermal velocity and they stick to the surface of dust particles. In this fashion, solid particles acquire charge and become an extra super-heavy component of the plasma. The charge on the dust particles increases with the size of the particles i.e. with radius (r_d) of the particles. The typical size of the solid particles ranges from nanometer to micrometer accordingly charge on them ranges from $100e$ to $10,000e$, where e is elementary charge. Shielding to these dust particles are provided by the background electrons and ions. The Debye length of the shielding is given by the following formula:

$$\lambda_D = \left(\frac{Z_i^2 n_i}{\epsilon_0 k_B T_i} + \frac{e^2 n_e}{\epsilon_0 k_B T_e} \right)^{-\frac{1}{2}} \tag{1.1}$$

Where Z_i, n_i, and T_i are the charge, density, and temperature of the plasma ions, and e, n_e, and T_e are charge, density, and temperature of the plasma electrons. If $a > \lambda_D >> r_d$, then medium is called "dust in plasma". Here, a is average inter particle distance between dust grains. On the other hand, If $\lambda_D > a >> r_d$, then medium is called "dusty plasma". In the later case, dust particles participate in the collective phenomena. The inclusion of dust to the plasma increases the complexity of the medium by introducing new physical processes viz. effects associated with dissipation, plasma recombination on the particle surface and variation of particle charge as a function of time. So the medium is called complex plasma. These new physical processes change the energy influx in the medium. Therefore, complex plasmas are the non-Hamiltonian system [12]. Presence of dust component in plasma adds a rich class of collective phenomena viz. dust acoustic wave (DAW), dust lattice wave (DLW), transverse shear wave (TSW), Mach cones, vortex, solitons, and shocks in the medium. The dynamical time scale associated with these phenomena (for micron size particles) varies between 1 - 100 Hz. Therefore they can be seen from bare eyes and can easily be diagnosed (eg. by CCD camera) in experiments. Due to long time and length scales strongly coupled dusty plasmas offer a model system to study generic phenomenon such as self-organization, transport, phase transitions, waves, structures and instabilities at individual particle level which is of relevance in regular liquids, charged colloids, polymers, electrolytes and condensed matter system [12].

1.2.2 Strong coupling

The thermodynamics of the dusty plasma can be characterized by two dimensionless parameters $\Gamma = Q^2/4\pi\epsilon_0 a k_b T_d$ (known as the coupling parameter) and $\kappa = a/\lambda_D$ (known as the screening parameter). Here T_d and a are the dust temperature and the Wigner-Seitz (WS) radius, respectively. For 2-D and 3-D systems, Wigner-Seitz (WS) radius is $(n_{2d}\pi)^{-1/2}$ and $(3/4\pi n_{3d})^{1/3}$, respectively. Here n_{2d} and n_{3d} are the dust density for the 2-D and 3-D systems, respectively. Due to high charges on the dust grains ($\approx -10,000$e), the dusty plasmas can be easily found in the strongly coupled state (i.e. their electrostatic average potential energy can be made comparable to or higher than the average kinetic energy of particles easily and does not require extreme conditions of temperature and/or density).

Such a plasma can, therefore, have traits of a gas, a fluid and a solid depending upon where medium lies in the (Γ, κ) plane. (Γ, κ) plane for 2-D and 3-D Yukawa systems are shown by Hartman et al. [1] and Hamaguchi et al. [2], respectively. The phase diagram is also shown here in Fig. 1.3 and, Fig. 1.4, respectively. For a given κ, dusty plasma imbricate to crystalline state when the coupling parameter $\Gamma > \Gamma_c$, where Γ_c is the critical value for crystallization. At intermediate value of Γ ($1 < \Gamma < \Gamma_c$) the system behaves like a complex fluid with both fluid and solid like traits. Fluid nature of dusty plasma gives viscosity and solid nature provides the elasticity in the medium. Hence, both longitudinal and transverse wave modes can be excited in strongly coupled dusty plasmas. Different phases (phase transitions) in typical dusty plasma experiments are achieved by either varying RF power or by changing neutral gas pressure [13]. Increasing RF power leads to an increase in the ion density, resulting decrement in Debye length (or increment in κ) occurs so that the dust crystal melts down. On the other hand, increasing neutral gas pressure leads to a decrease in the dust temperature which results increment in Γ and hence liquid phase converts into crystalline phase. Strong coupling behavior, crystallization, and phase transitions in dusty plasma are shown experimentally by Chu et al. [5] and Thomas et al. [14]. Phase transitions by means of shock melting have also been studied in the dusty plasma experiment [15]. In addition to dusty plasmas many other systems viz. Inertial confinement fusion (ICF) plasmas, colloidal suspensions, ultracold-neutral plasmas, and warm dense matter also show strong coupling behavior and phase transitions. Dusty plasma offers a model system to study the strong correlations related phenomenon which is difficult to study in the previously mentioned system. So the study carried out in this thesis would also be relevant to these systems as well.

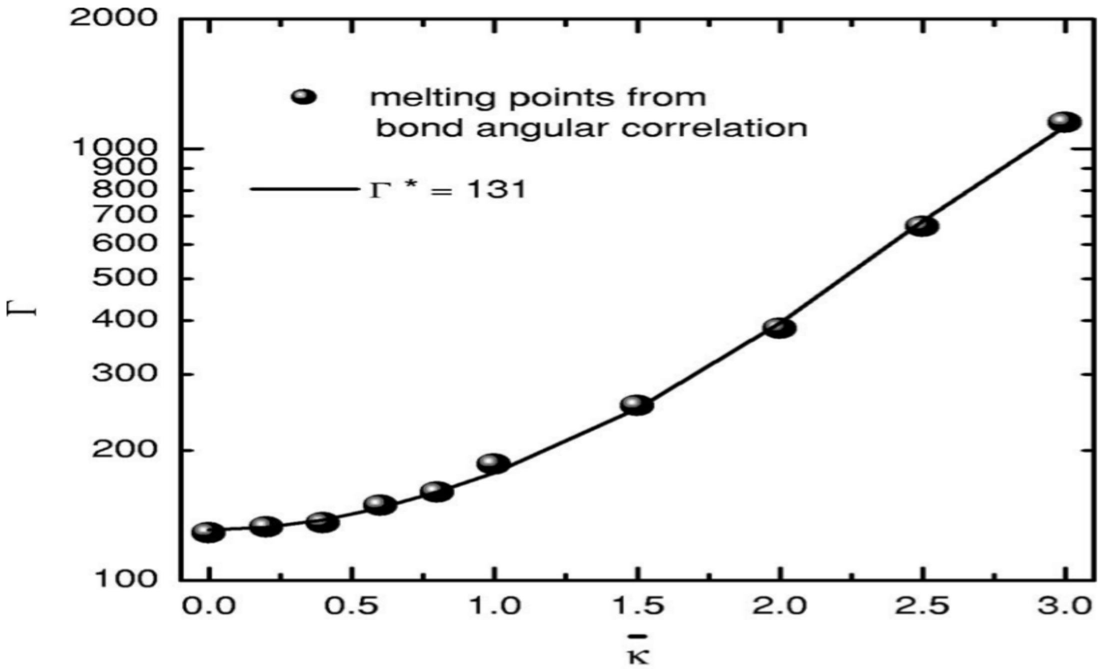

Figure 1.3: (Γ, κ) plane for 2-d Yukawa systems. Figure credit: Hartman et al., Phys. Rev. E. **72**, 026409 (2005) [1]

Strongly coupled plasmas are also known as non-ideal plasmas because $\Gamma > 1$ automatically sets $n_d\lambda_{dust}^3 < 1$, which can be seen as:

$$\Gamma = Q^2/4\pi\epsilon_0 a k_b T_d \propto 1/(n_d\lambda_{dust}^3)^{1/3} \tag{1.2}$$

Where $\lambda_{dust} = \sqrt{Q^2 n_d/\epsilon_0 k_B T_d}$, T_d and Q are dust temperature and charge on each dust particle, respectively. Unlike the ideal plasmas ($n_d\lambda_{dust}^3 > 1$), non-ideal plasmas are dominated by collective behavior and strong interaction with less probability of finding dust particles in the sphere of volume λ_{dust}^3.

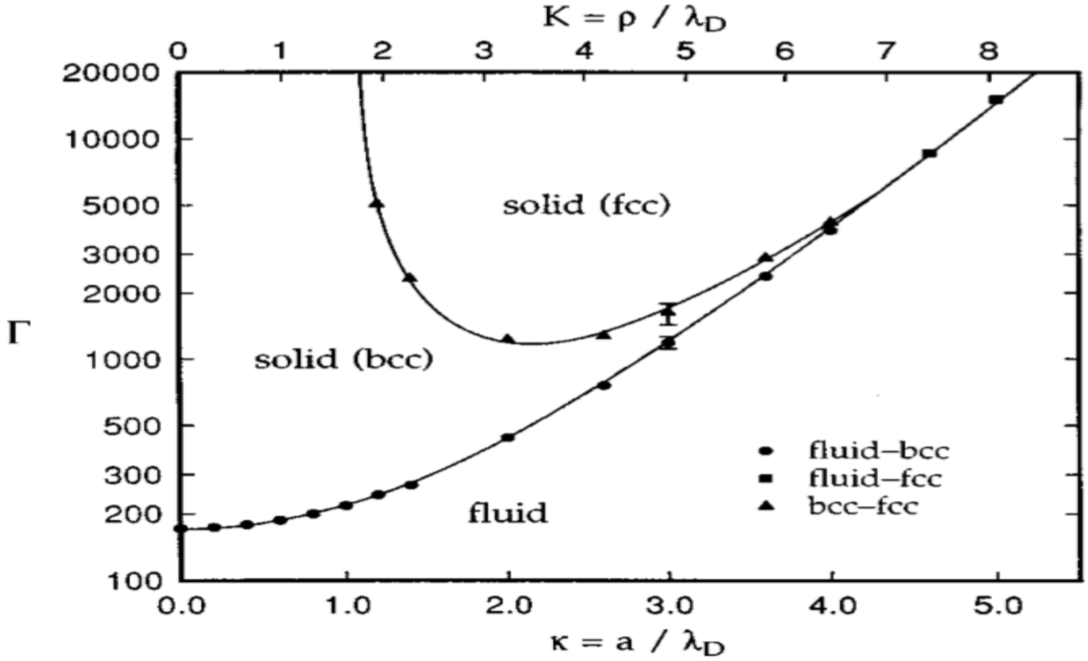

Figure 1.4: (Γ, κ) plane for 3-d Yukawa systems. Figure credit: Hamaguchi et al., Phys. Rev. E. **56**, 4671 (1997) [2]

1.3 Models to study dusty plasmas

In the literature, various models are used to study the dusty plasma characteristics. Among different models, here I am going to briefly discuss some simple models with outlining their advantage and disadvantage.

1.3.1 Generalized Hydrodynamic (GHD) model

Kaw and Sen introduced the Generalized Hydrodynamic model to study the strongly coupled dusty plasmas [16, 17]. In GHD model, dusty plasma is considered as a visco-elastic fluid which has both solid and fluid like traits. Fluid like nature of dusty plasma gives the viscosity and solid like nature provides elasticity in the medium. Due to elasticity dust fluid retains the memory of its past configurations.

The memory function has been modeled as exponentially decaying in time. It should be noted that GHD momentum equation reduces to the usual momentum equation for a charged viscous fluid in the limit when the dust has no memory. A finite memory represents the time for which the fluid retains the memory of its past configurations arising due to elastic behavior of the strongly coupled dusty plasma. GHD model have successfully explained DAW dispersion relation in both weak and strong coupling (phase velocity reversal in strong coupling) limits, predicts new mode called TSW, and explain various nonlinear structures viz. solitons and shocks, found in dusty plasma experiments. GHD model work well below crystalline Γ and in large wave vector (k) limit. Recently Murillo et al. have added some corrections in the GHD model by beginning with the exact equations of the Bogoliubov-Born-Green-Kirkwood-Yvon hierarchy [18].

1.3.2 Quasi-localized charge approximation (QLCA)

Kalman and Golden gave QLCA approach for the analysis of the dielectric response function and collective mode dispersion for various strongly coupled Coulomb systems [19–21]. In the QLCA model, dust particles are considered as quasi-localized charged particles trapped in the polarizable background. The location of dust charge sites are random (but strongly correlated) and they momentary oscillate around the local minima of the fluctuating potential. On a longer time scale, these site positions also change and a continuous rearrangement (by diffusion) of particle location configuration takes place. QLCA successfully explain the longitudinal and transverse mode dispersion relation of strongly coupled dusty plasma medium in the short wave vector (k) limit [22,23]. This model is only valid when the coupling parameter $\Gamma > 1$.

1.3.3 Particle-in-cell (PIC) simulations

In the PIC simulation method, dust, electron, and ion all species are considered as kinetic particles in the medium. Due to a large number of disparate mass particles in the medium, huge computation resources are required. In order to deal with this issue concept of super-particles are used in this simulation. Each super-particle contains large number of real particles and the dynamics of each super-particle is governed by Newton's law. The whole system is divided into the number of grids and on each grid charge density and current is being calculated. As the system evolves dust species charge and current density gets changed on each grid. This charge and current density variation goes into Newton's equation through the Maxwell equations and accordingly force on each particle gets modified. In this fashion dusty plasma medium evolve with time. By PIC simulation, we can study the dynamics of all the complex plasma species (electron, ion, and dust) but its working is limited within the weakly coupled regime. In the literature, various studies viz. charging of dust particle [24, 25], wake structures in steaming complex plasmas [26], and envelope solitary wave [27], dust acoustic instability [28], and ion-dust streaming instability [29] in the dusty plasma medium have been carried out by this simulation technique.

1.3.4 Molecular-dynamics simulation

In molecular-dynamic (MD) simulations, dust medium is considered as particles and they interact electrostatically via the Yukawa form of the interaction potential. The Yukawa interaction mimics the screening due to the presence of free electrons and ions between dust particle. The dynamics of particles is given by the first principle i.e. from Newton's law. MD simulation is a very popular tool to study the dusty plasmas. Using MD simulation people have studied normal modes, viscosity, phase transitions, diffusion, Mach cones, and nonlinear structures in the dusty plasmas. The disadvantage of MD simulation is that it requires huge computation and computation cost increases as square the number of particles. In addition to the number of particles computation problem, a huge difference in the response time scales of electron, ions, and dust make the study of all complex plasma species at a time in the MD simulation is not possible. Therefore, in these cases the MD simulations simply follow the dust dynamics interacting via screened Coulomb potential. The lighter electron and ion particles are assumed to provide instantaneous screening.

1.3.5 Vlasov approach

Rosenberg studied dust ion-acoustic and dust-acoustic instability analytically using Vlasov approach that was excited due to the weak electron and/or ion drifts [30]. By the Vlasov approach, all three components (electron, ion, and negatively charged dust) of the dusty plasma can be taken in the simulations. For the dynamics of medium, Vlasov equation for each species is evolved. The Electric potential of the medium is obtained by Poisson's equation. For the dynamics of plasma species electric potential coupled with the Vlasov equation. Using this simulation technique, Jenab et al. studied dust-ion acoustic wave and its Landau damping [31]. Recently Golden et al. have shown that the Vlasov approach for Yukawa interaction (dusty plasmas) is only tenable above a critical coupling parameter [32] and below which there can be no real solution to the collective modes dispersion relation.

1.4 Review of earlier work on collective structures in the dusty plasmas and the motivation

The dusty plasma constituents interact with each other electrostatically, therefore, various types of collective structures (both linear and nonlinear) can be excited by external perturbations in the form of electric fields or laser radiation pressure or self-excited by, viz., ion drag force, thermal fluctuations, and instabilities. Dusty plasma is a dispersive medium, the presence of nonlinearity in the normal mode perturbation leads to the formation of localized structures such as solitons and shocks. Due to the balance of dispersion and nonlinearity in the solitons, they can travel a long distance in the medium without altering their shape and size. In the literature, a considerable amount of studies carried out theoretically and experimentally on the collective structures viz. solitons, shocks, vortices (monopole, dipole and tripolar), and Mach cones in complex plasmas are present.

Rao et al. [33] motivated by the importance of dust particles in the planetary rings and cometary tails carried out a theoretical study of its collective modes. They name this collective mode dust acoustic wave (DAW). They have also studied the weakly nonlinear form of DAW and derived Korteweg-de Vries (KdV) equation using momentum, continuity, and Poission's equation of the dust fluid. Further, they have shown that the solution of KdV equation can propagate as solitons with either negative or positive electrostatic potential. After Rao et al.'s study, dusty plasma has achieved a huge attention of researchers. The first laboratory observation of DAW was reported by Barkan et al. [34]. They also compared their experimental results with the theories. Frank Melandso studied the linear and nonlinear waves in the dust crystal by using lattice vibrations, a prominent feature in solid state physics [35]. Melandso has called dust lattice wave (DLW) to the linear acoustic mode of the crystal. Later Farokhi et al. improved the results of Melandso et al. by considering the interaction with all grains (long range) rather than only a few nearest neighbor as Melandso et al. had taken [36]. Samsonov et al. [37] have studied dissipative longitudinal solitons in the experiments and found agreement with theoretical studies of Rao et al. and Melandso et al. Anisotropic plasma crystal compressional and shear solitons were reported analytically by Zhdanov et al. in the long-wavelength approximation [38]. They had also shown that the compressional solitons are always supersonic and weakly anisotropic but the shear solitons have strong anisotropy and can be both subsonic and supersonic, depending on the direction of propagation in the medium. Dark and bright dust-ion acoustic solitary waves (DIASWs) have been studied theoretically by Popel and Yu [39]. Popel et al. have also reported dissipative DISWs which occurs when the plasma absorption and ion scattering on dust particles were taken [40]. Experimental study on DISWs was carried out by Nakamura et al. [41]. Mamun and Shukla extended the dust-ion acoustic solitary study for the two and three dimensions and derived modified KdV equation for the cylindrical and spherical DIASWs [42]. They have found that the properties of nonplanar cylindrical or spherical DIASWs are different from the planar one-dimensional DIASWs. Head-on collision and associated phase shift of dust-acoustic solitary waves were studied both in weak and strong coupling regime theoretically by Ju-Kui Xue [43] and Jaiswal et al. [44], respectively. Sheridan et al. have studied solitary waves experimentally in the two-dimensional dusty plasmas [45]. They have excited solitary waves by pushing dust particles in a rectangular region using 18 W green laser. They have observed compressive solitary wave propagating in the forward direction and oscillating shock in the backward direction. The oscillating shock in the backward direction is in contrast to the theoretical finding of Avinash et al [46], in which they have shown a stable refractive soliton. Experimental study of low-frequency DASWs have been carried out by Bandyopadhyay et al. [47]; that was excited by a voltage pulse and DASWs head-on collision studied by Sharma et al. [48]. In the head-on collision study of solitary waves, Sharma et al. found that the phase shift during the collision increases with an increase in the amplitudes of colliding waves. Veeresha et al. have studied the effect of strong coupling on the nonlinear low-frequency waves in the dusty plasmas using GHD model [49]. In this study, they have also discussed the modulational stability of dust acoustic waves. Effect of polarization force (due to the presence of background (electron and ion) density inhomogeneity) on dust acoustic solitary waves was discussed by Bandyopadhyay et al [50]. Sanat et al. have observed cusp-like sharply peaked dust acoustic solitons in the one-dimensional fluid simulation of the dusty plasma medium [51]. Nonlinear waves studies such as precursor solitons, shocks in the flowing complex plasma was carried out by Surabhi et al [52, 53]. Linear [54, 55] and nonlinear [56] dust density waves which get self excited due to the ion drift relative to the dust particle have also been studied theoretically as well as experimentally. Envelope solitary waves of the dust particles have been studied by Zhang et al. using particle-in-cell (PIC) simulation method [27]. They have found that there is no phase shift after the head-on collision between two envelope solitary waves, unlike KdV solitary waves head on collision. Further, they have extended simulations and carried out study on the head-on collision and overtaking collision between an envelope solitary wave and a KdV solitary wave. It is observed that there are phase shifts of the KdV solitary wave in both head-on collision and the overtaking collision, while no phase shift occurs for the envelop solitary wave in any case [57].

Analytical studies on dust acoustic shocks were carried out by Melandso and Shukla and the mechanism of shock wave formation was balancing between the nonlinear wave breaking and the dissipation of wave energy due to the variation of dust particle charges [58]. Further Popel et al. have also studied shock waves formation due to dissipation associated with the dust charge variation (due to the charging of dust grains) [59]. Dust-acoustic monotonic/oscillatory shocks in a strongly coupled dusty plasmas which occur due to strong correlations among dust grains were studied by Shukla et al. using GHD model and they derived KdV-Burgers equation [60]. Later it was observed in the experiment by Sharma et al. [61]. Large amplitude non-dispersive dust acoustic shock waves in the dusty plasma were studied by Eliasson and Shukla [62,63]. Shock with various properties was also studies in many experiments [15,64–67]. V-shaped shocks produced by supersonic particle motion in the two-dimensional dusty plasma was studied by Samsonov et al. [68]. Linear and nonlinear dust drift waves in the the inhomogeneous and magnetized dusty plasmas was investigated by Shukla et al. [69]. They were also derived the nonlinear mode coupling equations. Vortices in both the unmagnetized and magnetized dusty plasmas theoretically as well as experimentally have been studied [70–79]. Dharodi et al. have studied coherent vortices in the strongly coupled dusty plasmas using fluid simulations and also compared their finding with the MD simulation [80].

Havnes et al. first proposed in his study that Mach cone structures can be generated in planetary dust rings by boulders moving through the dust [81]. They also showed that the Mach cone opening angle is dependent on the boulder velocity and the local dust acoustic velocity. Later Samsonov et al. studied Mach cones in the dusty plasma experiment and MD simulations [82]. In this experiment, Mach cones were excited by charged micro-spheres moving in the second incomplete dust layer that had a velocity faster than the lattice sound speed. Further, Melzer et al. had excited Mach cones in the dust crystal mono-layer using laser radiation pressure. The experimental results were also compared with the MD simulation [83]. Mach cone shocks have also been studied in the dusty plasma experiments [68]. Shear-wave Mach cones excited by the radiation pressure force in the two-dimensional dusty plasma crystal have also been observed experimentally [84].

Studies on collective structures in the micro-gravity condition have also been carried out by the many research groups. The advantage of the microgravity study is that 3-D dusty plasma studies can be carried out. Another advantage of the micro-gravity condition complex plasma system is that it has little free energy for parametric instabilities to occur. The first experiment on acoustic waves in complex (dusty) plasmas under microgravity conditions conducted with the PKE-Nefedov laboratory on the International Space Station (ISS) was reported by Khrapak et al. [85]. Shock waves in the micro-gravity condition in the PKE-Nefedov laboratory were excited by a sudden gas pulse [65]. Externally excited breathing mode and nonlinear waves in the PK-3 Plus set-up on board the International Space Station (ISS) were studied experimentally by Schwabe et al. [86]. Externally excited planar dust acoustic shock waves in the DC gas discharge chamber of Plasma Kristall-4 (PK4) were studied by Usachev et al. [87]. In this experiment, due to the facility of the polarity-switching DC discharge mode, dust particle electrostatic pressure have determined. The Hugoniot adiabat for the dust subsystem has also derived.

In this thesis, we focus on the study of collective structure (phenomena) using fluid and MD simulations. In particular, we have looked at the KdV soliton and multisoliton formation and their interaction using MD simulations. We have also studied the excitation and dynamics of spiral waves (structures) by both fluid and MD treatment.

1.5 Structure of the Thesis

There are six chapters in my thesis. In chapter 2, the details of simulation techniques (molecular dynamics and computational fluid dynamics) has been discussed. We also describe the various diagnostic tool that have been employed to extract the various physical quantities of interest from the simulation data. Benchmarking of the code with well known features of the dusty plasma medium such as dispersion relation, radial distribution function (RDF), diffusion coefficient and velocity autocorrelation function (VACF), and phase space distribution etc., are also shown in this chapter.

Chapter - III: In chapter 3, we have studied the KdV solitons in complex plasmas using molecular dynamics simulations. Solitons are robust and stable non-linear localized structures which have been observed in myriad different contexts such as optical fibers [88, 89], semiconductors [90], oceanography [91], and plasmas [92–94]. In our MD simulations studies, we have applied electric field perturbations of the experimental situation [45, 47, 48] to excite the solitonic structures. The collective response of the dust particles to such an applied electric field impulse gives an excitation of a compressible dust density pulse. This density structure propagates in one direction along with a train of negative perturbed rarefactive density oscillations in the opposite direction. We have also shown that by increasing the strength of electric field impulse, the amplitude of the solitonic structure increases and above a certain threshold, it splits to multiple solitons. Further, we have shown that by increasing the coupling parameter of the medium, the amplitude of the solitonic structures increases while their width decreases. We have carried out collisional interaction of these solitonic structures in many different configurations. As expected we find that the phase shift is more in overtaking collision compared to head-on collisions. Furthermore, we have observed that the phase shifts in the collisional interaction decrease with the increasing amplitude of the colliding solitonic structures. Though this is contrary to some experimental observation [48], our observations can be understood from the physical arguments.

Chapter - IV: In Chapter 4, we have studied a novel non-linear two-dimensional structure in dusty plasma using fluid simulations. This is essentially the observation of spiral wave excitation in dusty plasma medium. Spiral waves are ubiquitous structures found in a wide range of natural and laboratory scenario. In this chapter, the spatiotemporal development of spiral waves in the context of weak and strong coupling limits has been shown. While the weakly coupled medium has been represented by a simple charged fluid description, for strong coupling, a generalized hydrodynamic visco-elastic fluid [16] description has been employed. The medium has been driven by an external force in the form of a rotating electric field which is applied in a small circular region. It is shown that when the amplitude of force is small, the density perturbations in the medium are also small. In this case, the excitations do not develop as a spiral wave. Only when the amplitude of force is high so as to drive the density perturbations to nonlinear amplitudes does the spiral density wave formation occurs. We have found that the number of rings in the spiral pattern at a given time is proportional to the number of rotations made by the external forcing. Thus, if the frequency of the driver is high then the number of rings is also high. The radial propagation speed of the spiral is equal to the acoustic speed of the medium. The interplay between the acoustic speed of medium and frequency of forcing decides the spiral structure. In the charged compressible dust fluid, with increasing shear viscosity η the source of vorticity diffuses out. On the other hand in visco-elastic fluids, an additional traverse shear wave (TSW) generated from the forcing region. Thus, in our studies the expansion of this wave increases with an increase in the strong coupling (the ratio of η and τ_m) of the medium because its velocity is equal to $\sqrt{\eta/\tau_m}$.

Chapter - V: In chapter 5, the excitation of spiral waves in the context of driven two-dimensional dusty plasma (Yukawa system) has been demonstrated at particle level using molecular-dynamics (MD) simulations. The interaction amidst dust particles is modeled by the Yukawa potential to take account of the shielding of dust charges by the lighter electron and ion species. The spatiotemporal evolution of these spiral waves has been characterized as a function of the frequency and amplitude of the driving force and dust neutral collisions. The radial propagation of the spiral waves is governed by the dust lattice speed and the rotation gets decided by the forcing period. The interplay between the two decides the spiral wave structure. For distinctly clear spiral to form a proper combination of the two is essential. The parametric dependence is consistent with the continuum study carried out in Chapter 4 wherein the dusty plasma was considered as a visco-elastic fluid.

Further, we have shown that there are additional features which emerge when the discrete particle effects are taken into account using MD simulations. For instance, when the amplitude of force is high the particles at the center get heated by acquiring random thermal velocity. This, in turn, affects the spacing of subsequent rings and collective spiral structure. Furthermore, a large amplitude forcing throws the particle out of the external forcing regime. The restoring force to bring the particles back to the center would, however, depends on the interparticle interaction. When κ is chosen high, the shielding range is small and this restoring effect reduces. Thus for high amplitude and high κ the central region where external forcing has been chosen to be finite becomes devoid of particles. The spiral then fails to form adequately. Another interesting feature that has been observed when the dust medium is in two-dimensional hexagonal crystalline state. In this case, for high values of κ (for which the interparticle potential gets very weak) only a few neighboring particles participate in the interactions. The spiral waveform in such cases has a hexagonal front. This can be understood by realizing that for a hexagonal symmetry (triangular lattice) crystal, the nearest neighbors separation along different directions are different. Therefore, there is an anisotropy in the radial propagation speed along lattice axis and lattice diagonal directions and which leads to the formation of a hexagonal waveform.

Chapter - VI: In Chapter 6, the summary and conclusion of the thesis along with future directions has been provided.

This thesis comprises a series of studies on the collective structures in the two-dimensional strongly coupled dusty plasma using both hydrodynamic and particle simulations approach. These studies contribute significantly to the field of dusty (complex) plasma and also to the multidisciplinary fields of science.

2

Molecular dynamics and computational fluid dynamics

The objective of this chapter is to introduce the simulation techniques used for the studying of collective structures in the two-dimensional dusty plasmas. We have used both molecular dynamics and fluid simulations for the study of linear and non-linear structures. This chapter is organized as follows. Section 2.1 provides the basics for molecular dynamics (MD) simulation of dusty plasma. In this section, we have also benchmarked the MD code (LAMMPS [95]) with well known features of the dusty plasma. In section 2.2, the details of visco-elastic fluid simulation of dusty plasmas are provided.

2.1 Molecular dynamics simulations of dusty plasmas

Dusty plasma is essentially made of discrete charged particles viz. electrons, ions and micron or sub-micron size dust particles. Molecular dynamics simulations offer the possibility of simulating discrete particles which interact with each other via a specified potential. This is the first principle model and it track the dynamics of each individual particle unlike PIC and fluid simulations that track the averaged behavior. We have used open source classic code LAMMPS [95] for the MD simulations.

2.1.1 Interaction potential for MD simulations of dusty plasmas:

Dust particles are much heavier than electron and ion species ($\approx 10^{13} - 10^{14}$ times heavier than the ions) and hence, on dust response time scale electrons and ions are assumed to follow the Boltzmann distribution. Therefore, the electrostatic interaction potential between dust particles becomes Yukawa (shielded Coulomb) and has the following form:

$$U(r) = \frac{Q^2}{4\pi\epsilon_0 r}\exp(-\frac{r}{\lambda_D}),$$

Here, Q is the charge on a typical dust particle, r $(= r_i - r_j)$ is the separation between two dust (i-th and j-th) particles and λ_D is the Debye length of background plasma. In this thesis, Yukawa interaction potential is taken among dust particles for the MD simulations.

2.1.2 Trajectory evolution:

The motion of the i-th particle is governed by the Newton's second law:

$$\begin{aligned} m_d \ddot{r}_i &= -\sum_j \nabla U_{ij}, \\ f_i &= \sum_j \frac{Q^2}{4\pi\epsilon_0}\left(\frac{1}{r\lambda_D}\exp(-\frac{r}{\lambda_D}) + \frac{1}{r^2}\exp(-\frac{r}{\lambda_D})\right) \\ &= \sum_j (U_{ij}/\lambda_D + U_{ij}/r) \end{aligned}$$

The force on the i-th particle depends upon the position of other particles at that time. Velocity-Verlet algorithm has been used to integrate the equation motion. The first step in the Velocity-Verlet integration is to evolve positions of the particles:

$$r(t+\Delta t) = r(t) + v(t)\Delta t + [f(t)/2m](\Delta t)^2$$

From these positions force $f(t+\Delta t)$ on each particle can calculated. In the second step of integration velocities of the particles have been evolved using the following equation,

$$v(t+\Delta t) = v(t) + [(f(t+\Delta t) + f(t))/2m]\Delta t$$

This algorithm can be derived from the Taylor expansion of phase space variables about time t. The advantage of Velocity-Verlet integration is that both position and velocity are defined explicitly on the same instant of time. The choice of integration time step (Δt) is important in dusty plasma and is taken such that the generic phenomena occurs at dust response time scale can be easily resolved. Energy conservation during equilibrium simulation should also be taken into account in deciding Δt. If the chosen Δt is too large then particles traverse large distance in each step. This results a jump in the potential energy (or in the total energy). Therefore, in the simulation, we have taken $\Delta t = 0.0036\omega_{pd}^{-1}$ which satisfies both the criteria. Dust particle trajectories with varying coupling parameter Γ is shown in Figs. 2.1, 2.2, 2.3, 2.4. From the Figs, it is clear that at low Γ particle trajectories are diffusive but trajectories becomes localized at higher Γ. The diffusion coefficient shows the random mobility of the particles in the medium. We have calculated the diffusion coefficient D of the dust particles from the mean square displacement (MSD) as follows:

$$MSD = \left\langle \Delta\vec{r}(t)^2 \right\rangle = \frac{1}{N}\sum_{i=1}^{N}\left(\vec{r_i}(t+t_0) - \vec{r_i}(t_0)\right)^2 \tag{2.1}$$

Diffusion coefficient D and MSD are related through the following equation:

$$MSD = \left\langle \Delta\vec{r}(t)^2 \right\rangle = 4Dt + C_1 \tag{2.2}$$

From the above equation, diffusion coefficient D can be obtained from the slope of MSD vs t plot. Here C_1 is a constant and N is the number of particles in the simulation. Diffusion coefficient D of dust particles with varying Γ has been shown in Fig. 2.5. The velocity auto-correlation (VACF) shows the decay in the particle motion along the MD trajectory which is given by:

$$VACF = \left\langle \vec{v}(t+t_0).\vec{v}(t_0) \right\rangle = \frac{1}{N}\sum_{i=1}^{N}\vec{v_i}(t+t_0).\vec{v_i}(t_0) \tag{2.3}$$

Velocity-autocorrelation function (VACF) of dust particles with varying Γ has been shown in Fig. 2.6. The radial distribution function g(r), shows how particles are radially distributed around a given reference particle. Mathematically

$$g(r) = \frac{V}{N^2} \sum_{i=1}^{N} \sum_{j(\neq i)=1}^{N} [\vec{r} - (\vec{r_j} - \vec{r_i})] \tag{2.4}$$

Here V is the volume/area of the simulation box. Computationally, the g(r) is calculated in the form of histogram count by binning distance between all particle pairs from 0.0 to the maximum force cutoff and then it is normalized by the count if atoms were uniformly distributed like an ideal gas. RDF of dust medium with varying coupling parameter Γ has been shown in Fig. 2.7.

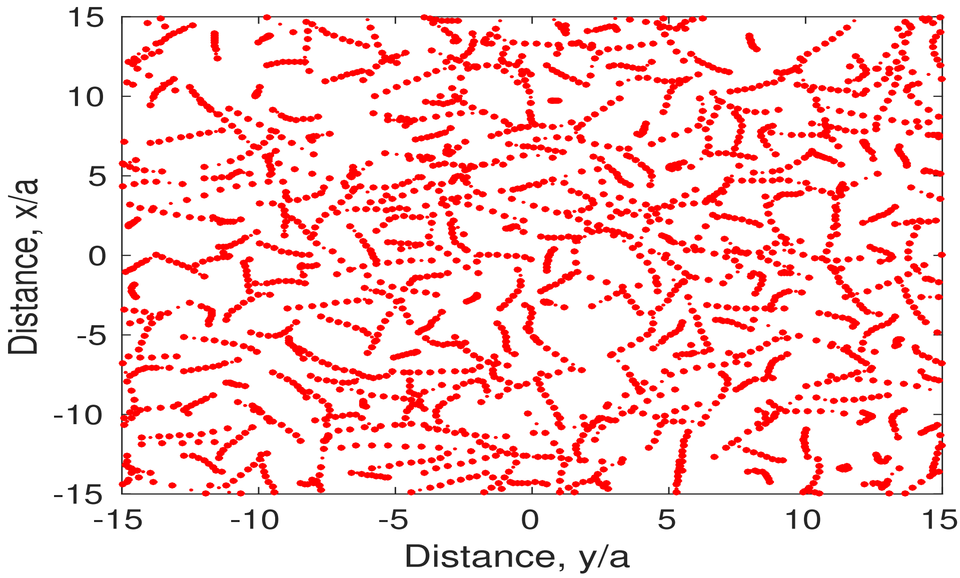

Figure 2.1: Particle trajectories for $\Gamma = 1$ and $\kappa = 0.5$. Trajectories are shown for a time interval $\omega_{pd}t = 2.86$. From the figure it is clear that particle trajectories are diffusive due to the weak coupling.

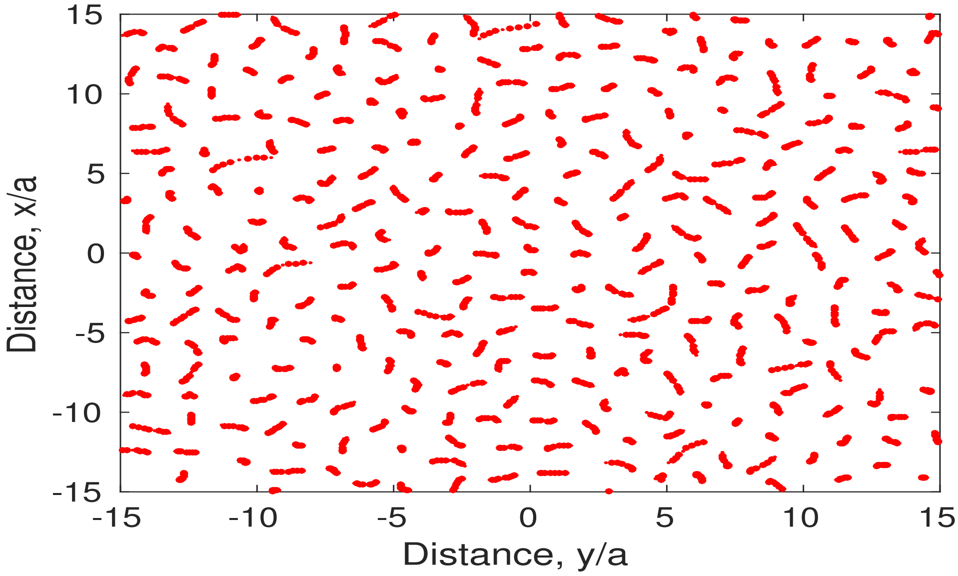

Figure 2.2: Particle trajectories for $\Gamma = 10$ and $\kappa = 0.5$. Trajectories are shown for a time interval $\omega_{pd}t = 2.86$.

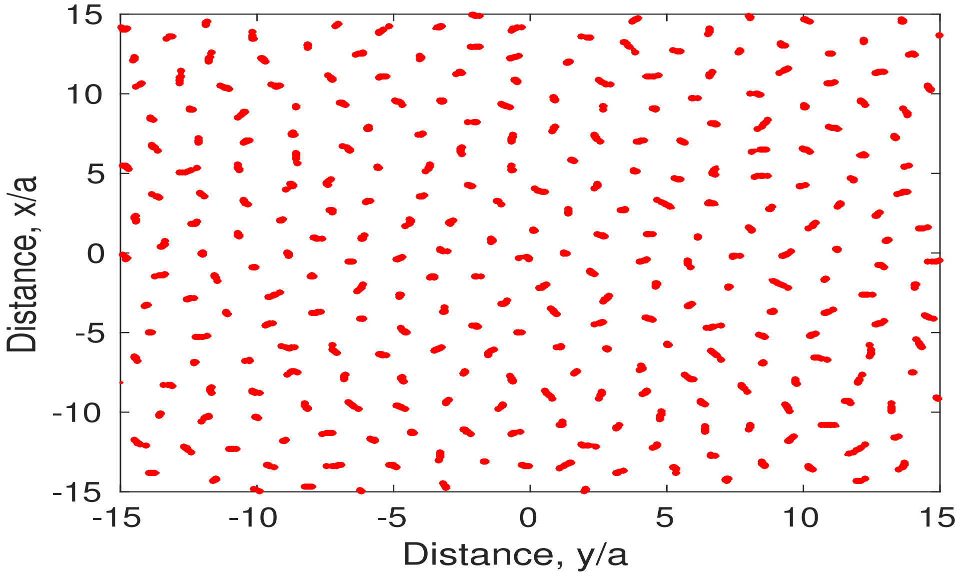

Figure 2.3: Particle trajectories for $\Gamma = 50$ and $\kappa = 0.5$. Trajectories are shown for a time interval $\omega_{pd}t = 2.86$.

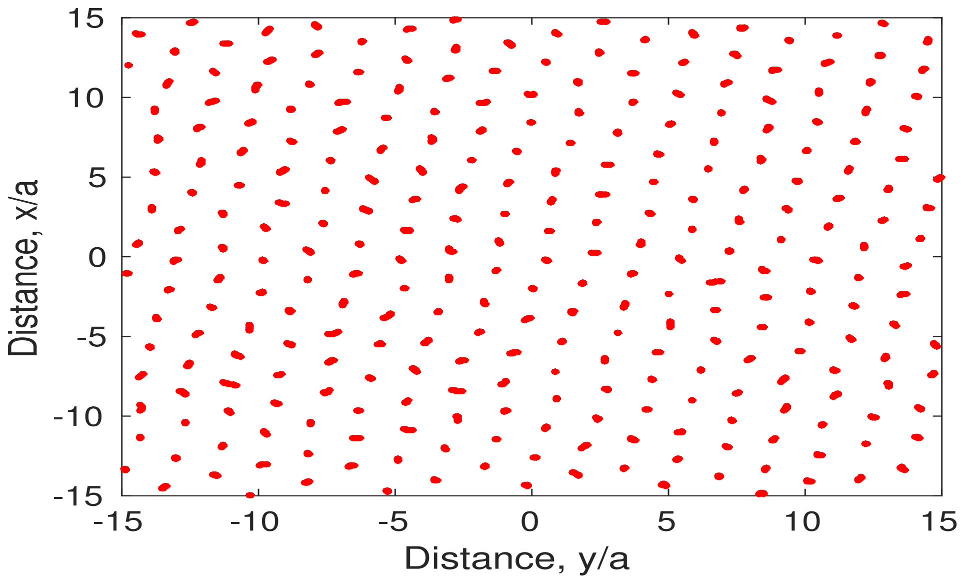

Figure 2.4: Particle trajectories for $\Gamma = 200$ and $\kappa = 0.5$. Trajectories are shown for a time interval $\omega_{pd}t = 2.86$. In this case particle trajectories are localized because average value of inter-particle electrostatic potential energy is much higher than average thermal energy of particles.

2.1.3 Addition of neutral force on the dust grains due to the background gas:

To include the effect of background neutral gas on dust micro - particles, we have added two additional force in the simulation. First is the neutral drag force due to the relative velocity $\vec{v}$ between the dust grains and neutral particles. It is given by [95–97]:

$$\vec{\mathrm{F}}_{\mathrm{f}} = -m_d \nu \vec{v},$$

Where m_d and ν are the mass of the dust particles and damping coefficient, respectively. The other force is random kicks experienced by the dust grains due to

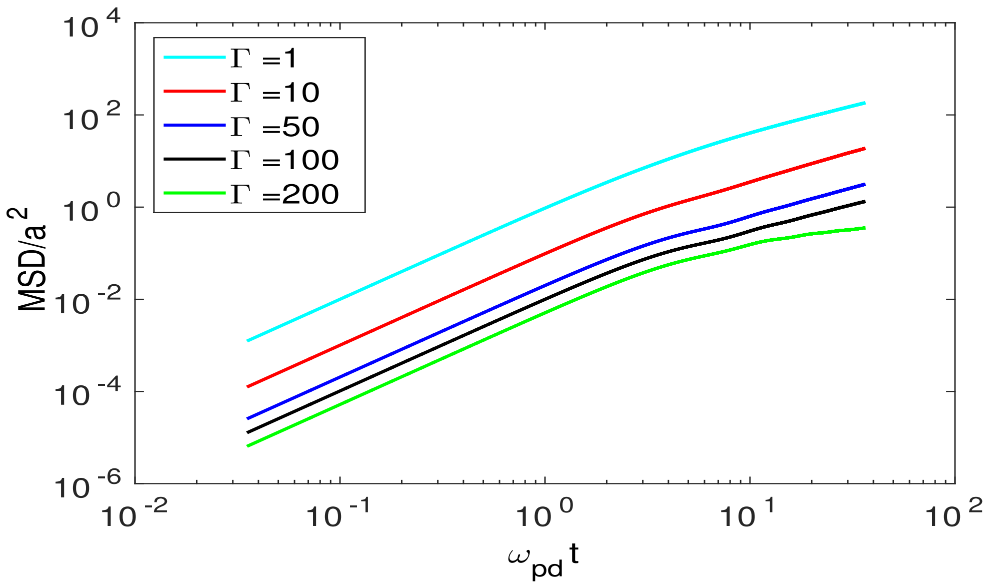

Figure 2.5: Mean square displacement (MSD) with varying Γ. Particles motion is ballistic at initial time with a slope of 2 but it becomes diffusive with a slope of 1 on later time. From the figure it is clear that motion is diffusive for Γ = 1, 50, 100, and 200 but non-diffusive for $\Gamma = 10$. [3]

collisions with neutral atoms. It is given by:

$$\mathrm{F_r} \propto \sqrt{\frac{k_B T_n m_d \nu}{dt}},$$

The direction and magnitude both of $\mathrm{F_r}$ are randomized [98]. Here dt and T_n are the time step of simulation and background neutral gas temperature, respectively. Both $\mathrm{F_f}$ and $\mathrm{F_r}$ together behave like a heat bath for the dust particles. The simulation including the effect of background neutral gas is runs by the Langevin MD dynamics and the motion of the i-th particle with mass m_d is given by the following equation:

$$m_d \ddot{r}_i = -\sum_j \nabla U_{ij} + \mathrm{F_f} + \mathrm{F_r} \tag{2.5}$$

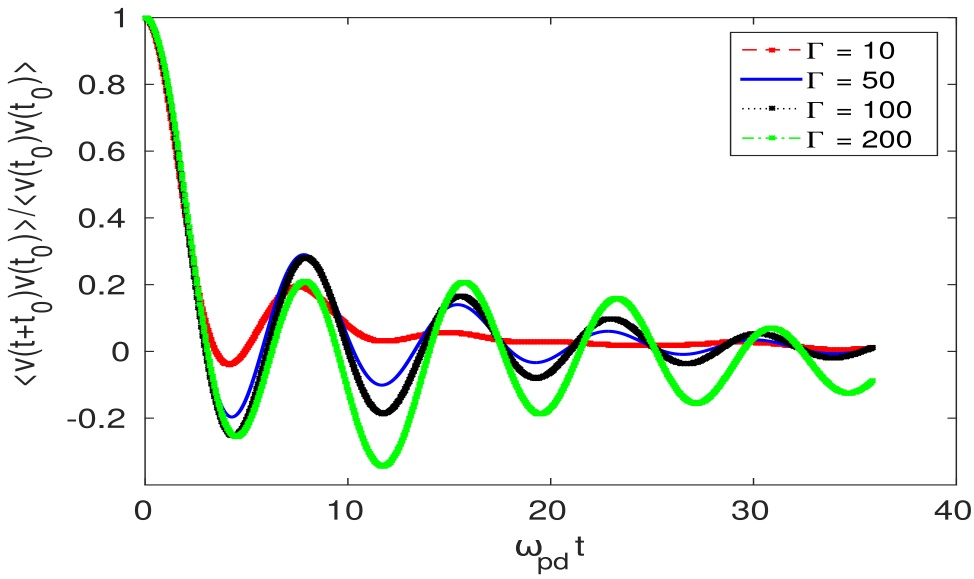

Figure 2.6: Velocity auto-correlation function (VACF) of the strongly coupled dusty plasmas. From the oscillations it is clear that velocities are less correlated in the weak coupled regime.

2.1.4 Details of a typical MD simulation:

The first task to start a MD simulation is to prepare a thermodynamically equilibrated system for desired Γ value. For this, the initial configuration of particle positions are chosen to be random and velocities are chosen to follow Gaussian distribution corresponding to temperature T_d. After initialization, we have achieved equilibrium temperature by generating positions and velocities from canonical ensemble using Nose-Hoover thermostat. After sufficient dust plasma period canonical run, we have disconnected the thermostat and run the system microcanonically in time. To test the equilibration of the system we check kinetic energy (KE), potential energy (PE), temperature (T_d), total energy (TE) fluctuation, and velocity distribution at different leading times. This is shown in Figs. 2.8, 2.9, 2.10, 2.11, 2.12, and 2.13, respectively. In these Figs., normalization parameter U_0 is equal to

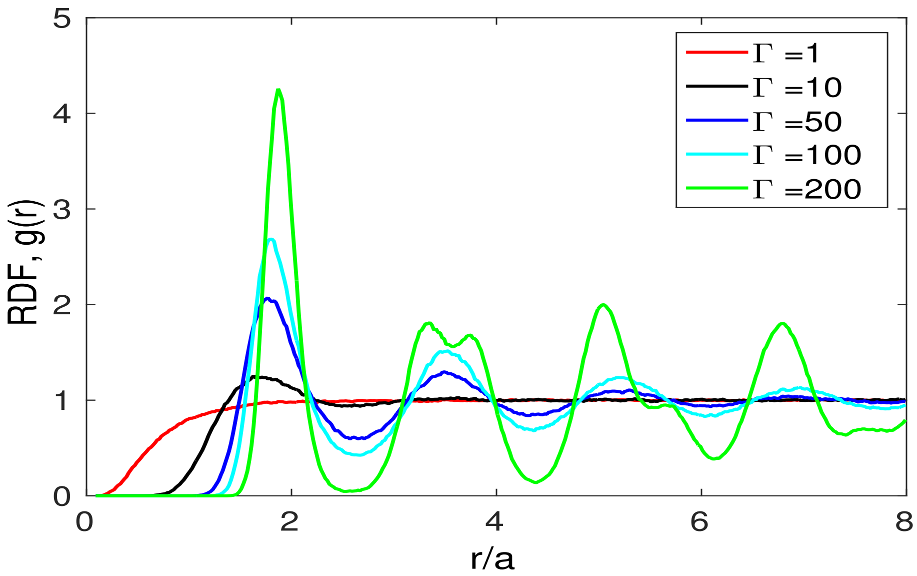

Figure 2.7: Radial distribution function (RDF) with varying Γ. Shielding parameter κ for all the Γ's are 0.5. With increasing Γ, peaks appear in g(r) which shows that now medium have not homogeneous distribution of particles. Splitting of second peak (peak lies just after sharp peak) at $\Gamma = 200$ shows that medium obtains crystalline phase and inter-particle distance is different along different directions.

$Q^2/4\pi\epsilon_0 a$. In the simulation, these quantities are calculated as follows:

$$KE = \frac{m}{2}\sum_{i=1}^{N}\vec{v_i}^2 \tag{2.6}$$

$$T_d = \frac{1}{2Nk_B}\sum_{i=1}^{N}\vec{v_i}^2 \tag{2.7}$$

$$PE = \sum_{i=1}^{N}\sum_{j(\neq i)=1}^{N} U_{ij} = \sum_{i=1}^{N}\sum_{j(\neq i)=1}^{N} \frac{Q^2}{4\pi\epsilon_0(r_i - r_j)}\exp(-\frac{r_i - r_j}{\lambda_D}) \tag{2.8}$$

$$TE = KE + PE \tag{2.9}$$

We consider the system to be in an equilibrium condition when the fluctuation in these quantities (δA/A) becomes very smaller e.g. fluctuation in total energy is

10^{-3} % (Fig. 2.11) and velocity distribution becomes Maxwellian then we consider the system is in an equilibrium condition. Fluctuation in the system also depends upon the number of particles N and varies as $1/\sqrt{N}$. Therefore, in order to reduce the statistical fluctuations in the thermodynamic quantities, we have taken sufficient number of particles in the simulations. After achieving equilibrium, we

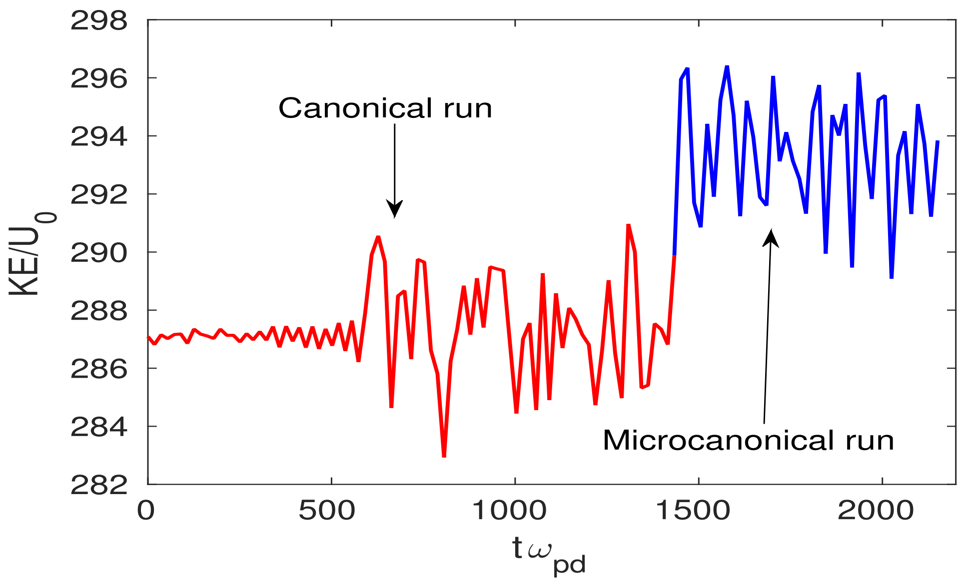

Figure 2.8: Evolution of the kinetic energy (KE) of the system during the equilibration of the 2D medium.

have applied perturbations/drive on the medium to excite the linear/nonlinear structures in the dusty plasmas. The coupling parameter of the dust medium is varied by changing the temperature (T_d) of the medium. For the low Γ values the temperature (T_d) of the system becomes higher than that for higher Γ values.

2.1.5 Diagnostic tools to extract Physics from the MD data:

In the MD simulation, the data obtained is the position and velocity of the individual entities or particles. Using "Matlab" we have extracted various physical

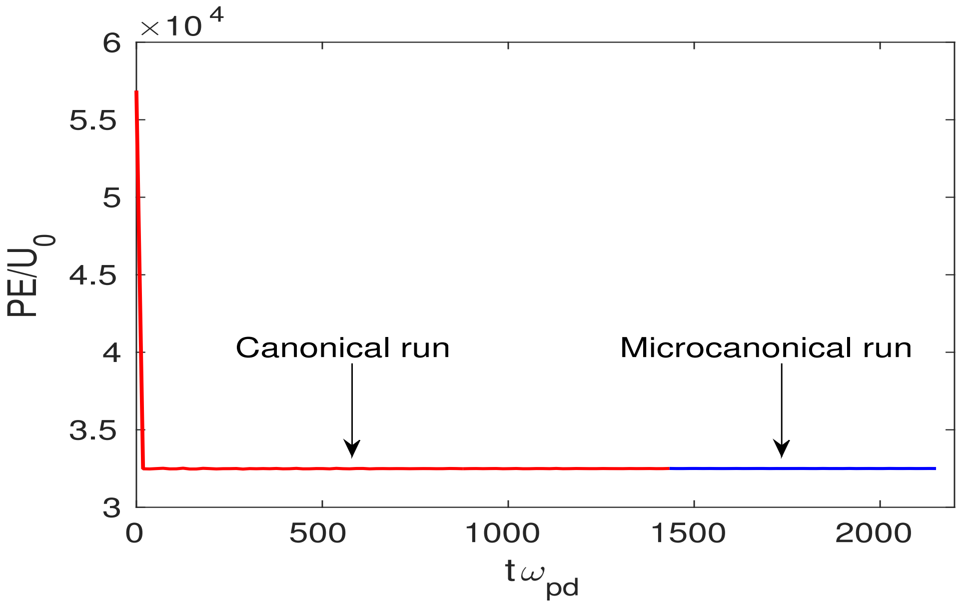

Figure 2.9: Evolution of the potential energy (PE) of the system during the equilibration of the 2D medium.

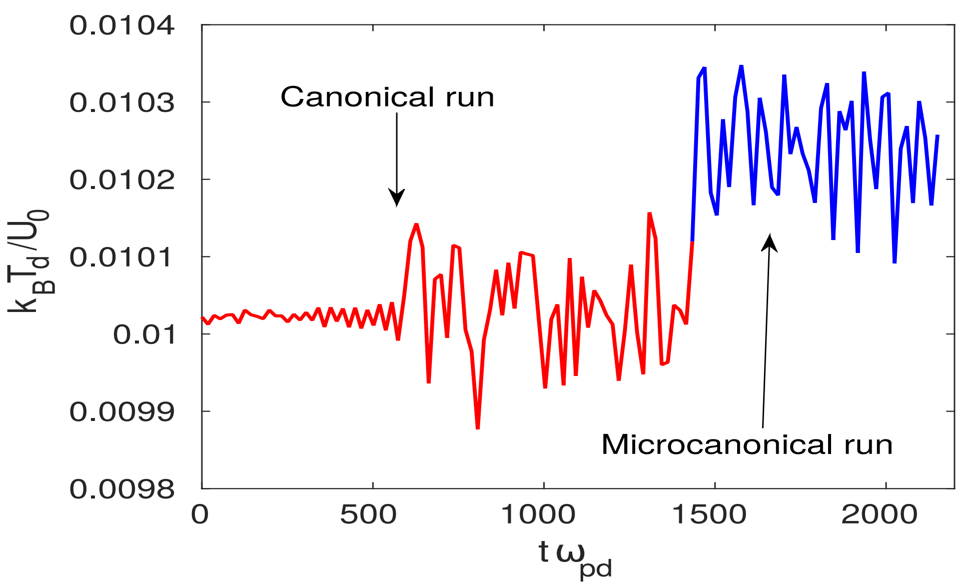

Figure 2.10: Evolution of the temperature (T_d) of the system during the equilibration of the 2D medium.

quantities of interest from these MD data to investigate physical phenomena responsible for the collective structures. In our case, we are interested in 1D and

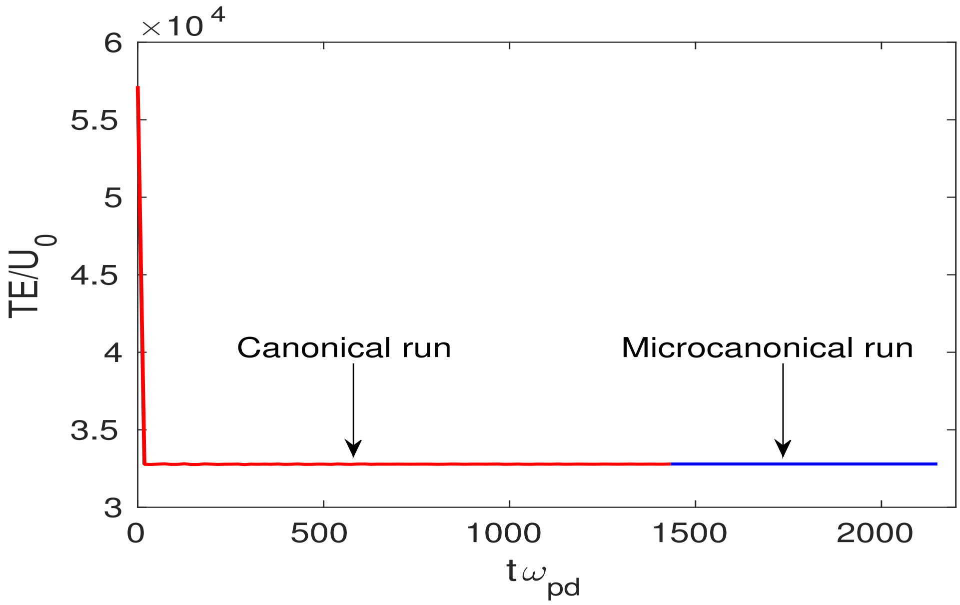

Figure 2.11: Evolution of the total energy (TE) of the system during the equilibration of the 2D medium.

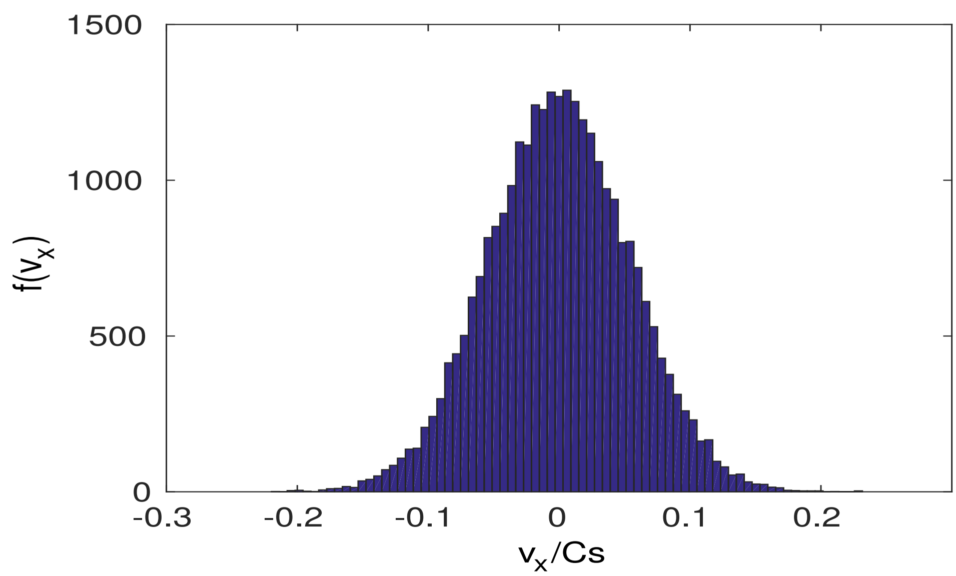

Figure 2.12: Equilibrium x-component velocity distribution $f(v_x)$ of the particles.

2D density and we evaluate it by counting the number of particles on the defined spatial grid. To find out rotation in the system, we have calculated the vorticity

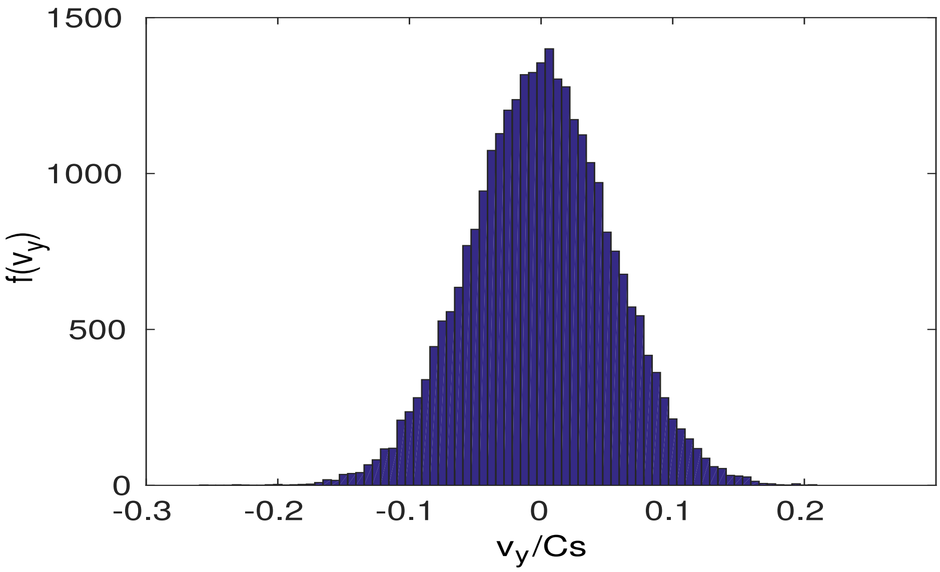

Figure 2.13: Equilibrium y-component velocity distribution $f(v_y)$ of the particles.

and enstrophy of the two-dimensional system. The enstrophy of the medium is calculated as:

$$\begin{aligned} \Omega &= \int \mid \vec{\nabla} \times \vec{v} \mid^2 dxdy, \\ &= \int \mid (\partial v_y/\partial x) - (\partial v_x/\partial y) \mid^2 dxdy \end{aligned} \tag{2.10}$$

Here, v_x and v_y are the fluidized velocities calculated at each grid point.

To find out characteristics modes in dusty plasma medium, we have plotted both dust acoustic wave and transverse shear wave dispersion relation from the naturally excited particle oscillations (phonons). These particle oscillations are excited by thermal or electrostatic fluctuations in the plasma. The dust acoustic and transverse shear spectrum are calculated from the longitudinal and transverse current-correlation, respectively as follows:

$$\lambda(k,t) = k \sum_j v_{jx} \exp(\iota k x_j) \tag{2.11}$$

$$\tau(k,t) = k \sum_j v_{jy} \exp(\iota k x_j) \tag{2.12}$$

Here $k = 2\pi n/L_x$ is the wave vector which is chosen along X-axis. Where n (= 1, 2, 3, 4......) and L_x are the integer number and simulation system length along the X-direction, respectively. We have calculated the longitudinal $L(k,\omega)$ and transverse $T(k,\omega)$ current fluctuation spectra by taking the Fourier transform of $\lambda(k,t)$ and $\tau(k,t)$, respectively as follows:

$$L(k,\omega) = \mid F(\lambda(k,t)) \mid^2 \tag{2.13}$$

$$T(k,\omega) = \mid F(\tau(k,t)) \mid^2 \tag{2.14}$$

The collective modes are the peaks in the spectra of $L(k,\omega)$ and $T(k,\omega)$ that represents the maximum energy of the wave mode. The plot of this peak value vs wave vector (k) gives the dispersion relation of the longitudinal and transverse wave mode in medium as shown in Fig. 2.14 and Fig. 2.15, respectively.

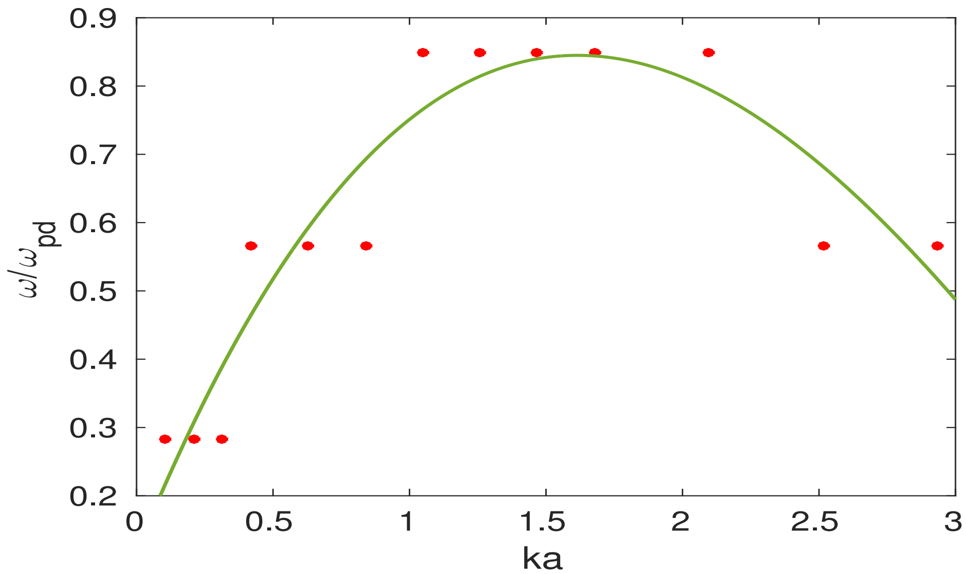

Figure 2.14: Dispersion relation for DLW in the two-dimensional dusty (Yukawa) plasmas. Γ and κ value of the medium for this plot is 100 and 0.5, respectively. At higher ka, $\partial\omega/\partial ka$ is < 0 means phase reversal occurs due to the strong coupling nature of the medium.

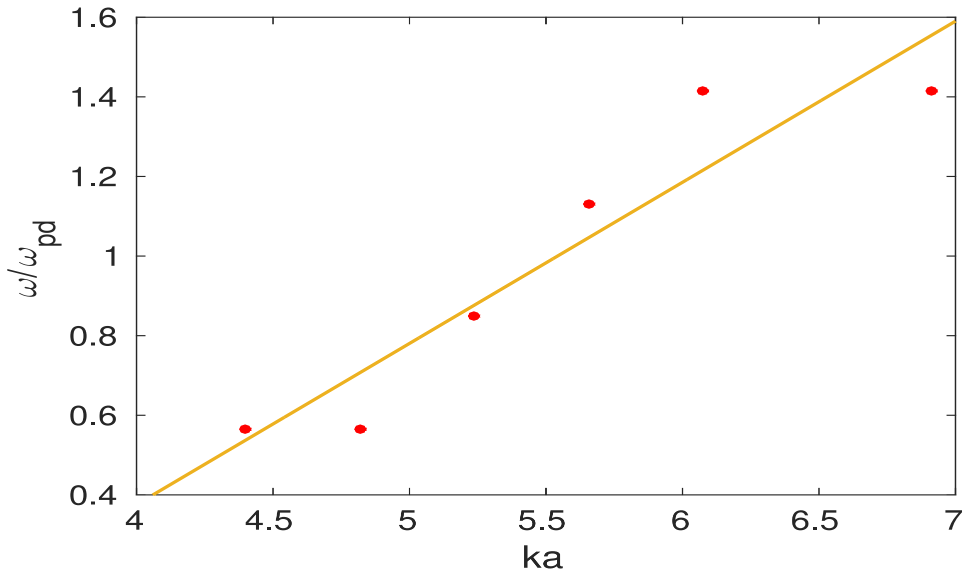

Figure 2.15: Dispersion relation for TSW in the two-dimensional dusty (Yukawa) plasmas. Γ and κ value of the medium for this plot is 100 and 0.5, respectively.

2.2 Fluid simulation of dusty plasma

In this section, we describe the 2-D fluid simulation techniques used for the study of excitation and dynamics of spiral waves in dusty plasmas. For the intermediate values of Γ ($1<\Gamma<170$), dusty plasma medium behaves like visco-elastic fluid which has often been depicted by the Generalized Hydrodynamic (GHD) model description. The equations depicting the evolution of the visco-elastic dusty plasma medium are represented by the coupled set of equations of GHD and the continuity equation for velocity and density evolution:

$$\left[1 + \tau_m(\frac{\partial}{\partial t} + \vec{v}\cdot\nabla)\right] \times \\ \left[\left(\frac{\partial \vec{v}}{\partial t} + \vec{v}\cdot\nabla\vec{v}\right) + \frac{\nabla P}{n_d} - \nabla\phi - \mathrm{F_{rot}}\right] = \eta\nabla^2\vec{v} \tag{2.15}$$

$$\frac{\partial n_d}{\partial t} + \nabla\cdot(n_d\vec{v}) = 0 \tag{2.16}$$

Where we have chosen the external force to be operative in a central circular patch with radii r_0 of the simulation box. Thus

$$\begin{aligned} \mathrm{F_{rot}} &= \mathrm{A}\sin(\omega_f t)\hat{x} + \mathrm{A}\cos(\omega_f t)\hat{y}; \quad \mathrm{r} < \mathrm{r_0} \\ \mathrm{F_{rot}} &= 0; \quad \text{otherwise} \end{aligned} \tag{2.17}$$

Where, A and $\omega_f = 2\pi/T_f$ are amplitude and angular frequency of force, respectively [99–101]. The magnitude of the force is constant but its direction rotates in time. Also, P here represents the dust pressure (for which equation of state is used) and ϕ represents the scalar potential. The scalar potential is determined by the Poisson's equation:

$$\nabla^2\phi = n_d + \mu_e \exp(\sigma_e\phi) - \mu_i \exp(-\phi) \tag{2.18}$$

with parameters $\sigma_e = T_i/T_e$, $\mu_e = n_{e0}/Z_d n_{d0}$ and $\mu_i = n_{i0}/Z_d n_{d0}$, where T_i and T_e are the ion and electron temperature, n_{i0}, n_{e0} and n_{d0} are the equilibrium density of ion, electron and dust fluid, respectively and Z_d is the negative charge on each dust particle. In unperturbed equilibrium situation dusty plasma medium satisfy the quasineutrality condition $n_{i0} = Z_d n_{d0} + n_{e0}$. Here, we have considered the Boltzmann distribution for electrons and ions on dust response time scale so as to have:

$$n_e = \mu_e \exp(\sigma_e\phi); \quad n_i = \mu_i \exp(-\phi), \tag{2.19}$$

In the GHD model Eq. (2.15) strong coupling is incorporated through the non-local visco-elastic operator. Non-local visco-elastic operator contains the memory effects and the short range order that develops in the system with increased correlation. In strong coupling regime dust fluid retain the memory of its past configurations. The memory function has often been modeled as exponentially decaying in time i.e as $\exp(-t/\tau_m)$ [49,102]. Here, τ_m is a time constant representing the relaxation time. It should be noted that Eq. (2.15) reduces to the momentum equation for a viscous compressible fluid in the limit when $\tau_m \to 0$, for which η represents the viscosity. A finite τ_m represents the time for which the fluid retains memory of its past configurations arising due to elastic behavior resulting from strong coupling features. Thus, if one is looking for a phenomena with time scales for which the condition $\tau_m \frac{d}{dt} << 1$, is satisfied the dust fluid would exhibit essentially a behavior of normal viscous fluid. However, at faster time scales for which $\tau_m \frac{d}{dt} > 1$, the dust fluid retains its memory and characteristic new elastic response can be observed. The variables v, ϕ and n_s ($s = e, i, d$) are the dust fluid velocity, potential, and number density of the charged species (electrons, ions, and dust), respectively. The normalized number densities are $\bar{n_d} = n_d/n_{d0}$, $\bar{n_i} = n_i/n_{i0}$, $\bar{n_e} = n_e/n_{e0}$. Time and length are normalized by ω_{pd}^{-1} and λ_D $(= k_B T_i/4\pi Z_d n_{d0} e^2)^{\frac{1}{2}}$. The normalized scalar potential is $\bar{\phi} = Z_d e\phi/k_B T_i$. The pressure is determined using equation of state $P = \mu_d \gamma_d n_d k_B T_d$. Here $\mu_d = \frac{1}{T_d}\frac{\partial P}{\partial n_d}|_{T_d}$ is compressibility parameter and γ_d is adiabatic index. The parameters μ_d, τ_m, and η are supposed to be empirically related to each other [16, 103, 104].

A flux-corrected transport scheme proposed by Boris et al., [105] has been used to evolve Eqs. (2.15,2.16). Since the scheme numerically solves the continuity form of equations with source and sink terms, we split Eq. (2.15) as two separate equations of the following form:

$$\left[1 + \tau_m\left(\frac{\partial}{\partial t} + \vec{v}\cdot\nabla\right)\right]\vec{\psi} = \eta\nabla^2\vec{v}$$

$$\left(\frac{\partial}{\partial t} + \vec{v}\cdot\nabla\right)\vec{v} + \alpha\frac{\nabla n_d}{n_d} - \nabla\phi - \mathrm{F}_{\mathrm{rot}} = \vec{\psi} \tag{2.20}$$

Where, $\alpha = \mu_d\gamma_d T_d/T_i Z_d$ represents the square of sound speed of the medium. The basic principle of this scheme is based on the generalization of two-step Lax-Wendroff method [106]. As the simulation system modeled in x-y plane, therefore, the above equations 2.16 and 2.20 have following form in Cartesian geometries x-y as,

$$\frac{\partial n_d}{\partial t} + n_d\frac{\partial v_x}{\partial x} + v_x\frac{\partial n_d}{\partial x} + n_d\frac{\partial v_y}{\partial y} + v_y\frac{\partial n_d}{\partial y} = 0 \tag{2.21}$$

$$\frac{\partial \psi_x}{\partial t} + v_{dx}\frac{\partial \psi_x}{\partial x} + v_{dy}\frac{\partial \psi_x}{\partial y} = \frac{\eta}{\tau_m}\frac{\partial^2 v_{dx}}{\partial x^2} + \frac{\eta}{\tau_m}\frac{\partial^2 v_{dx}}{\partial y^2} - \frac{\psi_x}{\tau_m} \tag{2.22}$$

$$\frac{\partial \psi_y}{\partial t} + v_{dy}\frac{\partial \psi_y}{\partial y} + v_{dx}\frac{\partial \psi_y}{\partial x} = \frac{\eta}{\tau_m}\frac{\partial^2 v_{dy}}{\partial x^2} + \frac{\eta}{\tau_m}\frac{\partial^2 v_{dx}}{\partial y^2} - \frac{\psi_y}{\tau_m} \tag{2.23}$$

$$\frac{\partial v_{dx}}{\partial t} + v_{dx}\frac{\partial v_{dx}}{\partial x} + v_{dy}\frac{\partial v_{dx}}{\partial y} = -\frac{\alpha}{n_d}\frac{\partial n_d}{\partial x} + \frac{\partial \phi}{\partial x} + \psi_x + F_{rot}\hat{x} \tag{2.24}$$

$$\frac{\partial v_y}{\partial t} + v_y\frac{\partial v_y}{\partial y} + v_x\frac{\partial v_y}{\partial x} = -\frac{\alpha}{n_d}\frac{\partial n_d}{\partial y} + \frac{\partial \phi}{\partial y} + \psi_y + F_{rot}\hat{y} \tag{2.25}$$

The right-hand sides of the above equations are separated into two parts, the x-direction, and the y-direction terms. Putting equations in this fashion separate the x-derivatives and the y-derivatives in the divergence and gradient terms into parts that is used sequentially by a general one-dimensional continuity equation solver in the LCPFCT package of subroutines. LCPFCT is an open source fluid code base on flux corrected transport scheme [105]. This subroutine solves the 2-D fluid equations by splitting the time steps in the x and y directions. Keeping this methodology in mind, we first solve the integration along x-direction and then, subsequently, along y-direction in the same time interval t to t+Δt. The numerical technique of integration using time-step splitting is discussed in detail in reference [105]. This technique can also be used for other geometries viz. three-dimensional, spherical, and cylindrical. We have chosen the simulation time step small enough to avoid the significant change in the cell-averaged values during the time steps t to t+Δt. This approach is second-order accurate as long as the time step is small and changed slowly, but there is still a bias that gets built is dependent on which direction, (x or y), is integrated first. For removal of this bias, the results from two calculations for each time step can be averaged. The averaged value is computationally expensive but has better value.

In the simulations, we have employed periodic boundary conditions (PBC) along x and y directions. The spatial resolution (grid size) Δx or Δy has been chosen in such a way that the Debye length (λ_D) is adequately resolved in both the directions. The temporal resolution i.e. time step (Δt) is then calculated from Courant-Friedrichs-Lewy (CFL) condition $\Delta \mathrm{t} = C_n(\Delta)/u_{max}$, where u_{max} and C_n are the maximum fluid velocity and CFL number [105]. Here Δ is the minimum value between Δx and Δy. We have taken $C_n = 0.2$ in the simulations. In our study, the maximum fluid velocity u_{max} depends upon the amplitude of the forcing. Therefore, in our simulations, the value of Δt has been varied according to change in the u_{max} for a good temporal resolution and stability. The numerical observations have also repeated by changing the grid size Δx or Δy, and C_n. The results of the simulation have been recorded at each time step in terms of n_d, ψ_x, ψ_y, v_x, v_y, and ϕ.

To solve non-linear Poisson's equation 2.18, we have used the Newton-Raphson method. First of all, we have decomposed Poisson's equation (two-dimensional) into the following form using finite difference scheme:

$$\begin{aligned} &C_0\phi_{i+1,j} + C_0\phi_{i-1,j} + C_1\phi_{i,j+1} + C_1\phi_{i,j-1} - C_2\phi_{i,j} \\ &= nd_{i,j} + \mu_e \exp(\sigma_e\phi_{i,j}) - \mu_i \exp(-\phi_{i,j}) \end{aligned} \tag{2.26}$$

Here, $C_0 = 1/(\Delta x)^2$, $C_1 = 1/(\Delta y)^2$, and $C_2 = 2[(\Delta x)^2 + (\Delta y)^2]/[(\Delta x)^2(\Delta y)^2]$ are the constants. Index (i, j) in the Eq. 2.26 are running from 1 to N (number of grids) along X and Y directions, respectively. Periodic boundary conditions are employed in the simulations, therefore $\phi_{1,1} = \phi_{N+1,1}$; $\phi_{1,1} = \phi_{1,N+1}$; $\phi_{1,N+1} = \phi_{N+1,N+1}$; and $\phi_{N+1,1} = \phi_{N+1,N+1}$.

The Eqs. 2.26 are like the system of equations

$$A\phi_{i,j} = F_0 + F_1(\phi_{i,j}) + F_2(\phi_{i,j}) \tag{2.27}$$

The first term on the right-hand side is a constant vector, second and third terms are the nonlinear terms. We can also write above equation as follows:

$$G(\phi_{i,j}) = A\phi_{i,j} - F = 0 \tag{2.28}$$

Here vector $F = F_0 + F_1(\phi_{i,j}) + F_2(\phi_{i,j})$. From here, we can get the new function by Newton-Raphson root finding method as:

$$\phi_{i,j}^{new} = \phi_{i,j}^{old} - \frac{G(\phi_{i,j}^{old})}{G'(\phi_{i,j}^{old})} \tag{2.29}$$

Where $G'(\phi_{i,j}^{old}) = \frac{\partial G(\phi_{i,j})}{\partial \phi_{i,j}}$ is the Jacobian matrix. Further, we have applied two step numerical technique to obtain the second term of the above equation as follows:

$$G'\psi = G \tag{2.30}$$

The advantage of two step numerical technique is that it avoids the inverse calculation of matrix $G'(\phi_{i,j}^{old})$. From above equation, we have calculated ψ using the linear solver. The final solution of Eq. 2.29 is obtained as

$$\phi_{i,j}^{new} = \phi_{i,j}^{old} - \psi \tag{2.31}$$

The iterations of the linear solution ψ is being continue until it obtains a given predefined tolerance i.e. $||\psi|| <$ tolerance value.

3

Korteweg-de Vries (KdV) solitons in molecular dynamics simulations of a dusty plasma medium

*The objective of this chapter is to study the KdV solitons in the strongly coupled dusty plasma using MD simulations. We have applied an experiment like electric field perturbations [45, 47, 48] on the dust particles to excite solitons in the simulation *. The collective response of the dust particles to such an applied electric field impulse gives an excitation of a perturbed density pulse (compression) propagating in one direction along with a train of negative perturbed rarefactive density oscillations in the opposite direction. The head-on and overtaking collision and associated phase shift have also been studied. We have also shown that by increasing the strength of electric field impulse, the amplitude of the solitonic structure*

Sandeep Kumar, Sanat Kumar Tiwari, and Amita Das, Physics of Plasmas* ***24**, 033711 (2017)* *increases and above a fixed strength, it splits in the form of multiple solitons. Further, we have studied the effect of strong coupling of the medium and neutral drag on the solitonic structures.*

3.1 Introduction

Solitons are robust and stable localized nonlinear structures observed in variety of natural and laboratory scenario including optical fibers [88, 89], semiconductors [90], oceanography [91], plasmas [92–94, 107], laser plasma interaction [108–110] etc. [111–113]. Mathematically, solitons are solution of non-linear equations such as Korteweg-de Vries (KdV) equation, Klein-Gordan equation and Schrodinger equation etc. [57, 114]. In plasmas both electrostatic [43, 51, 71, 115–117] and electromagnetic solitary waves [110, 118] are observed. The robust and stable existence of solitons can be utilized for communication as well as transport of energy [119]. Observing solitons in ordinary electron-ion plasmas in general would require sophisticated diagnostics. However, experimental observations of solitonic structures in the context of dusty plasma can be carried out with relative ease. This is because the temporal and spatial length scale of excitations typically lie within the perceptible grasp of human senses [120].

The dusty plasma contains highly charged (mostly negative) and heavy (10^{13} – 10^{14} times heavier than the ions) dust grains along with electron and ion species. The inclusion of heavy dust species makes such a plasma exhibits a rich class of collective phenomena occurring at longer time scales. There have been several experimental studies reported excitation of dust acoustic soliton [37, 45, 47, 48], their collisional interaction and the associated phase shift [48, 121]. More recently the excitation of multiple solitons have also been reported by Boruah et al. [122].

In this work we show that all these aspects can be very well depicted by treating the dust species in the plasma as particles interacting via Yukawa potential which mimics the screening due to the electron and ions species and has the following form [123]:

$$U(r) = \frac{Q^2}{4\pi\epsilon_0 r}\exp(-\frac{r}{\lambda_D}) \tag{3.1}$$

Here $Q = -Z_d e$ is the charge on a typical dust particle, r is the separation between two dust particles, λ_D is the Debye length of background plasma. Typical one component plasma (OCP) is characterized by two dimensionless parameters $\Gamma = \frac{Q^2}{4\pi\epsilon_0 a k_b T_d}$ and $\kappa = \frac{a}{\lambda_D}$. Here T_d and a are the dust temperature and the Wigner-Seitz radius respectively.

The present simulation studies employ the electric field perturbations of the experimental situations [47, 48] to excite the solitonic structures. We study the effect of the amplitude of the electric field and the width corresponding to the region where it is applied on the characteristics of the excited coherent structure. It has been observed that increasing the amplitude of the electric field paves the way for the formation of multiple solitons in the medium as observed recently by Boruah et al. [122]. It should be noted that by considering the response of the dust particles to the imposed electric field one makes a specific choice of the sign of the dust charge. The response of the dust species (with specified sign of the charge) to the applied electric field breaks the left and right symmetry, as a result of which one observes a positive train of solitons in one direction, whereas in the other direction rarefactive density oscillations are observed as per the KdV prescription. Our results are also in line with the experimental observations of KdV solitons by Sheridan et al. [45] where authors reported a stable solitary pulse in leading direction and a dispersive wave moving in the backward direction. This is in contrast to an earlier simulation study by Tiwari et al. [4], where arbitrary Gaussian density perturbation splits in two solitons moving in opposite directions. This difference in observation can be understood as in the case of Tiwari et al. [4] there was nothing in the excitation to break the left and right symmetry.

This chapter is organized as follows. Section 3.2 provides details of simulation. Section 3.3 explains the excitation of solitonic structures and reports on various features which confirm them as KdV solitons. In section 3.4, we discuss the collisional interaction amidst solitons. Section 3.5 shows the details of the excitation of multi-solitons, effect of the coupling parameter and neutral drag. Section 3.6 contains the summary.

3.2 Description of MD simulations

Molecular Dynamics (MD) simulations have been carried out for a two-dimensional system of point dust particles interacting with each other through the Yukawa form of interaction potential. A two dimensional box (with periodic boundaries) is created with $L_x = 20a$ and $L_y = 1000a$ along X and Y directions respectively. Here $a = (\pi n_{2D})^{-\frac{1}{2}}$ and n_{2D} is the dust density [124] in two dimensions. Parameters [99] chosen for the present set of simulations are as follows: the dust grain mass $m = 6.99 \times 10^{-13}$ Kg, charge on dust $Q = 11940e$ (e is an electronic charge) and $a = 0.418 \times 10^{-3}$ m. Shielding parameter $\kappa = \frac{a}{\lambda_D}$ is chosen to be 0.5 for all simulations leading to plasma Debye length to be $\lambda_D = 8.36 \times 10^{-4}$ m. For these parameters, $E_0 = \frac{Q}{4\pi\epsilon_0 a^2} = 98.39\ \frac{V}{m}$ and equilibrium density $(n_{d0}) = 1.821 \times 10^6$ m^{-2}. The cut-off for particle interaction potential in the simulation here has been chosen to be at $20a$. Characteristic dust plasma frequency of the particles $\omega_{pd} = \sqrt{\frac{Q^2}{2\pi\epsilon_0 m a^3}} \simeq 35.84\ s^{-1}$, which corresponds to the dust plasma period to be

0.175 s. We have chosen simulation time step as $0.0072\omega_{pd}^{-1}$ so that phenomena occurring at dust plasma frequency can be easily resolved. In this chapter, distance, density, time and electric field are normalized by a, n_{d0}, ω_{pd}^{-1} and E_0 respectively.

The first task is to prepare an equilibrated system. For this, the initial configuration of particle positions is chosen to be random and velocities were chosen to follow Gaussian distribution corresponding to the temperature T_d. Furthermore, we achieved equilibrium temperature by generating positions and velocities from canonical (NVT) ensemble using Nose-Hoover [125, 126] thermostat. To test the equilibration of system, we checked temperature fluctuation and velocity distribution at different leading times. After about an NVT run for $2867\omega_{pd}^{-1}$ time, we disconnected the canonical thermostat and ran a simulation for microcanonical (NVE) ensemble for about $1433\omega_{pd}^{-1}$ time. After NVE run temperature becomes steady and equal to T_d. Now system is in equilibrium and ready for further explorations. For most of our studies we have chosen the value of $\Gamma = 100$ and $\kappa = 0.5$. We have, however, also studied cases with different choice of Γ.

3.3 Excitation of solitons and dispersive waves

We have applied an electric field perturbation along $-\hat{y}$ direction in a narrow rectangular region (to mimic a wire) as shown in Fig. 3.1, mathematically $-E\delta(t-t_0)\hat{y}$ at time t_0, where δ is Dirac's delta function. The pulse duration of the electric field perturbation is $0.0716\ \omega_{pd}^{-1}$. This electric field results in an electrostatic force $F_E = QE\hat{y}$ on the dust particles. The direction of force is along $+\hat{y}$ as we choose the dust charge to be $-Q$ negative. The evolution shows an excitation of a solitary wave propagating in $+\hat{y}$ direction and a damped dispersive wave in the $-\hat{y}$ direction. The time evolution of density (n_d) is shown in Fig. 3.2. These observations are consistent with the property of the solitons permitted by the KdV equation which is given by the equation:

$$\frac{\partial n_d}{\partial t} + C n_d \frac{\partial n_d}{\partial y} + D \frac{\partial^3 n_d}{\partial^3 y} = 0 \tag{3.2}$$

Where C and D depend upon density, temperature and mass of particles in the medium [47, 48]. Second and third term in equation (2) give the nonlinearity and dispersion in the medium respectively. H. Segur [127] and P. G. Drazin [114] have shown that in addition to soliton solutions which is obtained from the balance of nonlinearity and dispersion, negative amplitude dispersive waves solutions propagating in opposite direction with a slower velocity are also permitted. The dispersive waves is the solution of initial-value problem for linearised KdV equation:

$$\frac{\partial n_d}{\partial t} + D \frac{\partial^3 n_d}{\partial^3 y} = 0$$

The amplitude of such dispersive wave have been shown to decays with time as $A_0 \times (3t)^{-\frac{1}{3}}$. Where A_0 is the initial amplitude. Comparison of decaying amplitude of the dispersive wave observed numerically has been provided with the analytic expressions of $A_0 \times (3t)^{-\frac{1}{3}}$ in Fig. 3.3. It can be seen that there is a close agreement between the two plots.

The above observations of propagating solitons in one direction and dispersive wave in other are in contrast to earlier studies carried out by Tiwari et al. [4], where two oppositely propagating solitonic structures were observed when an arbitrary initial Gaussian density perturbation was evolved. This has been reproduced here by us in Fig. 3.4. In the case of an initial Gaussian perturbation in density, there is no way to distinguish between the forward and reverse directions. On the other hand when one considers the response of dust particles with specified charge to an applied electric field the left and right directional symmetry gets broken up. Another well known property of KdV soliton is that the parameter AL^2 is

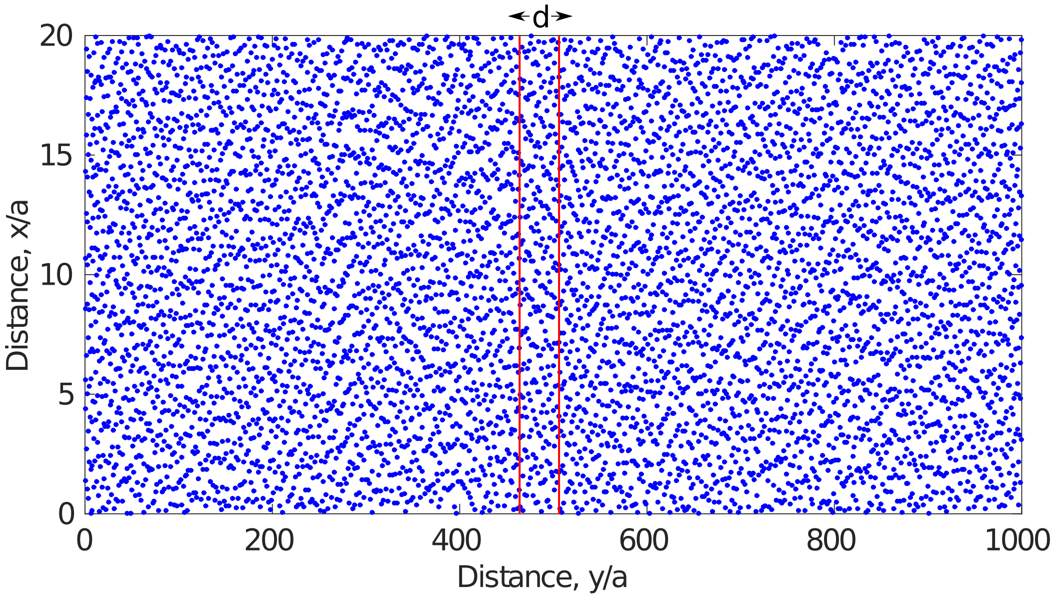

Figure 3.1: Schematic representation of the two-dimensional simulation system used for the KdV soliton study. Here, width "d" represents the region on which electric field perturbation is applied for the KdV excitation.

constant [47,128]. Where A is amplitude and L is full-width at half the maximum amplitude (FWHM) of soliton structure. In Table - 3.1 we list some parameters associated with the numerically observed solitonic structures. This include the normalized Electric field amplitude, the Mach number, the normalized value of the soliton width $\frac{L}{a}$, the normalized density amplitude $A = \frac{\delta n}{n_{d0}}$ and AL^2 in various columns. The Mach number is the ratio of soliton velocity to the dust acoustic speed, i.e., $M = \frac{v}{C_s}$. The dust acoustic wave speed (C_s) of medium at $\Gamma = 100$ and $\kappa = 0.5$ is equal to 1.94×10^{-2} $\frac{m}{s}$. The soliton velocity is calculated from the slope of the plot of the soliton trajectory with respect to time. From table - 3.1, we find that with increasing amplitude (A) the width (L) of solitary wave

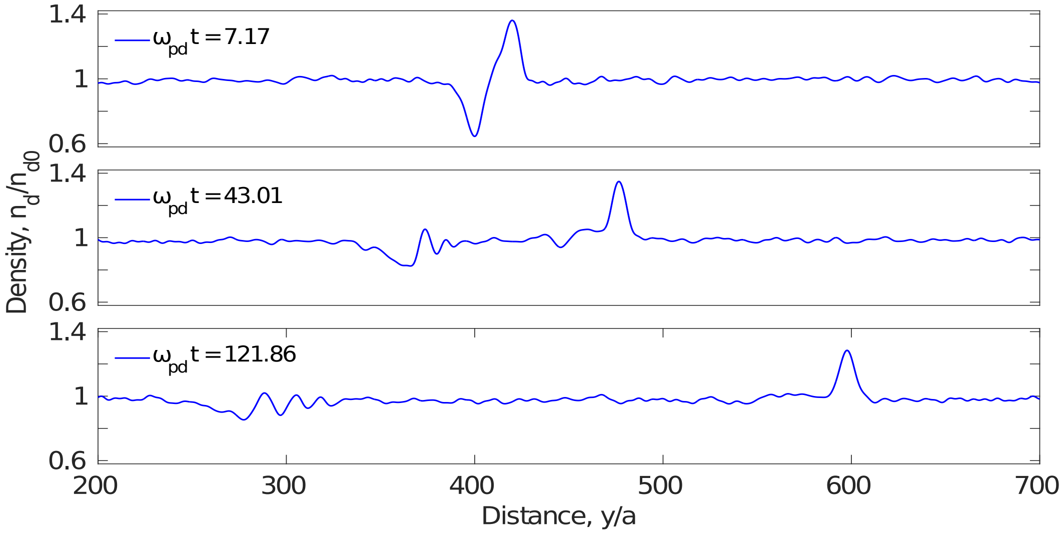

Figure 3.2: Time evolution of a solitary pulse (moving $+\hat{y}$ direction) and a dispersive mode (moving $-\hat{y}$ direction) excited through the electric field perturbation ($E = 25.40$) in the medium.

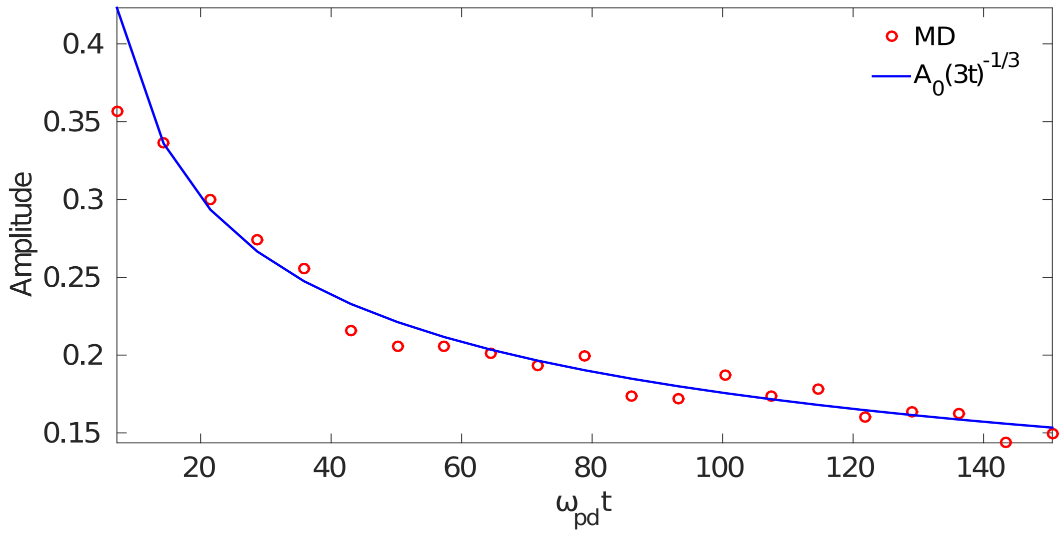

Figure 3.3: Comparison of theoretical and simulation results of amplitude ($\frac{\delta n}{n_{d0}}$) damping for rarefactive dispersive wave.

decreases as expected. From the table, it is also clear that soliton parameter AL^2 remains fairly constant for solitons with different Mach numbers (M). This can be understood from the fact that even though the percentage variation in the data between the minimum and maximum value of L^2 is about 27%, in A about 21%;

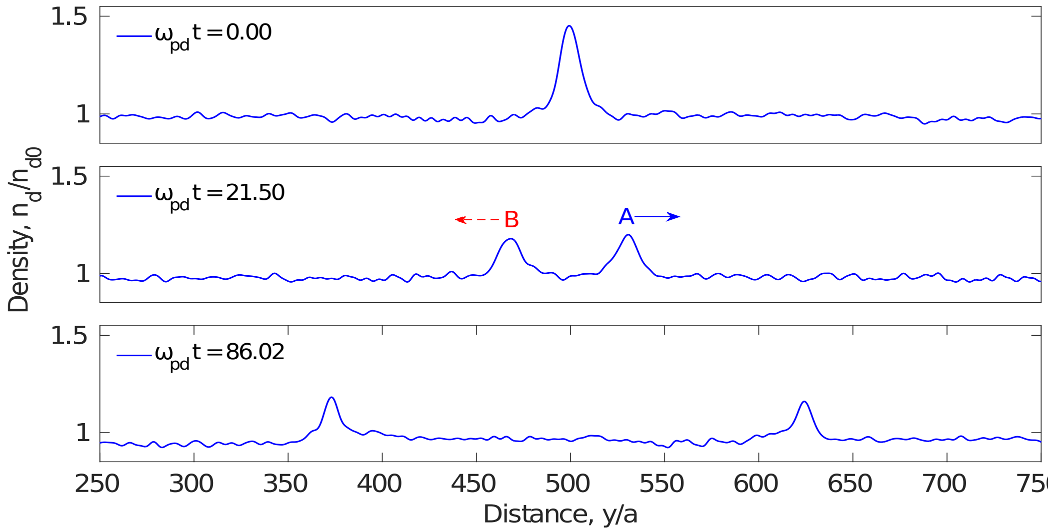

Figure 3.4: Time evolution of a Gaussian form of density perturbation in the medium. The Gaussian pulse splits in two A ($+\hat{y}$) and B ($-\hat{y}$) oppositely propagating symmetric pulses due to the left and right symmetry in the medium [4].

Table 3.1: Soliton Parameter with varying amplitude of perturbation (E). Parameters are taken at the time $55.91\omega_{pd}^{-1}$.

$\frac{E}{E_0}$	M	$\frac{L}{a}$	$A\ (\frac{\delta n}{n_{d0}})$	AL^2
20.32	1.15	9.5	0.307	27.70
22.86	1.16	9.0	0.324	26.24
25.40	1.18	8.5	0.346	24.99
28.96	1.20	8.5	0.365	26.37
30.49	1.22	8.1	0.393	25.78

the variation in AL^2 is limited to 7% only. This can be attributed to be well within the inaccuracy in estimation.

3.4 Interaction between solitons

We also report on the collisional interaction characteristics of the numerically evolved structures which show clear solitonic behaviour.

3.4.1 Head-on collision of same amplitude solitons:

By applying suitable electric field perturbations at different locations we create two counter propagating solitons of same amplitude. Time evolution of these structures are shown in Fig. 3.5. The structures collide and cross each other with no change in their shape and size. We also observe that during the time they overlap while colliding the resultant amplitude (0.589) of solitary wave is less than the sum of the individual soliton amplitudes ($0.318 + 0.318 = 0.636$). The trajectories of the two solitons with initial amplitudes of perturbation $E = 25.40$ and $E_0 = 12.70$ are shown in Fig. 3.6 and Fig. 3.7 respectively. Since the solitons are of equal amplitude the structures remain static for some time when they overlap. Time difference (δt) between the two points (intersection of incoming and outgoing trajectories) is termed as phase shift and it is about $4.3\omega_{pd}^{-1}$ and $8.6\omega_{pd}^{-1}$ for the two cases as shown in Fig. 3.6 and Fig. 3.7 respectively. The phase shift clearly decreases with increase in the amplitude of the solitons. This particular result is in contrast to the experimental findings of Sharma et al. [48]. The reason for this difference is not clear at the moment. However, intuitively one would expect the collision between higher amplitude solitons to have smaller phase shifts as they move with greater speeds. Conclusion similar to ours on phase shift has been theoretically inferred in some previous studies [128, 129].

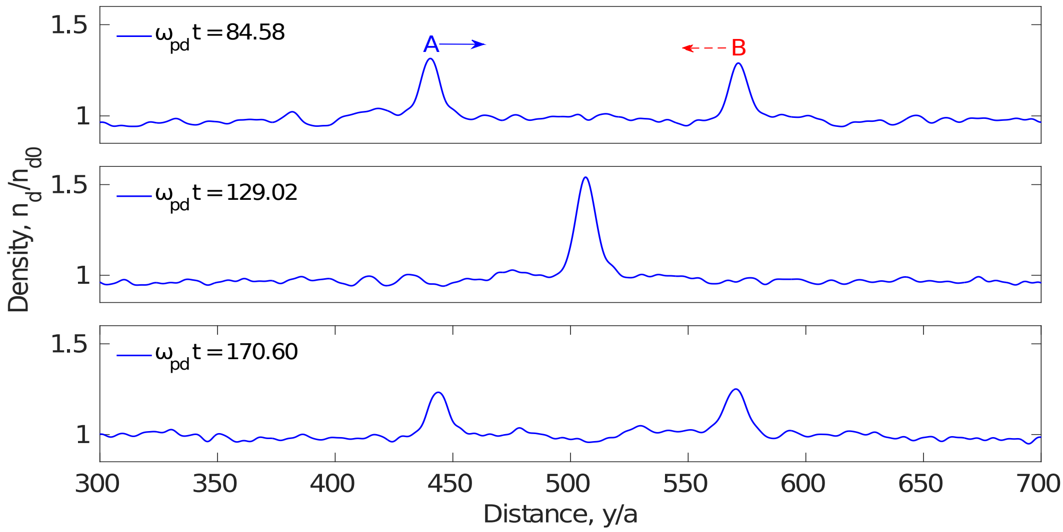

Figure 3.5: Collision of two same amplitude counter propagating solitons. Oppositely moving solitons (A and B) were excited with same amplitude electric field ($E = 25.40$) in $+\hat{y}$ and $-\hat{y}$ directions respectively.

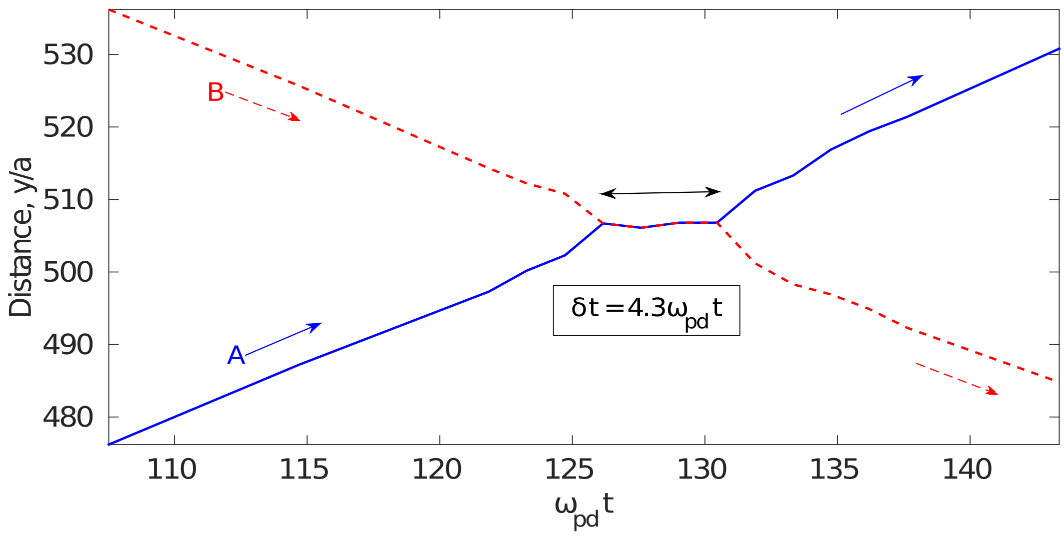

Figure 3.6: Phase shift during same amplitude soliton collision. An initial electric field to excite them is $E = 25.40$.

3.4.2 Head-on collision of different amplitude solitons:

We have also considered the case of head on collision amidst two counter propagating solitonic structures with unequal amplitude. Again the two structures emerge

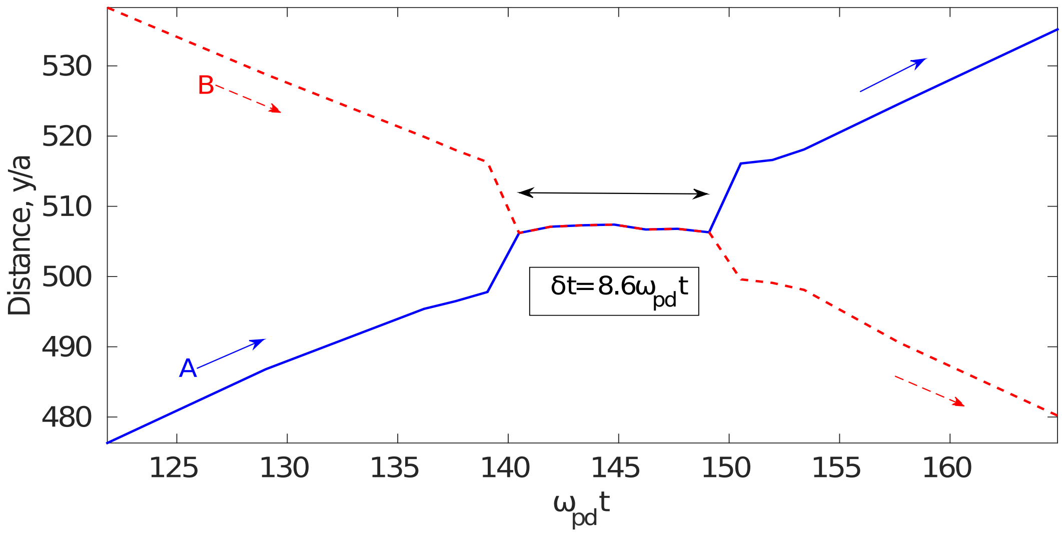

Figure 3.7: Phase shift during same amplitude soliton collision. An initial electric field to excite them is $E = 12.70$.

unchanged after suffering collision as shown in Fig. 3.8. From the plot of Fig. 3.9, which shows the trajectories of the two solitons, it can be observed that after the collision the low amplitude soliton in this case gets dragged in the direction opposite to its own propagation, by the high amplitude structure for a while. This is in confirmation with the analytical results obtained by Surabhi et al. [44]. This time phase shift is about $5.7\omega_{pd}^{-1}$ which is shown in Fig. 3.9. Thereafter the two structures get separated and move in their respective directions. In this case too the resultant amplitude (0.436) of the structure during collision is less than the sum of the individual amplitudes ($0.308 + 0.185 = 0.493$) of the solitons.

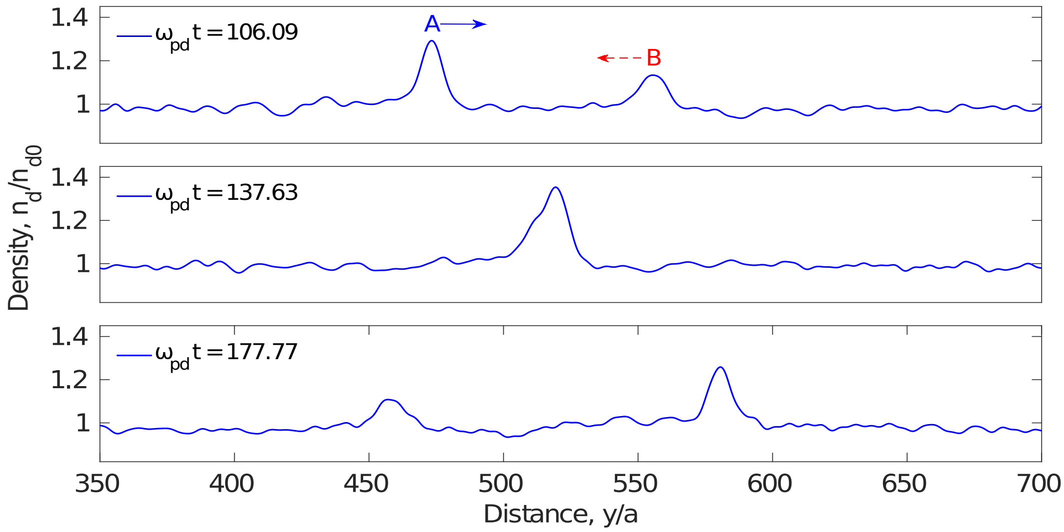

Figure 3.8: Head-on collision of different amplitude solitons A ($E = 25.40$) and B ($E = 15.24$) moving in opposite direction.

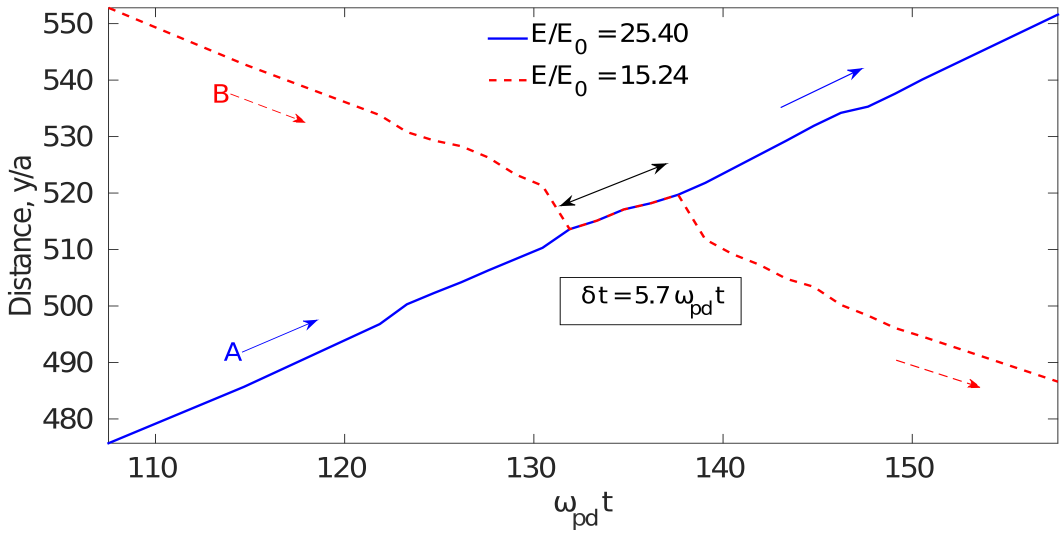

Figure 3.9: Phase shift for head-on collision of different amplitude solitons A ($E = 25.40$) and B ($E = 15.24$).

3.4.3 Overtaking collision amidst different amplitude solitons:

In this case we excite two solitons propagating in the same directions. The smaller amplitude soliton with slower phase velocity is placed ahead of the high amplitude soliton which is moving faster. After some time the faster soliton catches up with the slower soliton ahead of it and collides with it. This has been shown in Fig. 3.10. We have found that phase shift in the overtaking collision is larger than head-on collision.

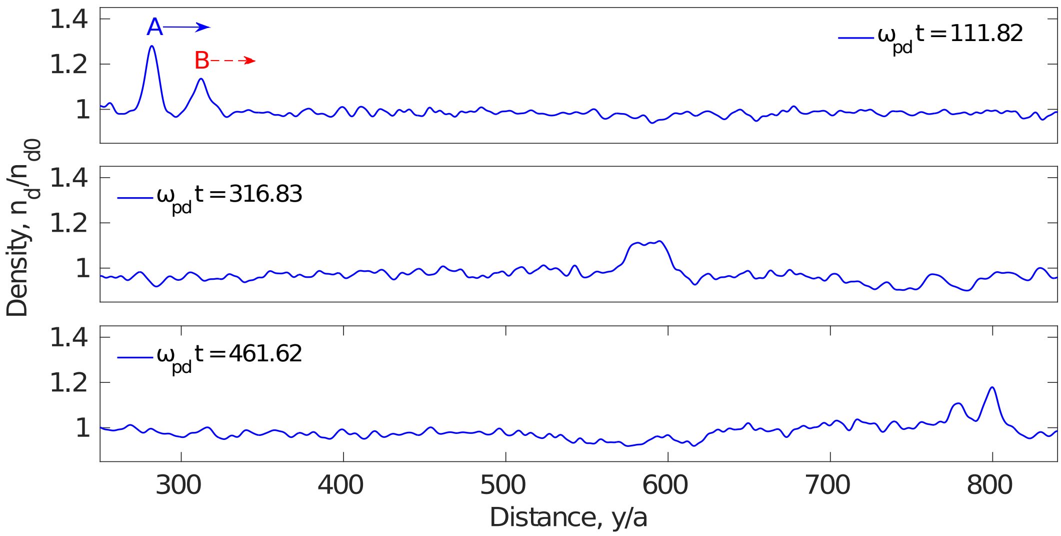

Figure 3.10: Density evolution for overtaking collision of A ($E = 25.40$) and B ($E = 15.24$) amplitude solitons.

3.5 Excitation of Multi-solitons, effect of the coupling parameter and neutral drag:

When we increase either the amplitude (E) or the spatial width (d) of the electric field impulse, the solitary pulse excited in the forward $+\hat{y}$ direction breaks up into more than one solitons. In Fig. 3.11 it is shown that for a fixed value of $d = 10$, as the amplitude of electric field perturbation is increased, multiple solitons appear. Similarly when the electric field amplitude is fixed and the width d is increased, multiple solitons get formed as shown in Fig. 3.12. Each of these multiple structures propagate along the same direction. They arrange themselves in the order of decreasing amplitude A (increasing width L). Interestingly the crests of each of the structures lie close to a straight line. These multiple solitons are termed as multi-solitons. In one of the recent experiments done by Boruah et al. [122] of dusty plasmas the multi-soliton formation has been clearly demonstrated by increasing the electric field impulse. The MD simulations with Yukawa interaction thus seems to be a good depiction of the properties of the dusty plasma medium. It should be noted that the formation of multiple solitons had been theoretically predicted by Zabusky et al. in the context of electron-ion plasma [92].

We have also investigated the role of coupling parameter on the formation of these soliton structures. We observe that with increasing coupling parameter Γ of the dust medium, amplitude (magnitude) of each soliton increases and consequently the width decreases as shown in Fig. 3.13. Further, we have also investigated the role of neutral drag ν on the formation of these soliton structures. We observe that with increasing neutral drag ν on the dust particles, amplitude (magnitude) of each soliton decreases and consequently the width increases as shown in Fig.

3.14.

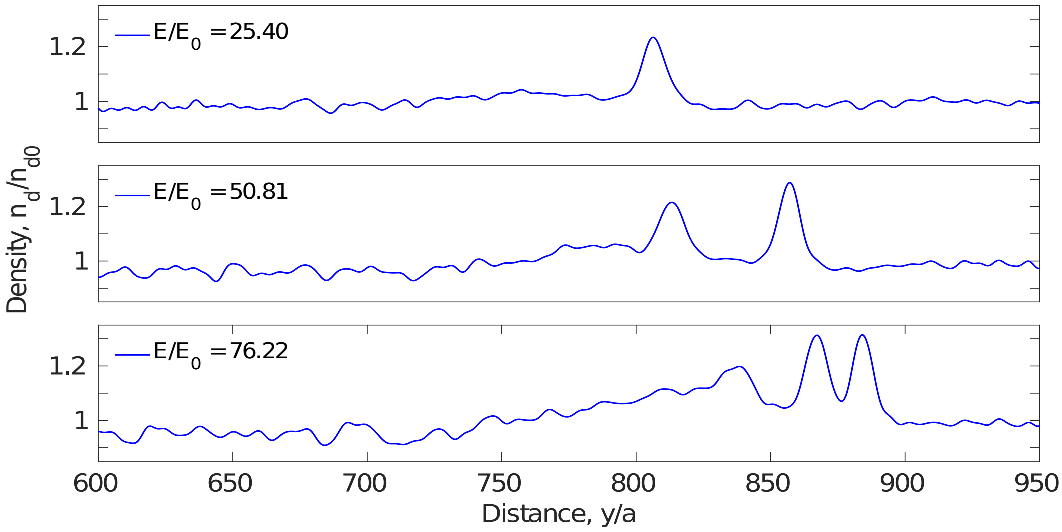

Figure 3.11: Formation of multi-soliton due to the increase in electric field strength (E). Density of medium for all E is taken at time $263.78\omega_{pd}^{-1}$. In all three cases perturbation width (d) is 10.

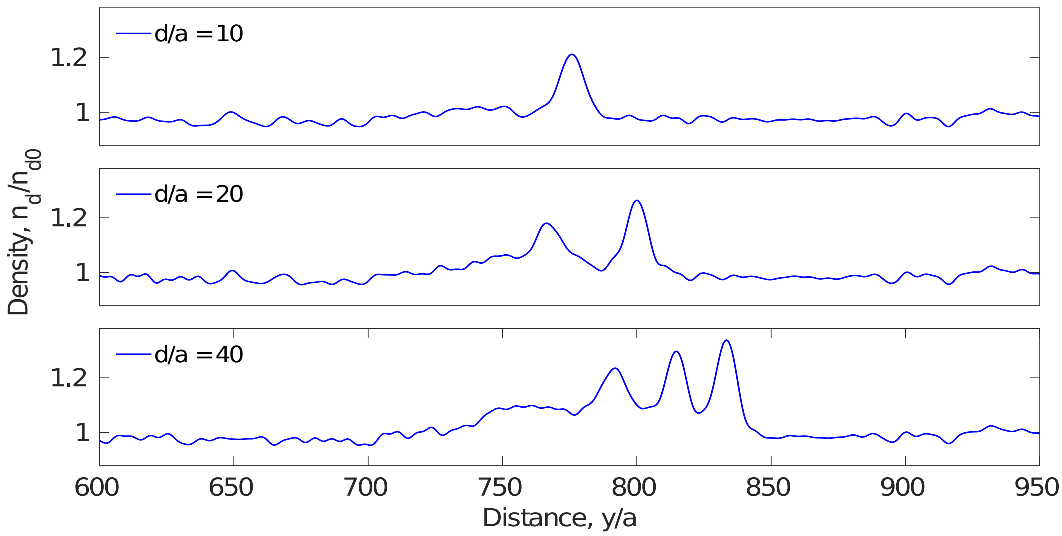

Figure 3.12: Formation of multi-soliton due to the increase in perturbation width (d). Density of medium for all d is taken at time $242.28\omega_{pd}^{-1}$. In all three cases perturbation strength of electric field (E) is 25.40.

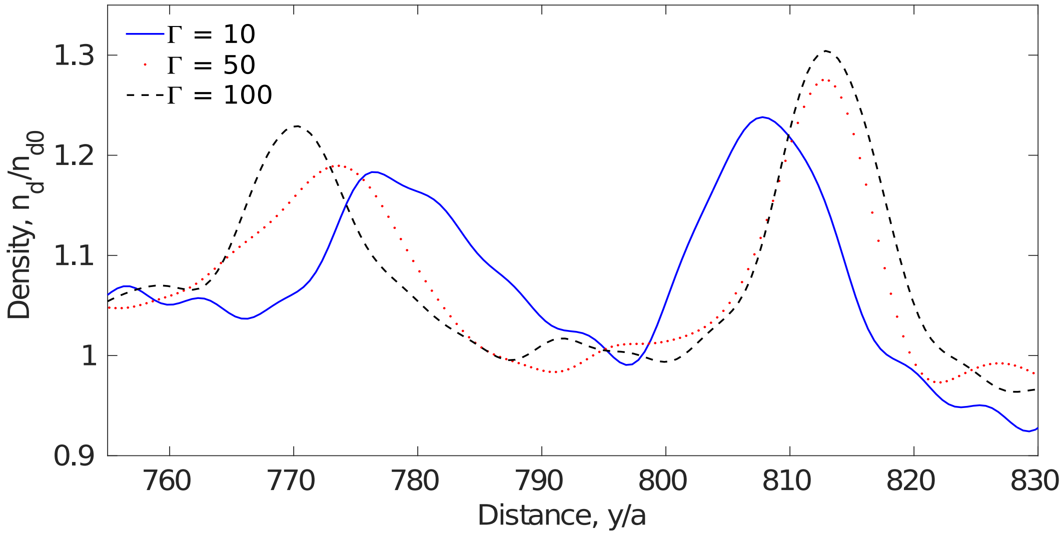

Figure 3.13: Density of medium for three Γ = 10, 50 and 100 is taken at time $235.11\omega_{pd}^{-1}$. For all three cases magnitude and width of electric field perturbation is 50.81 and 10 respectively.

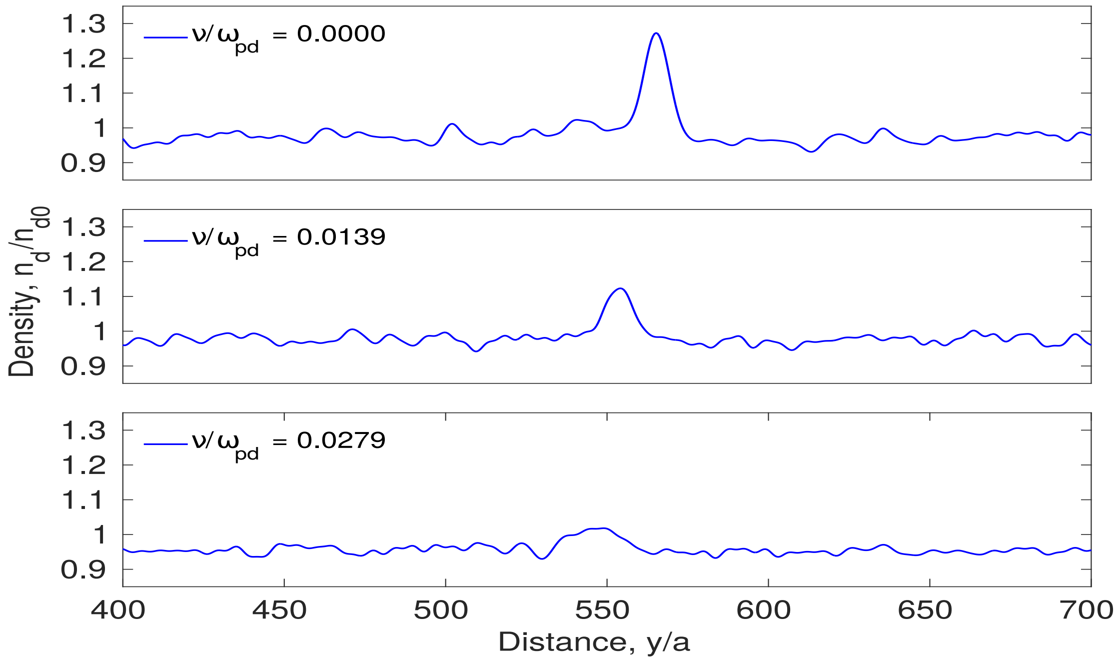

Figure 3.14: Density of medium for three neutral drag parameter ν/ω_{pd} = 0.00, 0.0139 and 0.0279 is taken at time $101.78\omega_{pd}^{-1}$. For all three cases magnitude and width of electric field perturbation is 25.40 and 10 respectively.

3.6 Summary

We have carried out the MD simulations for dusty plasma medium, treating the medium as collection of dust particles interacting with Yukawa interaction. We study the response of the dust medium to an imposed electric field impulse and provide clear evidence of the formation of KdV solitons. These evidences are in terms of following features: (a) a creation of positive density pulse propagating in one direction along with a train of negative perturbed density oscillations in the opposite direction (b) relative constancy of AL^2 (here A is the amplitude and L is the full width at half maxima of the structure) (c) the structures are shown to be remain intact after undergoing collisional interaction amidst them. Interestingly, the results (a) and (b) are supported by an experimental observation of dusty plasma made by Sheridan et al. [45].

We have also demonstrated that by increasing the strength of electric field impulse the amplitude of the solitonic structure increases and after a point it starts to splits in the form of multiple solitons. This is in agreement with recent experiments which have reported the formation of multiple solitons [122]. This suggests that the depiction of the dusty plasma medium in terms of a simple model of a collection of dust particle interaction via Yukawa potential is fairly good. Another observation made in the present study is related to studying the role of coupling parameter on the formation of solitonic structures. We have shown that by increasing the coupling parameter of the medium the amplitude of the solitonic structures increases while its width decreases. We have also shown that with an increase in the neutral drag on the dust particles the amplitude of the solitonic structures decreases and its width increases.

Furthermore, we have observed that the phase shifts in the collisional interaction seems to decrease with the increasing amplitude of the colliding solitonic structures. In one recent experimental observations [48] as well as in some other literature [44] contrary to this has been reported. We feel that our observations appears consistent with intuition, as one would expect the interaction time between two rapidly moving solitons (which have higher amplitude) to be smaller compared to slowly moving low amplitude solitons. We, therefore, feel that a relook of this issue in experiments as well as theoretical analysis is necessary.

4

Spiral wave (structure) in driven dusty plasmas: Fluid (continuum) simulations

The objective in this chapter is to investigate the excitation and dynamics of spiral waves (structures) in the dusty plasmas using fluid simulations[*]*. These spiral waves have been driven by a rotating forcing. In the fluid simulations, dusty plasma considered as a visco-elastic fluid. Characteristics of spiral waves with varying strength and frequency of rotating force and sound speed of the medium have also been studied. The visco-elastic simulation results have also been compared with the viscous (that have no elasticity) dust fluid results.*

4.1 Introduction

Rotating spiral waves are ubiquitous structures found in a wide range of natural and laboratory scenario. For instance, Belousov-Zabotinsky (BZ) reaction (Fig.

[*] *Sandeep Kumar, Bhavesh Patel, and Amita Das, Physics of Plasmas* ***25****, 043701 (2018)*

4.1) [130], excitable reaction-diffusion media [131,132], liquid crystals [133], cardiac tissue (Fig. 4.2) [134, 135], rotating fluids [136], spiral galaxy (Fig. 4.3) [137, 138], Saturn ring (Fig. 4.4), coupled oscillators [139,140], etc. [141–144], all demonstrate the existence of spiral waves. The self organization of excitations in the form of spiral wave patterns continues to remain an intriguing topic. It has often been interpreted on the basis of an interplay between propagator and controller fields in the excitable medium. The spiral wave tip can rigidly rotate or meander depending upon control parameters of the medium. A vast amount of literature is present in which people claim that meandering occurs via a Hopf bifurcation [131, 145]. Mathematically, FitzHugh-Nagumo (FHN) model has been widely employed for the spatiotemporal development of spiral waves in excitable media [146–149]. For incompressible fluid system, the thermal spiral wave pattern has been observed resulting from temperature gradient excitations [136]. In this chapter, we show that a compressible fluid system can also be forced to form spiral wave density patterns. These waves are shown to propagate in a spiral pattern even after the forcing is switched off.

For definiteness, we consider dusty plasma medium for our study. A dusty plasma is mixture of highly charged (mostly negative) and heavy ($10^{13} - 10^{14}$ times heavier than the ions) dust grains along with electron and ion species. A typical dust particle of micron size has approximately -10^4e charges. At slow dust time scales the inertialess response of electrons and ions are considered which essentially follow a Boltzmann distribution. The inclusion of heavy dust species makes such a plasma exhibit a rich class of collective phenomena. Depending on the value of its coupling parameter it can have both fluid like viscous as well as solid like elastic traits wherein it preserves memory of its past configurations

Figure 4.1: Patterns in the Belousov-Zhabotinsky (BZ) reaction image. Image credit: Michael C. Rogers and Stephen Morris, University of Toronto.

for some amount of time. This has led to the adoption of visco - elastic fluid depiction in terms of Generalized Hydrodynamic (GHD) fluid model [16, 17]. The dusty plasma medium has been shown to exhibit a variety of normal modes such as the longitudinal acoustic [150–155] and transverse shear waves [80, 156–158]. In the nonlinear regime the dusty plasma medium can excite self-sustained non-linear propagating waves that can form solitons [159, 160], shocks [53, 61, 161], and vortices [70–72, 162, 163] etc. Experimental studies by externally driving the medium by energetic particles and or external rotating electric fields (REF) have also been considered [99, 164–166]. In this work, we numerically study the response of the dusty plasma medium in the presence of external forcing by a rotating electric field using the generalized hydrodynamic model. Both weak (wherein the equations reduce to simple charged fluid description) and strong coupling regimes have been investigated in detail.

This chapter has been organized as follows. In section 4.2 we report the ob-

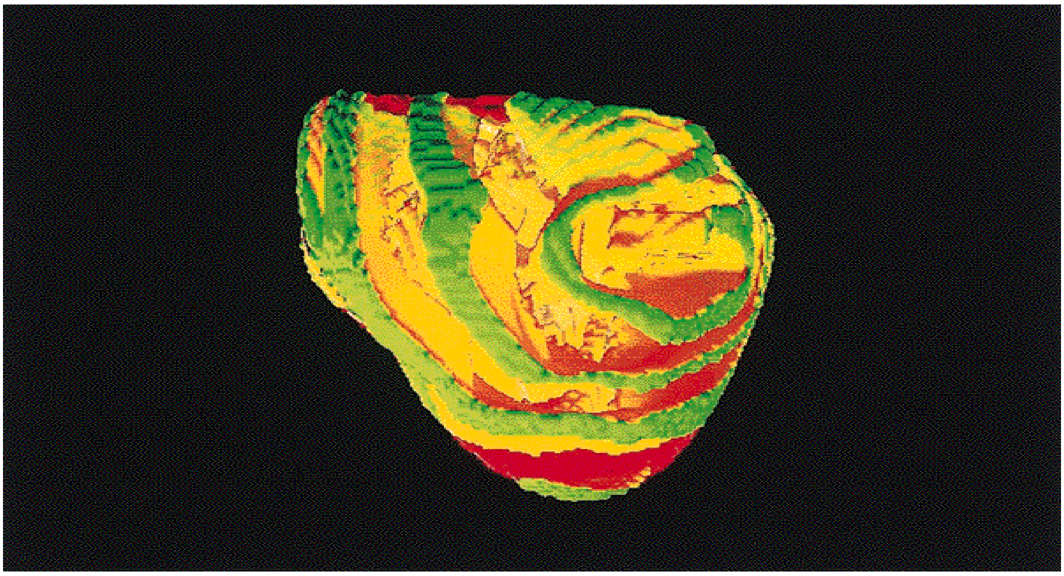

Figure 4.2: Rotating spiral waves of electrical activity on a heart surface. Image credit: A. V. Holden, Nature 392, 20 (1998)

servation of the excitation of spiral density waves in the presence of forcing. The salient features of spiral density wave with respect to various parameters of the medium and forcing characteristics are discussed in detail in various subsections. Section 4.3 provides the summary and conclusion on the study.

Figure 4.3: Spiral galaxy NGC 6814 is captured by NASA/ESA Hubble Space Telescope. Image credit: ESA/Hubble and NASA

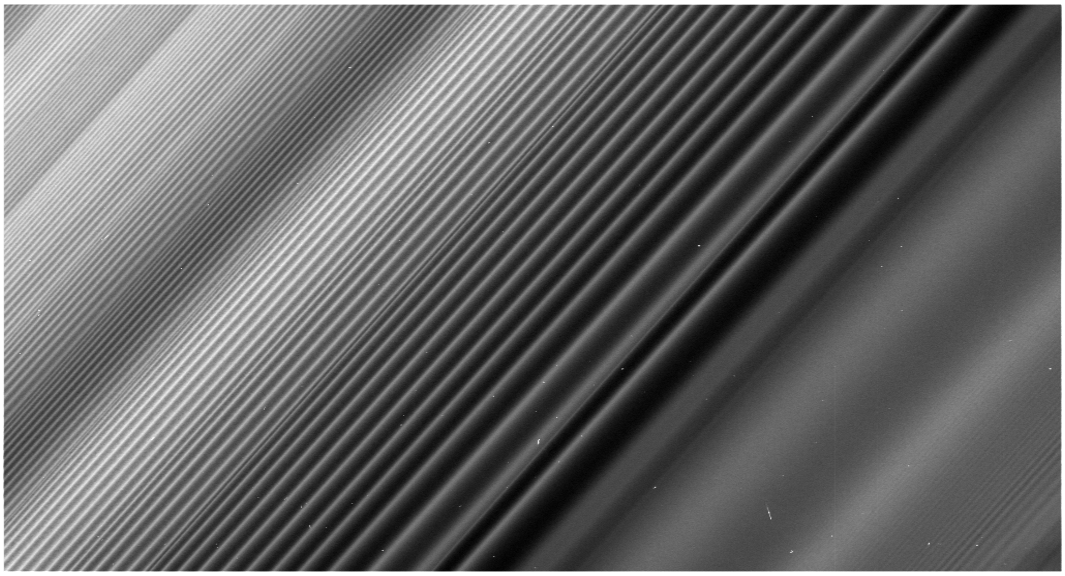

Figure 4.4: Recently NASA's Cassini spacecraft shows this figure which is taken from the Saturn's ring and concluded that it is a spiral density wave structure in the Saturn's ring. Image credit: NASA/JPL-Caltech/Space Science Institute

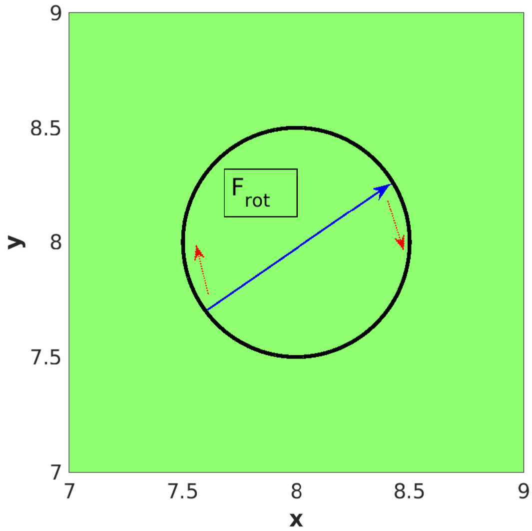

Figure 4.5: Schematic representation of the circularly rotating force ($\mathrm{F_{rot}}$). Here, $\mathrm{F_{rot}} = \mathrm{A}\sin(\omega_f t)\hat{x} + \mathrm{A}\cos(\omega_f t)\hat{y}$ which is only acting within the circular region on each grid point. The Absolute value of the $\mathrm{F_{rot}}$ is constant but direction rotating clockwise with leading time. The solid large arrow depicts the direction of $\mathrm{F_{rot}}$ and small dotted arrows direction of rotation. This force creates perturbation in the density ($\vec{\nabla} n_d$) and potential ($\vec{\nabla}\phi$) of the medium.

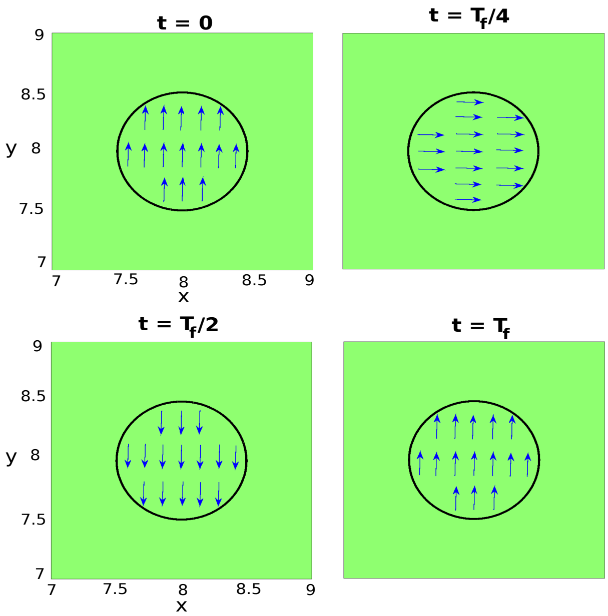

Figure 4.6: Schematic representation of the circularly rotating force ($\mathrm{F_{rot}}$) at different times. The direction of REF shown in the subplots of this Fig. is obtained by putting t $= 0, T_f/4, T_f/2, T_f$, respectively in Eq. 2.17.

4.2 Numerical observations

We carry out numerical simulation studies for the coupled set of Eqs. (2.15,2.16) along with Poisson equation (2.18) in a 2-D $x-y$ plane. The simulation details are present in section 2.2 of Chapter 2. The boundary condition are chosen to be periodic. The box dimension have been chosen as $L_x = 16$, $L_y = 16$. The dust fluid is chosen to have a zero velocity and homogeneous density distribution initially. A rotating electric field (REF) forcing is applied in a small circular domain at the center of $x-y$ plane with a radii $r_0 = 0.5$. The schematic of REF is shown in Fig. 4.5 and Fig. 4.6. Both cases, where forcing continues to be present throughout the simulation and/or is switched off after a certain duration has been considered in our studies.

4.2.1 Weak coupling: Fluid regime

In the weak coupling case, the dust momentum equation satisfies the evolution equation of a normal charged fluid. The form of the equation can be recovered by choosing $\tau_m = 0$ in Eq. (2.15). The evolution of vorticity in the compressible fluid regime (i.e. when $\tau_m = 0$) can be obtained by taking the curl of Eq. (2.15) along with the continuity equation Eq. (2.16). Using the vector identity of

$$\vec{v} \cdot \nabla \vec{v} = \nabla(v^2/2) - \vec{v} \times (\nabla \times \vec{v})$$

and assuming that the pressure is simply a function of density through equation of state we have vorticity equation:

$$\frac{\partial \vec{\Omega}}{\partial t} - \vec{\nabla} \times (\vec{v} \times \vec{\Omega}) = \nabla \times \vec{\mathrm{F}}_{\mathrm{rot}} + \eta \nabla^2 \vec{\Omega} \tag{4.1}$$

Here, $\vec{\Omega} = \nabla \times \vec{v}$ is the vorticity. In the two-dimension (2D)

$$\vec{\nabla} \times (\vec{v} \times \vec{\Omega}) = -\Omega(\vec{\nabla} \cdot \vec{v}) - (\vec{v} \cdot \vec{\nabla})\Omega$$

From continuity equation:

$$(\vec{\nabla} \cdot \vec{v}) = -\frac{1}{n_d}\left(\frac{\partial \vec{n_d}}{\partial t} + \vec{v} \cdot \nabla n_d\right)$$

Using above two equations into Eq. 4.1 it becomes

$$\frac{\partial \vec{\Omega}}{\partial t} + (\vec{v} \cdot \vec{\nabla})\Omega = \frac{\Omega}{n_d}\left(\frac{\partial n_d}{\partial t} + \vec{v} \cdot \nabla n_d\right) + \nabla \times \vec{\mathrm{F}}_{\mathrm{rot}} + \eta \nabla^2 \vec{\Omega}$$

Dividing both side of this equation by n_d it implies

$$\frac{\partial}{\partial t}\left(\frac{\vec{\Omega}}{n_d}\right) = \vec{v} \cdot \left(\frac{\Omega}{n_d^2}\nabla n_d - \frac{\nabla \Omega}{n_d}\right) + \frac{1}{n_d}\left(\nabla \times \vec{\mathrm{F}}_{\mathrm{rot}} + \eta \nabla^2 \vec{\Omega}\right)$$

On rearrangement of terms it becomes

$$\frac{\partial}{\partial t}\left(\frac{\vec{\Omega}}{n_d}\right) + \vec{v} \cdot \nabla\left(\frac{\vec{\Omega}}{n_d}\right) = \frac{1}{n_d}\left(\nabla \times \vec{\mathrm{F}}_{\mathrm{rot}} + \eta \nabla^2 \vec{\Omega}\right) \tag{4.2}$$

From Eq. (4.2) in the absence of forcing and viscosity, the field $\vec{\Omega}/n_d$ is convected by the fluid. Integrating over space it can be shown that

$$\frac{d}{dt}\int\left(\frac{\vec{\Omega}}{n_d}\right)dxdy = \int\left(\frac{\vec{\Omega}}{n_d}\right)\nabla\cdot\vec{v}\,dxdy \tag{4.3}$$

We denote the left and right hand side of Eq. (4.3) by I_1 and I_2, respectively. We have shown the evolution of I_1 and I_2 with time in Fig. 4.7. Both I_1 and I_2 are initially zero as the medium is unperturbed in the beginning. The forcing is responsible for the generation of vorticity and density perturbations. The vertical line shows the time at which the forcing is stopped. It can be seen that for $\eta = 0$, once the forcing is stopped there is a close agreement between I_1 and I_2 as expected. It is, however interesting to observe the behavior of density perturbations in the 2-D plane, the snapshot of which has been shown at various time in Fig. 4.8. It shows a clear development of a spiral wave (density compression and rarefaction) with time. In this case the forcing is present throughout the simulation duration, however, it is applied only within a spatial region of $r < r_0 = 0.5$. The observed spiral wave, however, is extended beyond this spatial domain. Thus the spiral wave pattern are an intrinsic response of the medium in the presence of such a forcing. The number of spiral rings at the various snapshots match with the number of forcing periods covered in that duration. For instance, the normalized forcing frequency $\omega_f = 10$ correspond to a time period of $T_f = 2\pi/\omega_f = 0.628$. Thus for the four subplots, we have $t/T_f = 0.605, 1.24, 2.91, 3.78$, which corresponds approximately to the number of rings that one observes in the subplots for this figure. In Fig. 4.9 where we show the variation of the 2-D density plots with respect to the forcing frequency. From this figure too it is pretty evident from all the subplots except the first one that the spiral rings denote the number of

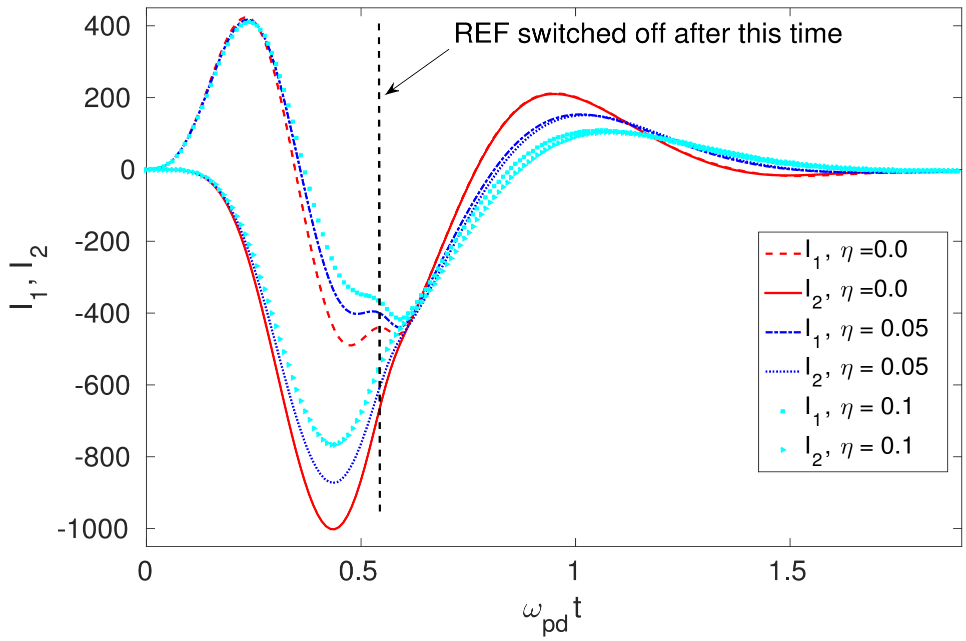

Figure 4.7: Time evolution of I_1 and I_2 (Eq. 4.3) for compressible HD fluids with different values of η. Simulation parameters for this plot are $A = 10$, $\alpha = 5$ and $\omega_f = 10$. Here, applied force switched off after $\omega_{pd}t = 0.55$ time. In the plot I_1 and I_2 for different η are represented by different line styles. There is perfect matching of I_1 and I_2 (dash and solid line, respectively) for the value of $\eta = 0$.

forcing periods covered in a given duration for which the plot has been shown. In the first subplot of this figure the forcing frequency seems to be very high for the natural response of the medium to keep pace. The natural response of the medium is typically the acoustic waves. It should be noted that the typical radial extent of the structure for all the cases remains approximately the same as the acoustic speed in all the four cases of this figure is same. Since the rotation frequency is fast, the radial expansion is unable to keep pace with it and the spiral rings get smeared up to be distinguished clearly for the case of $\omega_f = 15$. For the other cases, the number of rings are in agreement with the law mentioned above.

It appears that the radial expansion of the structure is typically governed by

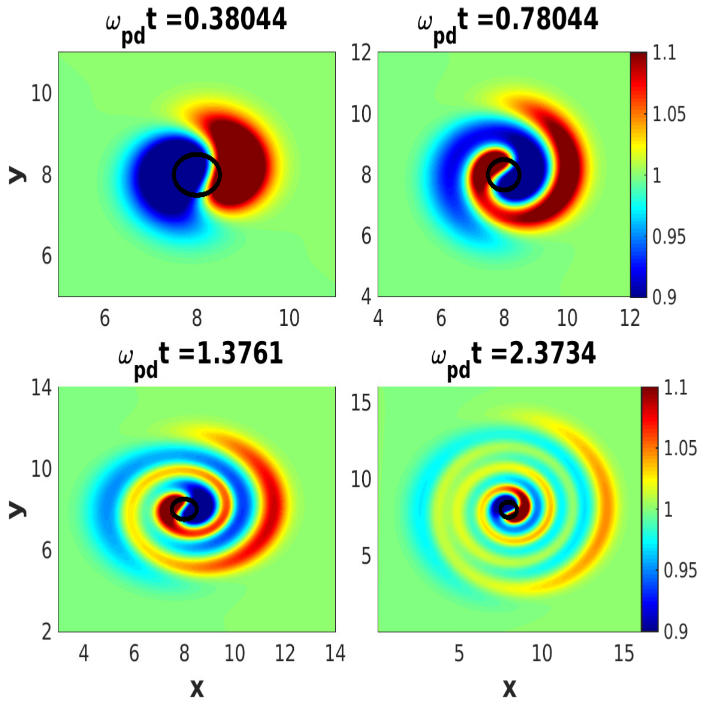

Figure 4.8: Time evolution of the density for HD fluid. Here, F_{rot} applied for whole duration of simulation. For simulation, we have taken $A = 10$, $\omega_f = 10$, $\alpha = 5$ and $\eta = 0.1$. Small circle in the figure represent the region where REF applied. Color bar in the figure represents the density of the medium: equal to 1.00 shows equilibrium density, greater than 1.0 is density compression, and less than 1.0 is density rarefaction. The Density evolution of the medium show the formation of spiral wave.

the acoustic speed of the medium and the number of spiral rings by the forcing frequency. In fact for this case the value of α has been chosen as $\alpha = 5$. This typically corresponds to the acoustic speed (small corrections due to nonlinearity might exist at higher amplitudes) of 2.23. This reasonable explains the radial expansion for $\omega_f = 10$ wherein the disturbance typically has propagated along $+\hat{x}$ direction from $r_0 = 8.5$ to $r = 12.4$ in a time duration of $t = 1.6$. The plot in Fig. 4.10 shows variations with α also suggests that the radial expansion in our system is essentially governed by the value of α. Another feature to note from Fig. 4.9 and Fig. 4.10 is that for a proper unbroken spiral to form an appropriate combination

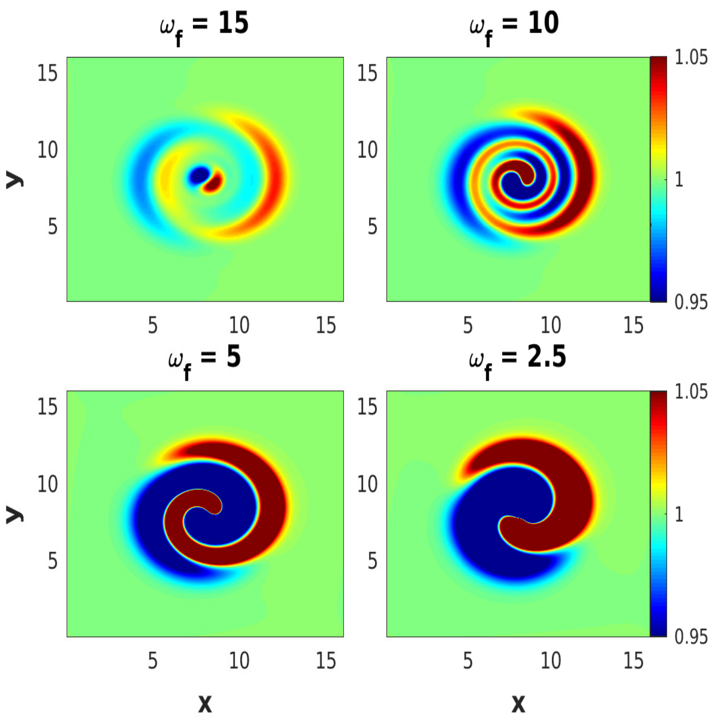

Figure 4.9: Spiral wave for different frequency of forcing. In this case rotating external forcing applied for whole duration of simulation. Simulation parameters for this plot are $A = 10$, $\eta = 0.1$, and $\alpha = 5$. Density for all subplots are taken at time $\omega_{pd}t = 1.60$. First subplot elucidate that when driver frequency is high then radial velocity cannot pace with it resulting spiral becomes smeared out.

of α and forcing frequency ω_f is required. This is because the radial expansion has to keep pace with the rotation. We have also observed the behavior of the spiral with respect to the amplitude A of forcing. This has been shown in the plot of Fig. 4.11. With increasing amplitude, the density perturbations are stronger as the amplitude of density perturbations also increase. On the other hand in the presence of viscosity the density perturbations and $\vec{\Omega}/n_d$ die away as is shown in Figs. (4.12,4.13) and the spiral waves get damped as expected. Fig. 4.13 also elucidate that the source of spiral vorticity (small circular forcing region) diffused with the increase in the viscosity of the medium which is also in agreement with the Eq. (4.2).

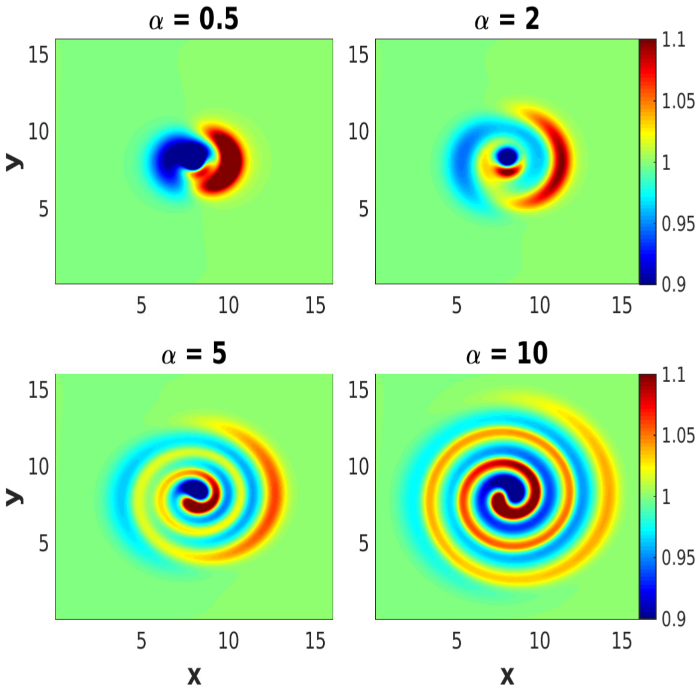

Figure 4.10: Dynamics of spiral wave for different value of sound velocity of medium ($\sqrt{\alpha}$). Simulation parameters for this plot are $A = 10$, $\omega_f = 10$, and $\eta = 0.1$. In this case rotating external forcing applied for whole duration of simulation. Density for all subplots are taken at time $\omega_{pd}t = 1.84$. Here by increasing α inner part of spiral wave breakup avoided. For higher value of α, radial expansion is larger than azimuthal expansion.

4.2.2 Strong coupling: GHD regime

We now present the evolution of the complete set of GHD fluid equations for the dusty plasma medium. Again the initial configuration of homogeneous plasma density with zero velocity in 2-D $x - y$ plane is chosen. The dust fluid is subjected to time dependent forcing within a central circular spatial domain of the 2-D simulation box. In this case by taking the curl of the two coupled equations 2.20. we obtain

$$\left(1 + \tau_m \frac{\partial}{\partial t}\right) \vec{\nabla} \times \vec{\psi} + \tau_m \vec{\nabla} \times \left((\vec{v} \cdot \vec{\nabla})\vec{\psi}\right) = \eta \nabla^2 \vec{\Omega} \tag{4.4}$$

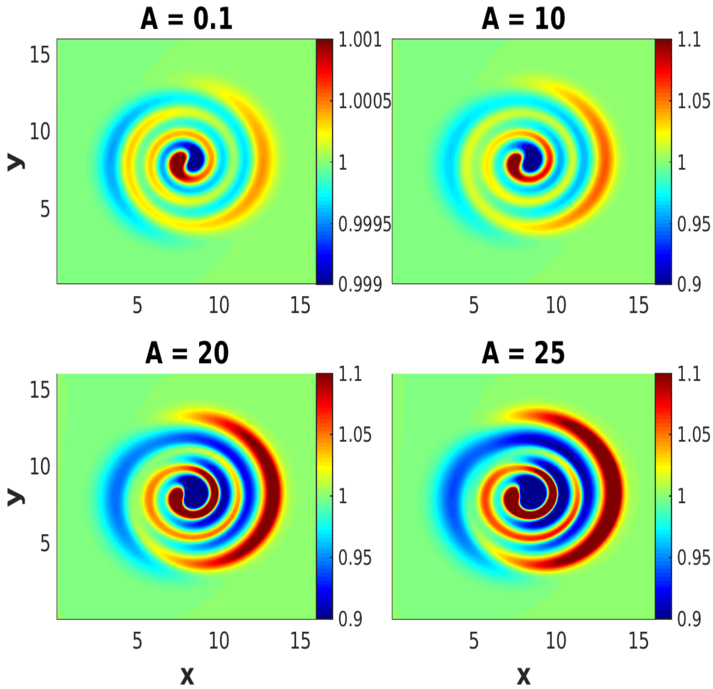

Figure 4.11: Spiral wave with varying amplitude of forcing. In this case rotating external forcing applied for whole duration of simulation. Simulation parameters are $\omega_f = 10$, $\alpha = 5$ and $\eta = 0.1$. Density plots for all amplitudes are taken at time $\omega_{pd}t = 1.97$.

Vector identity:

$$(\vec{v} \cdot \vec{\nabla})\vec{\psi} = (\vec{\nabla}\psi) \cdot \vec{v} - \vec{v} \times (\vec{\nabla} \times \vec{\psi}) \tag{4.5}$$

On using this vector identity in Eq. 4.4, it becomes

$$\left(1 + \tau_m \frac{\partial}{\partial t}\right) \vec{\xi} + \tau_m \vec{\nabla} \times (\vec{v} \times \vec{\xi}) + \tau_m \vec{\nabla} \times (\vec{\nabla}\psi \cdot \vec{v}) = \eta \nabla^2 \vec{\Omega}$$

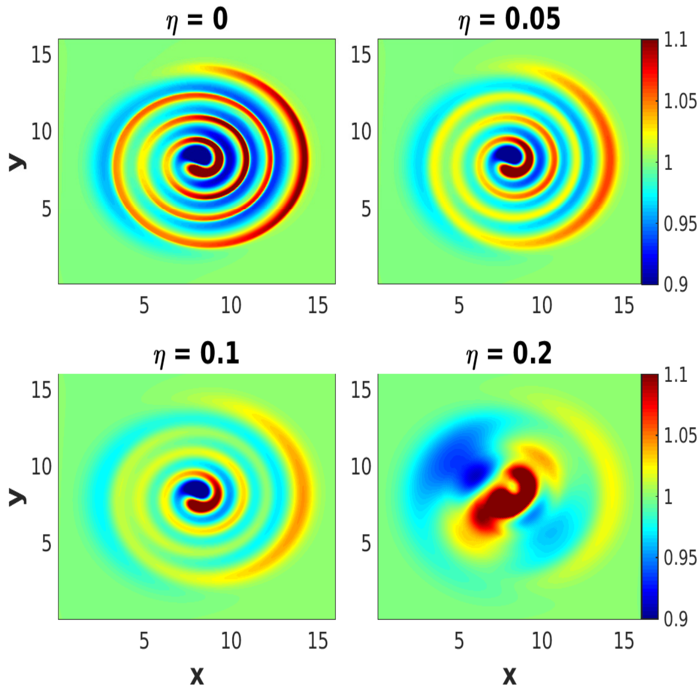

Figure 4.12: Density plot of spiral wave for different values of η in HD fluid. Simulation parameters in this plot are $A = 10$, $\alpha = 5$ and $\omega_f = 10$. Density plots for all values of η are taken at time $\omega_{pd}t = 2.45$.

Here $\vec{\xi}$ is $\vec{\nabla} \times \vec{\psi}$. Upon using continuity equation and two-dimensionality condition in above equation it gives

$$\frac{\partial}{\partial t}\left(\frac{\vec{\xi}}{n_d}\right) + \vec{v} \cdot \nabla \left(\frac{\xi}{n_d}\right) = \\ -\frac{1}{\tau_m}\left(\frac{\xi}{n_d}\right) + \frac{1}{n_d}\nabla \times (\nabla\psi \cdot \vec{v}) + \frac{\eta}{n_d\tau_m}\nabla^2\vec{\Omega} \tag{4.6}$$

Where

$$\frac{\vec{\xi}}{n_d} = \frac{1}{n_d}\vec{\nabla} \times \vec{\psi} = \frac{\partial}{\partial t}\left(\frac{\vec{\Omega}}{n_d}\right) + \vec{v} \cdot \nabla \left(\frac{\vec{\Omega}}{n_d}\right) - \frac{1}{n_d}\vec{\nabla} \times \vec{F}_{ext}$$

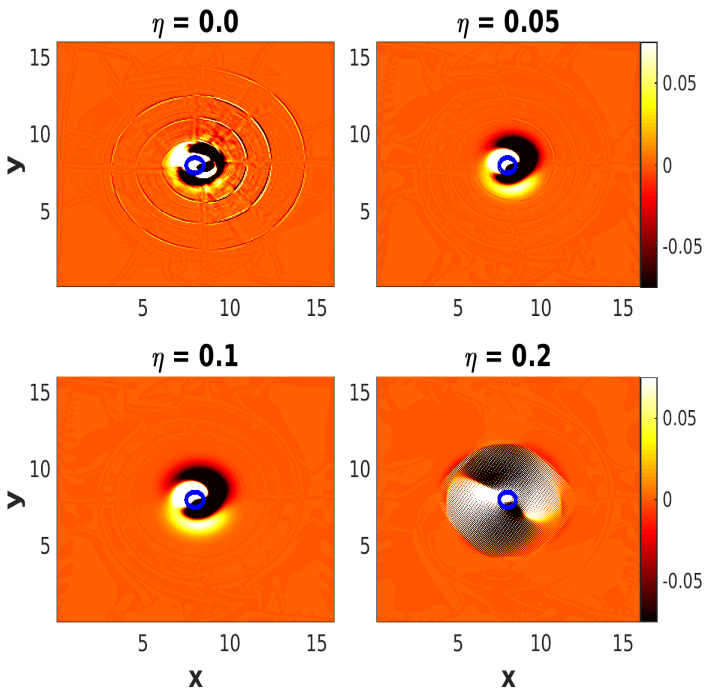

Figure 4.13: Ω/n_d (vorticity) of the HD fluid medium for different values of η. Simulation parameters in this plot are $A = 10$, $\alpha = 5$ and $\omega_f = 10$. Vorticity plots for all values of η are taken at time $\omega_{pd}t = 2.45$. From the figure it is clear that diffusion of source of vorticity increases with increase in the coefficient of viscosity of the medium.

Integrating over space one obtains:

$$\frac{d}{dt}\int\left(\frac{\vec{\xi}}{n_d}\right) dxdy = \int(\nabla\cdot\vec{v})\frac{\vec{\xi}}{n_d}\ dxdy - \int\frac{1}{\tau_m}\left(\frac{\vec{\xi}}{n_d}\right) dxdy$$
$$+\int\frac{1}{n_d}\nabla\times(\nabla\psi\cdot\vec{v})\,dxdy + \int\frac{\eta}{n_d\tau_m}\nabla^2\vec{\Omega}\ dxdy \tag{4.7}$$

It should be noted that when $\tau_m \to 0$, we recover the viscous charged fluid (no memory) vorticity equation 4.3. In the absence of forcing while the fluid satisfies the first order differential equation and shows damping, here on the other hand, there is a possibility of the vorticity to recur.

The snapshots of dust density evolution for the visco-elastic fluid are shown at

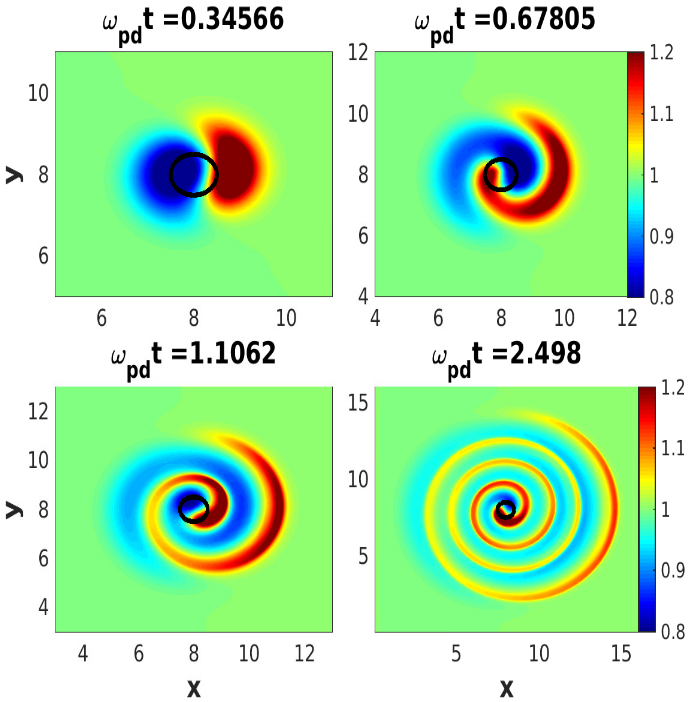

Figure 4.14: Time evolution of the density for strongly coupled visco-elastic fluid. Here F_{rot} applied for whole duration of simulation. For simulation, We have taken $A = 10$, $\omega_f = 10$, $\alpha = 5$, $\eta = 5$ and $\tau_m = 20$. Small circle in the figure represent the region where REF applied.

various times in Fig. 4.14. For this case, the amplitude of the forcing $A = 10$, the forcing frequency $\omega_f = 10$, $\eta = 5$, $\tau_m = 20$ and $\alpha = 5$ has been chosen. It should be noted that the periodicity of the forcing function being 10 (in units of ω_{pd}) the forcing function has completed several rotations at the time snapshot at which the four subplots of the Fig. 4.14 have been shown. The number of turns of the spiral rings in these snapshots are equal to the number of rotations of the forcing function here also similar to the weakly coupled case. However, even though the value of $\eta = 5$ is very high the spiral wave survives in this case when τ_m is finite. This is because η in the presence of finite τ_m plays the role of elasticity of the medium. This is unlike the role of pure damping in the weakly coupled case.

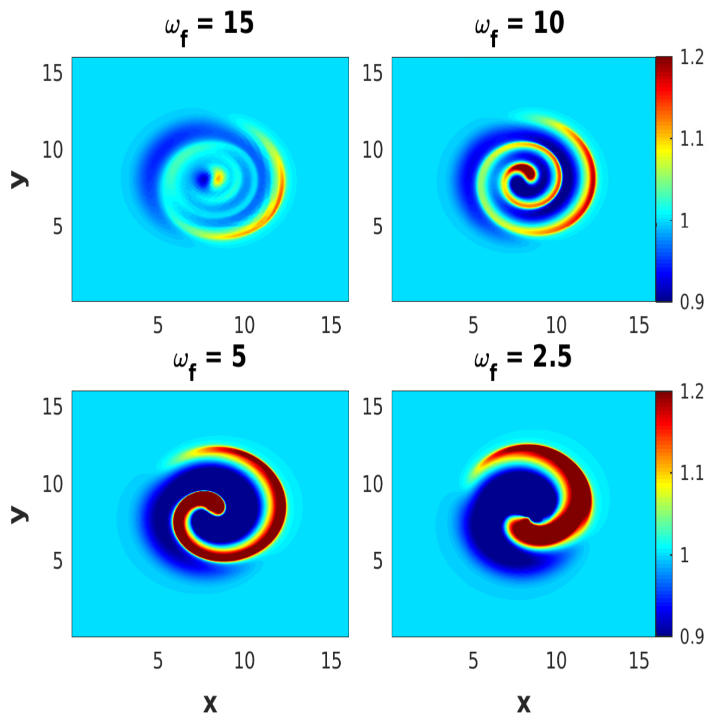

Figure 4.15: Spiral wave for different frequency of forcing. In this case too rotating external forcing applied for whole duration of simulation. Simulation parameters in this plot are $A = 10$, $\alpha = 5$, $\eta = 5$ and $\tau_m = 20$. Density for all subplots are taken at time $\omega_{pd}t = 1.55$. At higher ω_f (first subplot), angular velocity is not in pace with the radial velocity resulting spiral becomes smeared and broken out.

The behavior of the structure as a function of forcing frequency, α (representing the square of acoustic speed), amplitude (A) and strong coupling (η/τ_m) are shown in Figs. 4.15, 4.16, 4.17 and (4.18, 4.19, 4.20), respectively. It is clear from Fig. 4.15 that the number of rings gets decided by the forcing frequency. In this case too if the forcing frequency is very high the radial expansion of the medium is unable to keep pace with it and so in the $\omega_f = 15$ cases the rings get destabilized and broken up to be distinguished clearly. When the frequency is low the radial width of the spiral arms are broad. This can be understood by realizing that the density perturbations in this case are forced at low frequency. The acoustic waves which can resonate at such low frequency would have longer wavelengths. It can be

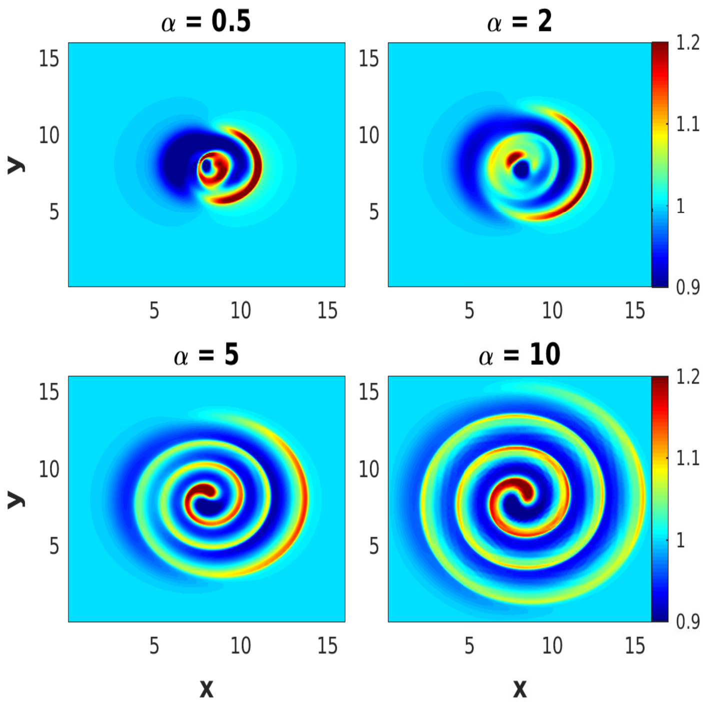

Figure 4.16: characteristic of spiral wave with varying sound velocity of the visco-elastic medium ($\sqrt{\alpha}$). Simulation parameters in this plot are $A = 10$, $\omega_f = 10$, $\eta = 5$ and $\tau_m = 20$. In this case rotating external forcing applied for whole duration of simulation. Density for all subplots are taken at time $\omega_{pd}t = 2.13$. Here by increasing α inner part of spiral wave breakup avoided. For higher value of α, radial velocity is larger than angular velocity.

observed that good spirals are not clearly formed when the radial speed determined by α is small (Fig. 4.16 top subplots). A certain combination of α and forcing frequency determines a good spiral wave structure and its propagation with time.

At a low amplitude A of force, one can observe that the spiral structure does not form as the perturbed density is too weak (Fig. 4.17 for $A = 0.1$). When the value is increased to $A = 10$, it can be observed that a good spiral wave structure gets formed. However, when the amplitude is increased further the density perturbation is high and the acoustic density perturbations would be nonlinear. This is visible

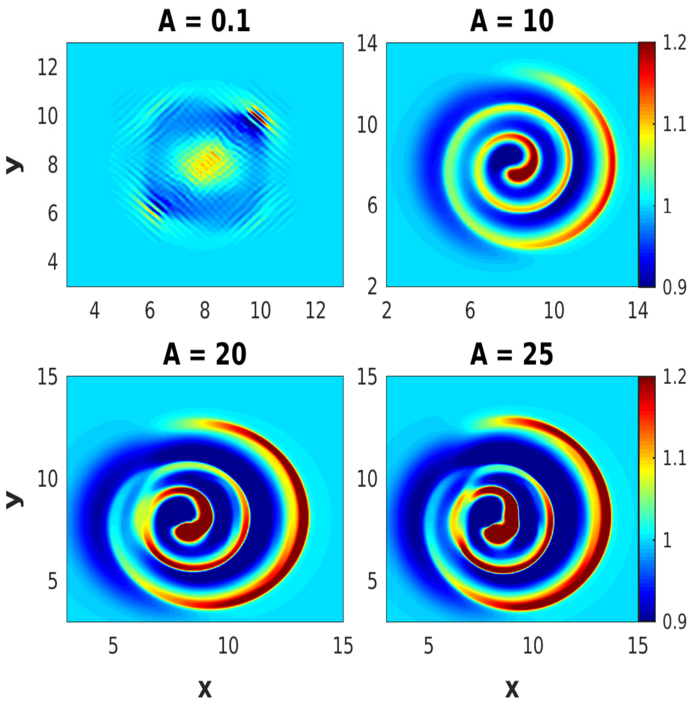

Figure 4.17: Spiral wave behavior in GHD fluid with varying amplitude of forcing. In this case rotating external forcing applied for whole duration of simulation. Simulation parameters are $\omega_f = 10$, $\alpha = 5$, $\eta = 5$ and $\tau_m = 20$. Density plots for all amplitudes are taken at time $\omega_{pd}t = 1.76$.

from the bottom subplots of Fig. 4.17, where one can observe the formation of defects in the spiral structure.

We have also observed the behavior of the spiral wave with respect to strong coupling of the medium. This has been shown in the plot of Figs. 4.18, 4.19 and 4.20. From the Figs. 4.19 and 4.20, it is clear that with increasing strongly coupling (ratio of η and τ_m) the source of spiral vorticity (small circular forcing region) expanding. This expansion is an additional traverse shear wave (TSW) in the medium which generated from the central forcing region. The expansion of this wave increases (Fig. 4.19) with an increase in the strong coupling (the ratio of η and τ_m) of the medium because its velocity is equal to ($\sqrt{\eta/\tau_m}$).

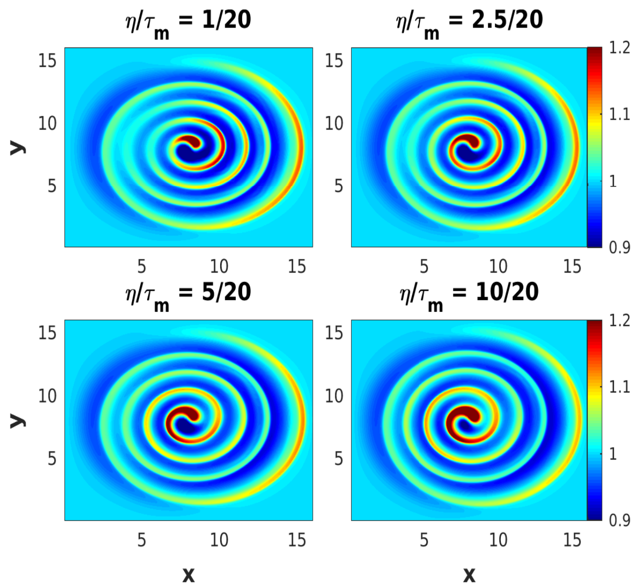

Figure 4.18: Density plot of spiral wave with increasing strong coupling. Simulation parameters in this plot are $A = 10$, $\alpha = 5$ and $\omega_f = 10$. In this case too external REF applied for the whole duration of simulation. Density plots for all ratio of η and τ_m are taken at time $\omega_{pd}t = 2.8068$.

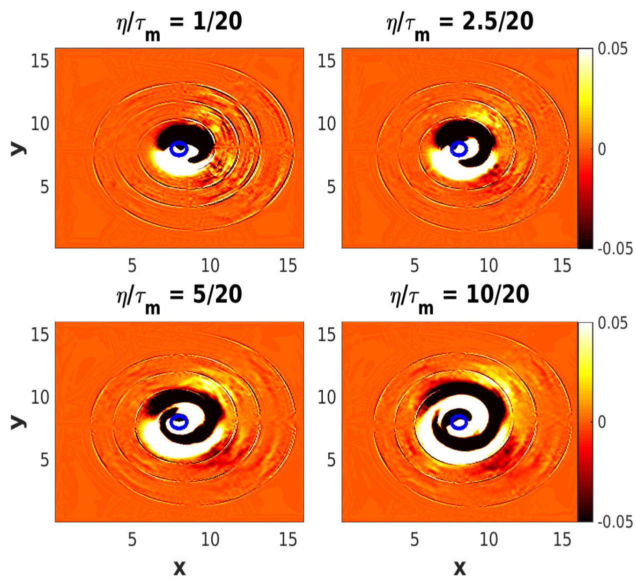

Figure 4.19: Ω/n_d (vorticity) of the GHD fluid medium with increasing ratio of η and τ_m. Simulation parameters in this plot are $A = 10$, $\alpha = 5$ and $\omega_f = 10$. Vorticity plots for all ratio of η and τ_m are taken at time $\omega_{pd}t = 2.8068$. From the figure it is clear that expansion of source of vorticity increases with increase in the ratio of η and τ_m.

4.3 Summary and conclusion

We have carried out the GHD visco-elastic fluid simulations for a driven dusty plasma medium. We study the response of the dust medium to an imposed rotating electric field in a small localized region and observed the formation of spiral waves. These spiral waves are observed to propagate radially outwards much beyond the spatial extent of the forcing. When forcing is weak and the density perturbations are in linear regime then we observe planar acoustic excitations. Only in nonlinear density perturbations does one observe spiral structure formation. Spiral wave has both angular as well as radial velocity. We have identified that the radial expansion velocity corresponds to the sound speed. The number of rings in the spiral correspond to the number of rotations of the forcing field at any given time. If the radial velocity is too fast then the rings are broad. However, when the forcing frequency is fast and the radial velocity is slow the spiral rings are sharp. When the radial velocity is too slow and is unable to keep pace with the forcing frequency the spiral structure gets destabilized and smeared out. For a proper clear spiral to form an appropriate combination of sound speed and forcing frequency is required. We have found that the source of spiral vorticity expanding with an increase in the strong coupling of the medium which elucidates the presence of additional TSW in the medium. We have observed only two armed (one of compression and other of rarefaction) spiral waves unlike Li et al. [136] multi-armed spiral waves.

Spiral wave formation are ubiquitously present in many natural phenomena in excitable media which requires a certain time duration to regain after a wave passes through it. In this case, the dust density perturbations created by the forcing requires the response of the dust before it can be again perturbed by the forcing.

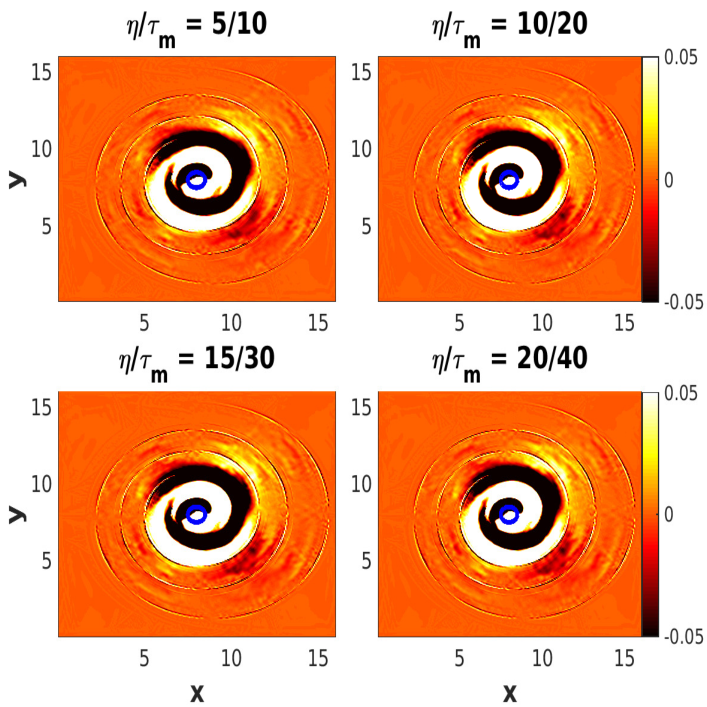

Figure 4.20: Ω/n_d (vorticity) of the visco - elastic fluid for the same ratio of η and τ_m. Simulation parameters for this plot are $A = 10$, $\alpha = 5$ and $\omega_f = 10$. Vorticity plots for all ratio of η and τ_m are taken at time $\omega_{pd}t = 2.8068$. Small circle in the figure represent the region where REF applied. From the figure it is clear that expansion of source of vorticity depends only upon the ratio of η and τ_m, not upon the individual values.

The exciter and controller fields are believed to be important in the excitation of spiral waves. Here forcing induces vorticity as well density perturbations which together propagate like a spiral wave pattern.

5

Spiral waves in strongly coupled Yukawa Systems: A molecular dynamics study

In chapter 4, we have studied spiral waves (structures) using fluid (continuum) simulation but it misses out on the kinetic particulate nature of the dust species. The objective of this chapter is to investigate the spiral wave in a dusty plasma medium by taking discrete particle effects into consideration[*]*. Molecular-dynamics simulations have been used for this purpose. In the crystalline state of dusty plasma, the spiral wavefront becomes hexagonal in shape which is understood by the difference in the phase velocity in directions associated with the crystal lattice (viz., lattice axis and lattice diagonal).*

[*] *Sandeep Kumar, and Amita Das, Physical Review E* ***97****, 063202 (2018)*

5.1 Introduction

Spiral wave formation is typically believed to arise as an interplay of propagator and controller fields in any excitable medium [167–169]. An excitable medium by definition is a nonlinear dynamical medium permitting wave propagation by means of local coupling between its constituents. However, the medium takes a certain time before a next wave can be excited through it. There are many examples of excitable media. For instance, oscillating chemical reactions such as Belousov-Zabotinsky (BZ) reaction [130,170] behave in this fashion. The pathological conditions in brain and heart activities have also been modeled as excitable medium [144,171]. There are many types of waves which can be observed in any excitable medium. For example, in one-dimension fronts and solitons, in 2-D curvature and spiral waves, and in 3-D scroll waves can be observed [167]. Mathematically, FitzHugh-Nagumo (FHN) model has been widely used to describe the spatiotemporal development of spiral waves in excitable media [146–149]. In the literature, spiral waves have also been reported for many others systems such as liquid crystals [133], spiral galaxy [137, 138], coupled oscillators [139, 140] and spread of disease in epidemiology [143]. Recently, thermal spiral wave excitation in incompressible fluid system has been demonstrated by Li et al. [172].

Propagation of spiral density waves under the influence of external force have been recently demonstrated in the fluid simulation of compressible dusty plasma medium [173]. The dusty plasma is essentially made up of discrete charged dust particles which are of macroscopic size compared to the lighter electron and ion species present in the medium. Dusty plasma offers a model system to study generic phenomena such as self-organization and transport at the particle level which is also of great importance for excitable media. The use of fluid model misses out on the kinetic particulate nature of the dust species. The Molecular Dynamics (MD) simulations, however, offer the possibility of investigating this. The aim of this chapter is to seek the excitation and dynamics of the spiral wave in a dusty plasma medium by taking discrete particle effects into consideration.

A dusty plasma is a mixture of highly charged (mostly negative) and heavy ($10^{13} - 10^{14}$ times heavier than the ions) dust grains along with the lighter electron and positive ion species. A typical dust particle of micron size has approximately -$10,000e$ electronic charge. Dusty plasma can be very well depicted by a collection of point particles which interact via Yukawa potential (which mimics the screening due to the presence of free electrons and ions between dust species) having the following form [123]:

$$U(r) = \frac{Q^2}{4\pi\epsilon_0 r}\exp(-\frac{r}{\lambda_D}),$$

Here, Q is the charge on a typical dust particle, r is the separation between two dust particles and λ_D is the Debye length of background plasma. The Yukawa system can be characterized in terms of two dimensionless parameters $\Gamma = Q^2/4\pi\epsilon_0 a k_B T_d$ (known as the coupling parameter) and $\kappa = a/\lambda_D$ (known as the screening parameter). Here T_d and a are the dust temperature and the Wigner-Seitz radius, respectively. Yukawa interparticle interaction also occurs in many other systems such as charged colloids [174, 175], electrolytes [176, 177] and strongly coupled e-i plasmas [178, 179]. So the studies carried out in this work would also suitably depict these systems.

Due to high charges on the dust grains, the dusty plasmas can be easily found in the strongly coupled state (i.e. their average electrostatic potential energy can be made comparable to or higher than the average kinetic energy of particles rather easily and does not require extreme conditions of temperature and/or density). Such a plasma can, therefore, have traits of a fluid or a solid depending upon where medium lies in the (Γ, κ) plane [1]. For a given κ, dusty plasma imbricate to crystalline state when coupling parameter $\Gamma > \Gamma_c$, where Γ_c is the critical value for crystallization. At intermediate value of Γ ($1 < \Gamma < \Gamma_c$) the system behaves like a complex fluid with both fluid and solid like traits. Hence, both longitudinal and transverse wave modes can be excited in dusty plasmas. Waves in dusty plasmas are either excited by external perturbations in the form of electric fields, or self excited by viz. ion drag force, thermal fluctuations, and instabilities. High amplitude perturbations in dusty plasma medium can lead to non-linear propagating waves that can form solitons [159, 180], shocks [161], and vortices [73, 74]. We have also studied shocks in the dusty plasma by moving a projectile in the medium and that it is part of someone else thesis [181]. There are some experiments where the medium is driven by rotating electric field (REF) [166, 182]. The REF in these experiments was operated over the entire domain of the system. In the present simulation studies, we show that by employing a rotating electric field only over a small circular patch in the system, spiral waves propagating radially outwards can get excited.

This chapter is organized as follows. Section 5.2 provides details of MD simulation. Section 5.3 provides numerical observations. Section 5.4 contains conclusion.

5.2 Simulation details

The simulation system modeled here is a two-dimensional square box of point dust particles interacting electrostatically with each other through the Yukawa form of interaction potential. A monolayer with 28647 grains (with periodic boundary conditions) is created in a simulation box with $L_x = L_y = 300a$ ($-150a$ to $150a$) along X and Y directions. Here, $a = (1/\sqrt{\pi n_d})$ is the Wigner-Seitz radius in two-dimension and n_d corresponds to dust density for the monolayer. We have assumed [99] the dust grain mass $m_d = 6.99 \times 10^{-13}$ Kg, charge $Q = -11940e$ (e is elementary charge) and $a = 4.18 \times 10^{-4}$ m. We have also considered all particles to have equal mass and charge. The screening parameter κ is chosen to be 0.5 which sets the plasma Debye length in the simulation as $\lambda_D = 8.36 \times 10^{-4}$ m. The typical inter-dust unscreened electric field, $E_0 = Q/4\pi\epsilon_0 a^2 = 98.39$ V/m. The equilibrium density (n_{d0}) of 2-D dust layer is $1.821 \times 10^6\ m^{-2}$. The characteristic frequency of the particles $\omega_{pd} = (Q^2/2\pi\epsilon_0 m a^3)^{1/2} \simeq 35.84\ s^{-1}$, which corresponds to the dust plasma period (t_d) to be 0.175 sec. We have chosen simulation time step as 0.0036 ω_{pd}^{-1} so that phenomena occurring at dust response time scale can be easily resolved. Results in this chapter are presented in normalized units, for which distance, time, and electric field are normalized by a, ω_{pd}^{-1}, and E_0, respectively.

Thermodynamical equilibrium state for a given Γ is achieved by generating positions and velocities from canonical ensemble using Nose-Hoover [125,126] thermostat. After about an canonical run for 1433 ω_{pd}^{-1} time, we disconnected the canonical thermostat and ran a simulation for about 716 ω_{pd}^{-1} time micro-canonically to test the energy conservation. After micro-canonical run the dust monolayer achieves thermodynamical equilibrium with the desired value of Γ.

The dust particles are then evolved in the presence of their Yukawa interactions and the external force due to the rotating electric field. The effect of background neutral gas on dust micro - particles has also been studied in some simulations. For this, we have added two additional forces in the simulation. First is the neutral drag force due to the relative velocity $\vec{v}$ between the dust grains and neutral particles and is given by [95–97]:

$$\vec{\mathrm{F}}_{\mathrm{f}} = -m_d \nu \vec{v},$$

Where m_d is the mass of the dust particles and ν is the damping coefficient. The other force is random kicks suffered by dust grains by collisions with neutral atoms. This is given by:

$$\mathrm{F}_{\mathrm{r}} \propto \sqrt{\frac{k_B T_n m_d \nu}{dt}},$$

Where, dt and T_n are the time step of simulation and background neutral gas temperature, respectively. The simulation including the effect of background neutral gas is run by Langevin MD dynamics and the motion of the i^{th} particle with mass m_d is governed by the following equation:

$$m_d \ddot{r}_i = -\sum_j \nabla U_{ij} + \mathrm{F}_{\mathrm{f}} + \mathrm{F}_{\mathrm{r}} + \mathrm{F}_{\mathrm{rot}} \tag{5.1}$$

Here, $\mathrm{F}_{\mathrm{rot}} = Q\mathrm{E}_{\mathrm{rot}}$ is the force due to the REF of the form $\mathrm{E}_{\mathrm{rot}} = A\cos(\omega_f t)\hat{x} + A\sin(\omega_f t)\hat{y}$. Where, A is the amplitude of REF and $\omega_f = 2\pi/T_f$. It should be noted that $\mathrm{F}_{\mathrm{rot}}$ is only acting on those particles who lies within the circular patch as shown in schematic representation of Fig. 5.1. For most of our simulations, unless otherwise stated, we have used the value of $\Gamma = 100$, $\kappa = 0.5$ and $\nu = 0$. However, in some cases to investigate the dependence on these parameters we have also varied these values as per the requirement. In the simulation, Γ and κ are varied by varying T_d and λ_D, respectively. The characteristics dust lattice wave

(DLW) velocity (C_s) of the medium at $\Gamma = 100$, $\kappa = 0.5$ and $\nu = 0$ is 1.94×10^{-2} m/s. [159]

5.3 Numerical Observations

We have applied a rotating electric field on a small circular region at the center of the two-dimensional simulation box to excite the spiral waves. In the present simulation, we have chosen the radius of circular region $r_0 = 15a$. A rotating electric field $E(t)$ is generated by choosing the following time dependence for the two components, viz., $E_x(t) = A\cos(\omega_f t + \psi)$ and $E_y(t) = A\sin(\omega_f t)$ along X and Y axis, respectively. Here, $\omega_f = 2\pi/T_f$ so that T_f is the period of rotation. Their superposition $E = (E_x, E_y)$ gives rise to a polarized electric field rotating in two-dimensions. The type of polarization depends upon the phase difference ($\Delta\phi$) among E_x and E_y. For linear polarization $\Delta\phi = 0$ or π, circular polarization $\Delta\phi = \pi/2$ or $3\pi/2$ and elliptical polarization $\Delta\phi = \pi/4$ or $3\pi/4$. In the present studies, the case of circular polarization has been employed. Schematic representation of REF is shown in Fig. 5.1. This electric field results in an electrostatic force $F_E = QE$ on the dust particles which creates spatial perturbation in dust density ($\vec{\nabla} n_d$). The forcing also imparts kinetic energy to the particles, which can randomize and create temperature gradients ($\vec{\nabla} T_d$) in the medium. The applied REF has been kept on for the entire duration of simulation.

The evolution of the medium is shown in Fig. 5.2. Particle snapshots clearly show the excitation of the collective mode of spiral waveform which is rotating as well as radially expanding. The handedness of the spiral motion depends upon the type of polarization (left or right circular) of the driver field. This spiral wave is manifestation of the forcing on the dust particles by the REF which is

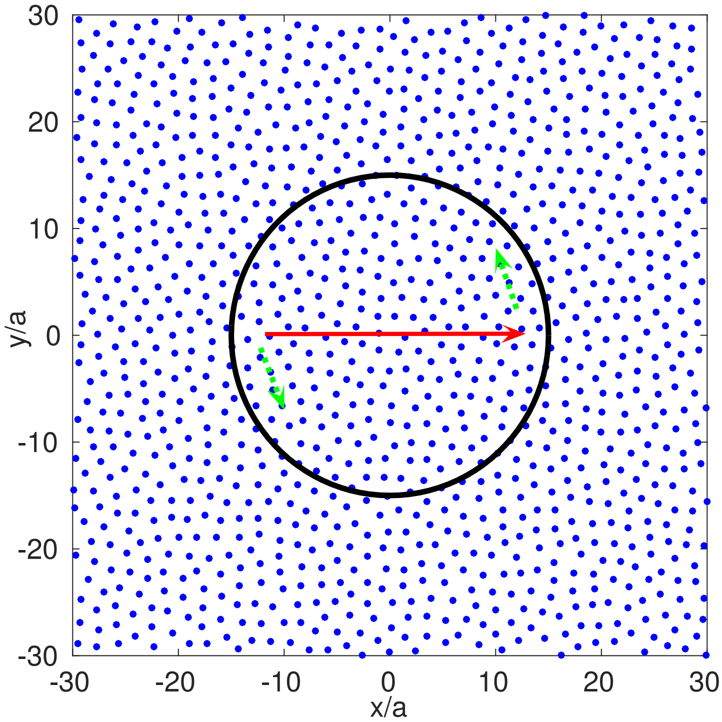

Figure 5.1: Schematic representation of the circularly rotating electric field. Here, REF is only acting within the circular region on each dust particle. The Absolute value of the REF is constant but direction rotating anti-clockwise with leading time. The solid large arrow depicts the direction of REF and small dotted arrows direction of rotation.

operative over the central circular region shown in the Fig. 5.2 by thick line. The number of rings in the spiral structure at a given time is proportional to the number of periods taken by the REF in that duration. In Fig. 5.2 number of rings according to number of periods from four plots (a), (b), (c), and (d) are $17.92/26.88 = 0.67$, $35.84/26.88 = 1.33$, $53.76/26.88 = 2.0$ and $71.68/26.88 = 2.67$, respectively as expected. We have calculated the radial velocity of the spiral wave from the propagation of the density peak radially outward (for instance the X-axis is specifically chosen here) with respect to time. The density data as a function of x are obtained by calculating the density of particles within spatial grids along X axis. Radial velocity for $A = 0.203$, $\omega_{pd}T_f = 26.88$, $\Gamma = 100$, $\kappa = 0.5$ and $\nu = 0$

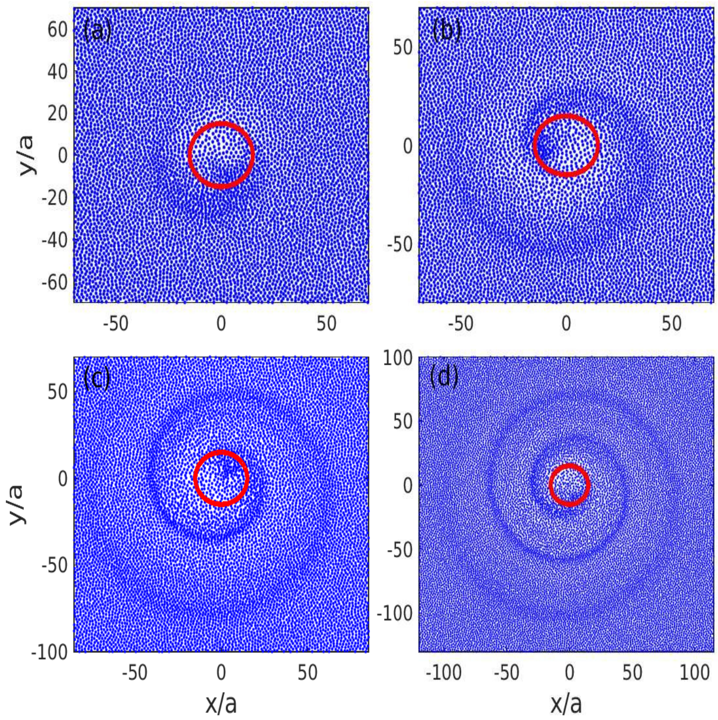

Figure 5.2: Time evolution of the medium for REF of amplitude $A = 0.203$, $\omega_{pd}T_f = 26.88$, $\Gamma = 100$, and $\kappa = 0.5$. Particle snapshots taken at time (a) $\omega_{pd}t = 17.92$, (b) $\omega_{pd}t = 35.84$, (c) $\omega_{pd}t = 53.76$, and (d) $\omega_{pd}t = 71.68$ are clearly showing the formation of spiral wave. Circle at the center represents the region of forcing.

is 1.97×10^{-2} m/s which is very close to the DLW velocity ($C_s = 1.94 \times 10^{-2}$ m/s) [159].

The number of spiral generated at a given time is a function of the frequency of the REF. With increasing frequency of REF the number of spiral rings increases as shown in Fig. 5.3 and Fig. 5.4. However, since the radial expansion is govern by the acoustic propagation speed therefore the radial separation between two consecutive density peaks reduces with increasing frequency. At very high frequency (plot (a) of Fig. 5.3), the spiral density compression and rarefaction is not very clear. In this case the radial expansion is unable to keep pace to distinctly identify the individual density peaks. When the amplitude of the driving force is increased, the density

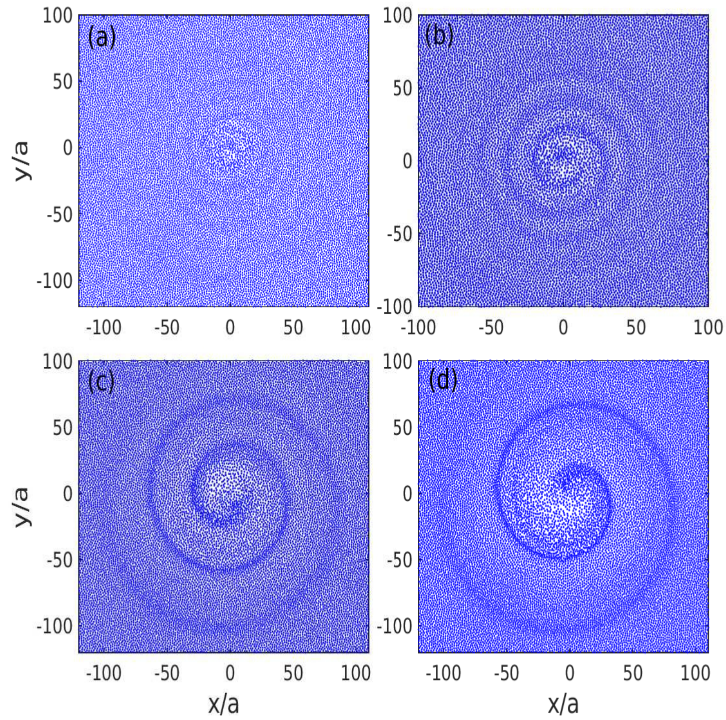

Figure 5.3: Spiral waves for different value of driver frequency (a) $\omega_{pd}T_f = 12.54$, (b) $\omega_{pd}T_f = 16.12$, (c) $\omega_{pd}T_f = 26.88$, and (d) $\omega_{pd}T_f = 35.84$ at $A = 0.203$, $\Gamma = 100$, and $\kappa = 0.5$. Snapshot of particles for all frequencies are taken at time $\omega_{pd}t = 71.68$.

perturbation ($\delta n = n_d - n_{d0}$) in the spiral are of higher amplitude and spiral rings are broader. This is evident from the plot of Fig. 5.5. Furthermore, one can observe that with increasing amplitude of the force the particles in central region acquire higher velocities which gets randomized. The consecutive rings, therefore, have varying radial speed of propagation and the spiral structure therefore does not form clearly. Therefore, in forming a good spiral structure the amplitude of driving force also plays a crucial role.

We have also applied frictional damping on the dust particles due to the presence of neutral particles in the dusty plasma medium. We have found that the spiral wave gets damped in the presence of frictional damping $\vec{\mathrm{F}}_{\mathrm{f}}$. The damping

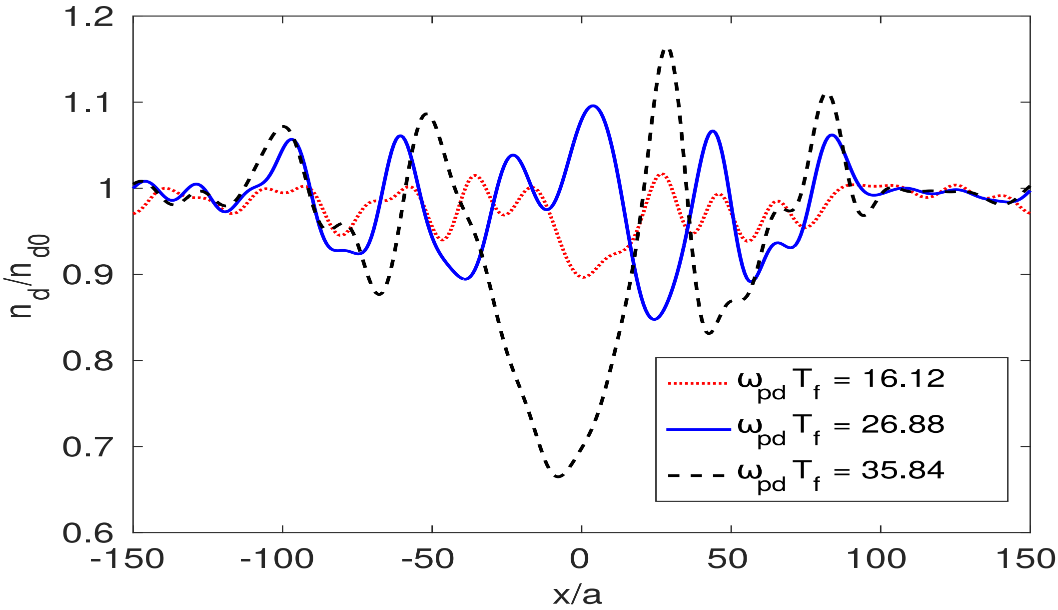

Figure 5.4: One-dimensional density of the medium for the different frequencies of driver at $A = 0.203$, $\Gamma = 100$, and $\kappa = 0.5$. Density plot for all frequencies are taken at time $\omega_{pd}t = 71.68$. From the plot it is clear that with decrease in the frequency of external driver, density compression, rarefaction and distance between two consecutive rings increases.

rate increases with increase in the damping coefficient ν as shown in Fig. 5.6.

We have also studied the effect of Γ and κ on the formation and evolution of spiral waves. When the value of coupling parameter Γ of the medium is increased one observes that spiral rings become more distinctly clear (Fig. 5.7). This can be understood from the fact that in weakly coupled case particle trajectories are diffusive, but it becomes localized in strongly coupled case. Another observation is that the coupling parameter Γ has a negligible influence on the radial propagation speed of the spiral wave. The screening parameter κ, however, has a strong effect. The radial propagation velocity decreases with increase in the value of κ. The role of Γ and κ parameters are illustrated in the plots (a), (b), (c), and (d) of Fig. 5.7 and Fig. 5.8, respectively. The dependency of the radial velocity of spiral on Γ and κ is also in accordance with the findings of Khrapak et al. [183] and Kalman et

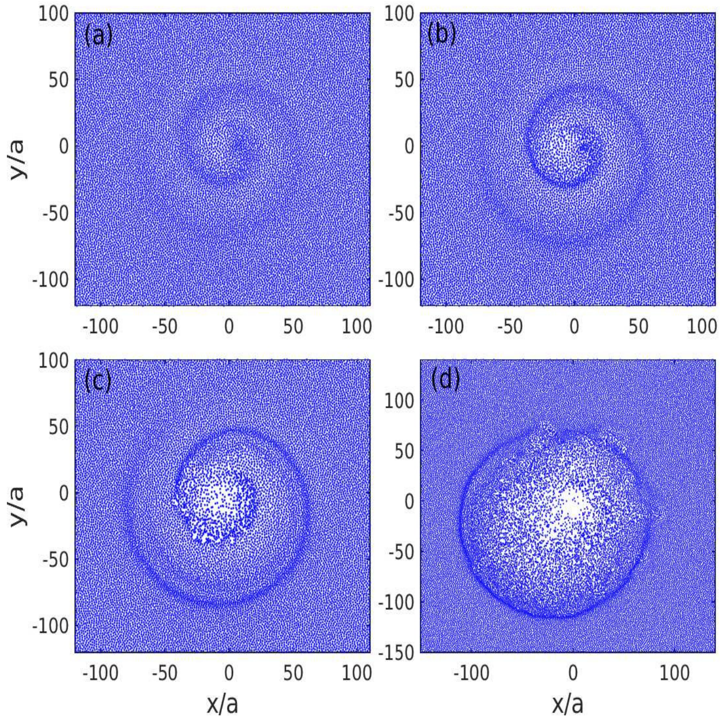

Figure 5.5: Characteristics of spiral waves with varying amplitude of REF (a) $A = 0.101$, (b) $A = 0.203$, (c) $A = 0.406$, and (d) $A = 1.27$. Coupling parameter, screening parameter, and time period of REF for all amplitudes are $\Gamma = 100$, $\kappa = 0.5$, and $\omega_{pd}T_f = 26.88$, respectively. Snapshot of particles for all amplitudes are taken at time $\omega_{pd}t = 50.17$. From the figure, it is clear that an undistorted (tip) spiral wave can be excited when the amplitude of REF is smaller than inter-dust unscreened electric field (E_0).

al. [23], that have been obtained for the sound velocity of strongly coupled Yukawa liquids. Kalman et al. suggested approximate expression for the sound velocity of the Yukawa liquids valid for $\kappa < 2.5$ is as following:

$$C_s = \omega_{pd}a\sqrt{(1/\kappa^2 + f(\kappa))}, \tag{5.2}$$

Where

$$f(\kappa) = -0.0799 - 0.0046\kappa^2 + 0.0016\kappa^4.$$

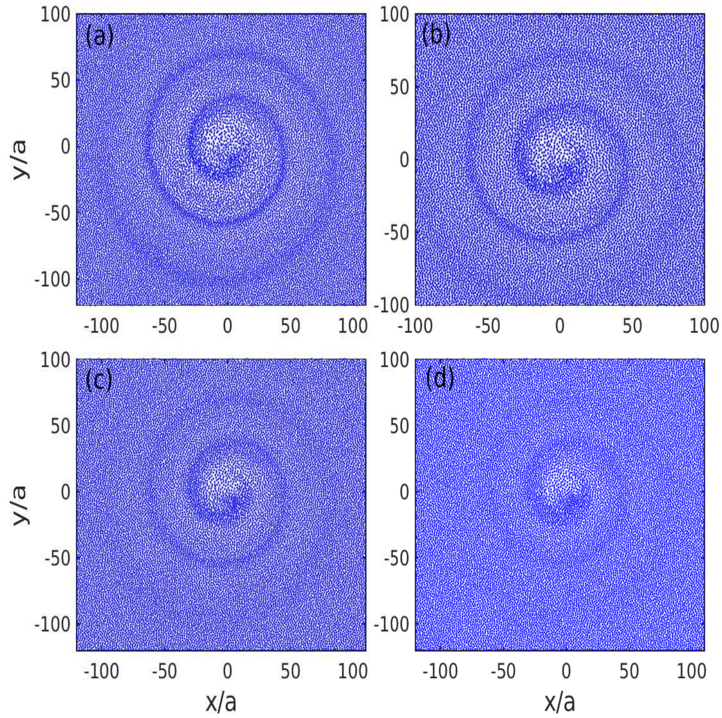

Figure 5.6: Effect of neutral damping (a) $\nu/\omega_{pd} = 0.0$, (b) $\nu/\omega_{pd} = 0.014$, (c) $\nu/\omega_{pd} = 0.0279$, and (d) $\nu/\omega_{pd} = 0.0558$ on the spiral wave are shown here. For all the plots, $A = 0.203$, $\omega_{pd}T_f = 26.88$, $\Gamma = 100$, and $\kappa = 0.5$. Snapshot of particles for all damping parameters are taken at time $\omega_{pd}t = 71.68$.

The radial propagation speed decreases with increasing κ. So that for a given κ, there is a critical frequency of REF above which the disturbance gets smeared out instead of forming distinctly clear spiral rings (shown in plot (d) of Fig. 5.8). It is thus clear that to form a proper unbroken spiral wave pattern, we require a proper combination of ω_f and κ so that radial and angular velocities can appropriately compliment each other.

The increasing value of κ essentially implies that the interparticle shielding gets stronger and hence the individual dust particle interactions reduces. Due to the reduction in interparticle interaction, when the REF throws the particle out of the radial patch of forcing, the particles are unable to return back to their original

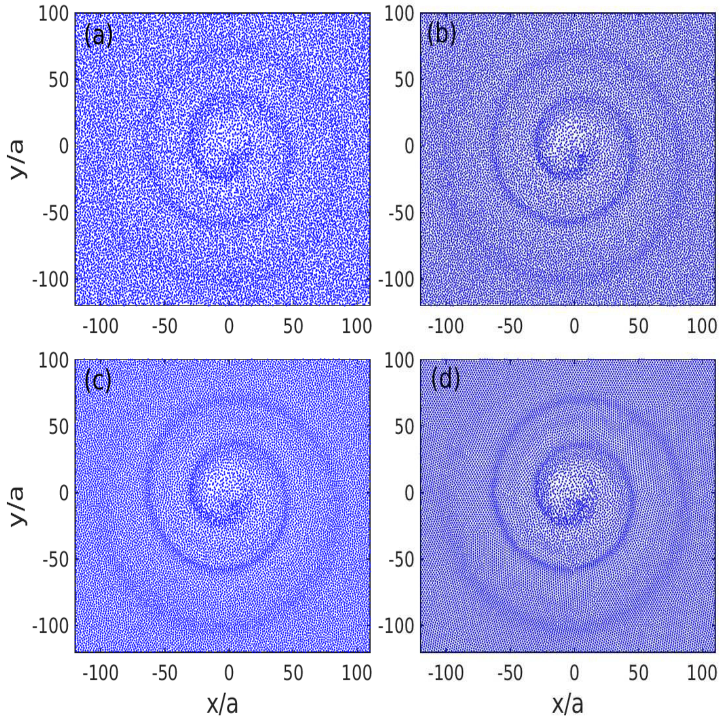

Figure 5.7: Characteristics of spiral wave with varying coupling parameter (a) $\Gamma = 10$, (b) $\Gamma = 50$, (c) $\Gamma = 100$, and (d) $\Gamma = 800$. Strength of REF, period of REF, and screening parameter for all the Γ are $A = 0.203$, $\omega_{pd}T_f = 26.88$, and $\kappa = 0.5$, respectively. Snapshot of particles for all Γ are taken at time $\omega_{pd}t = 71.68$.

location. Thus the particle density in the forcing region reduces. This is evident from Fig. 5.8 where one can easily notice (see the white patches in plot (c) and (d)) the reduction in particle number density in the central forcing region. As a result of this reduction in the number density the subsequent rings of the spiral do not form clearly for high values of κ.

We have also investigated the possibility of exciting spiral wave when the dust medium is initially in crystalline phase. For this purpose, we have chosen the case of $\Gamma = 2000$ for our studies. When the value of κ is small (plot (a) of Fig. 5.9), we observe the regular formation of spiral wave. However, as κ is increased one observes the spiral excitations to have a hexagonal wave front (plot (b), (c),

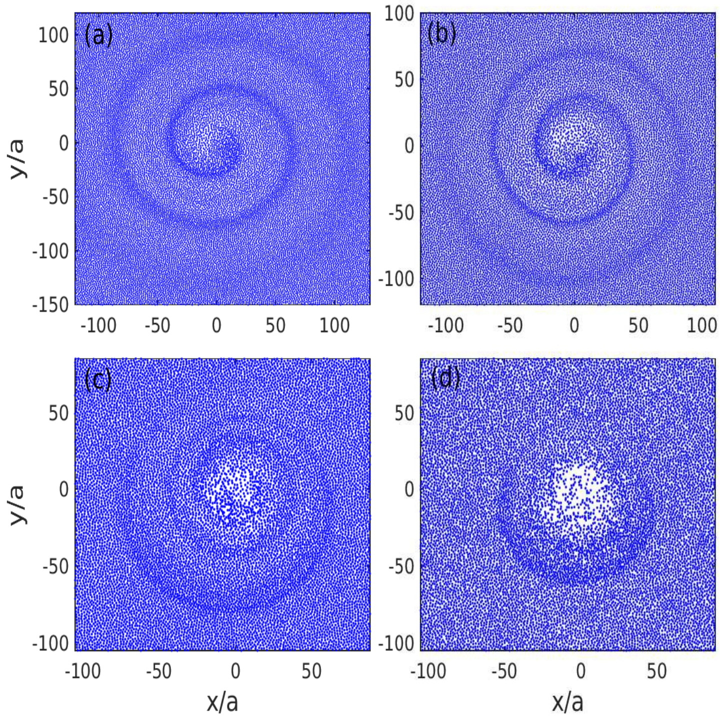

Figure 5.8: Dynamics of spiral waves for different values of screening parameter (a) $\kappa = 0.25$, (b) $\kappa = 0.50$, (c) $\kappa = 1.0$, and (d) $\kappa = 2.0$. Amplitude of driver, period of driver, and coupling parameter for all the plots are $A = 0.203$, $\omega_{pd}T_f = 26.88$, and $\Gamma = 100$, respectively. Snapshot of particles for all the κ are taken at time $\omega_{pd}t = 71.68$.

and (d) of Fig. 5.9). This observation can be understood by realizing that the original dust crystal lattice has hexagonal symmetry. When the value of κ is increased interactions amidst particles gets confined to a few nearest neighbors. In the hexagonal configuration as shown in the schematic of Fig. 5.10, the nearest neighbor distances along the lattice axis are smaller compared to those at lattice diagonal. The asymmetry in the interparticle distance in crystalline phase also influences the radial distribution function (RDF), which shows additional peaks in the distribution, as shown in Fig. 5.11. Furthermore, from Eq. 5.2, it is clear that the radial propagation speed depend on the κ (ratio of interparticle separation to Debye length). Thus, the spiral disturbance propagates faster along lattice axis

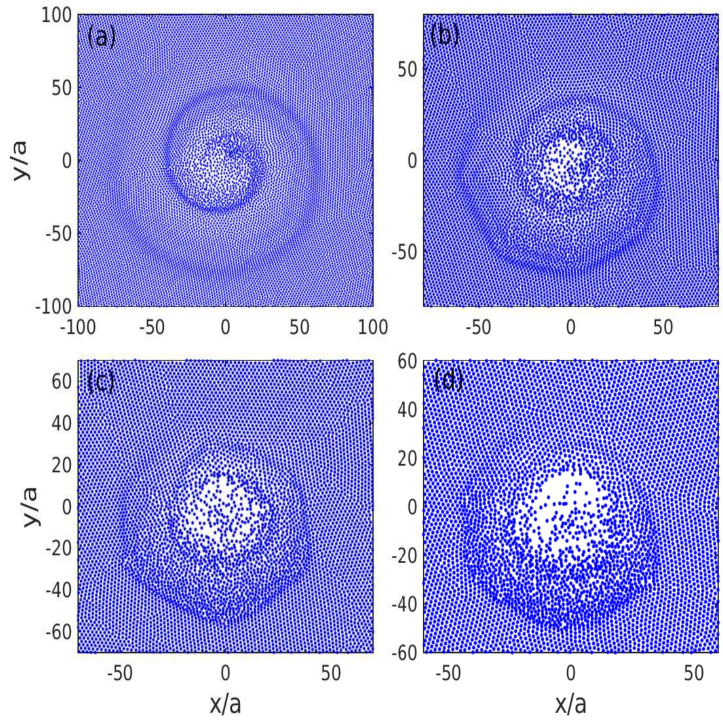

Figure 5.9: Effect of screening parameter (a) $\kappa = 0.5$, (b) $\kappa = 1.0$, (c) $\kappa = 1.5$, and (d) $\kappa = 2.0$ on the spiral structure when dust medium is in crystalline state. Amplitude of driver, period of driver, and coupling parameter for all the plots are $A = 0.203$, $\omega_{pd}T_f = 26.88$, and $\Gamma = 2000$, respectively. Snapshot of particles for all κ are taken at time $\omega_{pd}t = 53.76$.

(in this direction particles are aligned closer) and is slow along lattice diagonal.

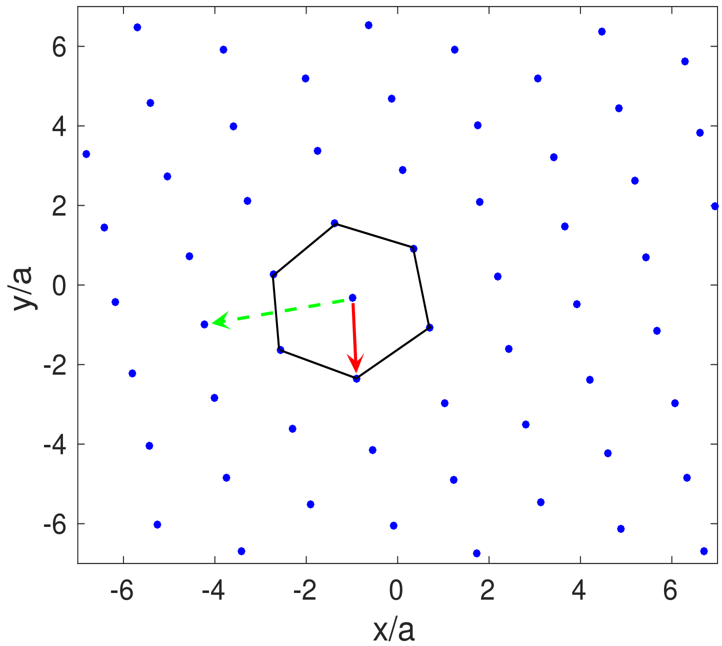

Figure 5.10: Schematic representation of interparticle distance asymmetry when dusty plasma is in crystalline phase. This is the equilibrium snapshot of particles for $\Gamma = 2000$ and $\kappa = 1.5$. Solid and dotted arrows depict the lattice axial and diagonal directions, respectively in the crystal. Asymmetry in the dust crystal spacing have also shown experimentally by J. H. Chu and Lin I [5].

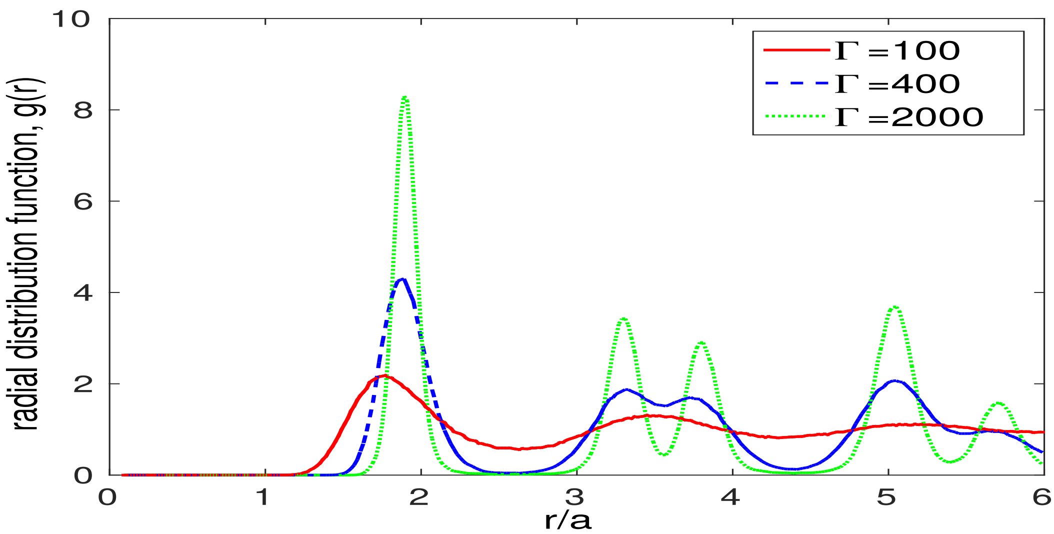

Figure 5.11: Radial distribution function (RDF) for three $\Gamma = 100, 400, 2000$ are shown here. Screening parameter (κ) for all Γ are 1.5. At $\Gamma = 2000$, appearance of one more peak near the second peak (peak comes just after sharp first peak) confirms the anisotropy in the interparticle distance of hexagonal crystal.

5.4 Conclusion

We have carried out the MD simulations for dusty plasma medium in the presence of forcing due to an external rotating electric field. We observe the formation of spiral waves. This ascertains that the dusty plasma behaves like an excitable medium. The radial propagation is governed by the dust acoustic speed and the rotation gets decided by the forcing period. The interplay between the two decides the spiral wave structure. For distinctly clear spiral to form a proper combination of the two is essential. In case the radial propagation is too slow the rings diffuse amongst each other and the spiral structure is not so distinctive. The parametric dependence is consistent with the continuum study carried out by Kumar et al. [173] wherein the dusty plasma was considered as a visco-elastic fluid.

Further, we have shown that there are additional features which emerge when the discrete particle effects are taken into account using MD simulations. For instance, when the amplitude of forcing is high the particles at the center get heated by acquiring random thermal velocity. This in turn effects the spacing of subsequent rings. Furthermore, a large amplitude forcing throws the particle out of the external forcing regime. The restoring force to bring the particles back at the center would, however, depends on the interparticle interaction. When κ is chosen high the shielding range is small and this restoring effects reduces. Thus for high amplitude and high κ the central region where external forcing has been chosen to be finite becomes devoid of particles. The spiral then fails to form adequately.

Another interesting feature that has been observed when the dust medium is in 2-D hexagonal crystalline state. In this case for high values of κ (for which the interparticle potential gets very weak) only a few neighboring particles participate in interactions. The spiral waveform in such cases has a hexagonal front. This can be understood by realizing that for a hexagonal lattice the nearest neighbors separation along different directions varies as has been illustrated by the schematic of Fig. 5.10. Thus, there is an anisotropy in the medium and the radial propagation speed to be dependent on the strength of nearest neighbor interaction.

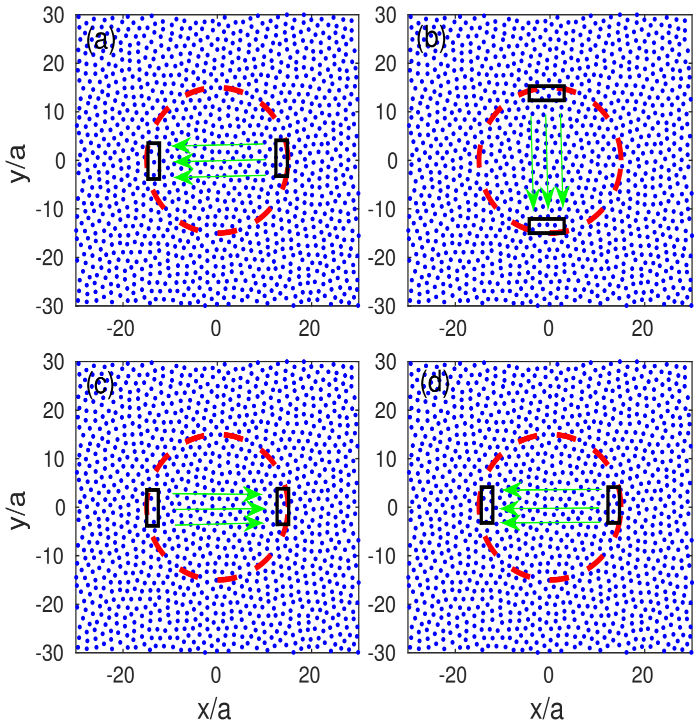

Figure 5.12: Schematic representation of the suggested experimental system. Rectangular black regions on circumference of the circle represents the two prongs of the fork and arrows depicts the direction of electric field. Plots (a), (b), (c), and (d) shows the spatial location of the fork at time 0.0, $T_f/4$, $T_f/2$ and T_f, respectively. where, T_f is the time period of rotation of the fork.

It is our firm belief that spiral waves as observed in our simulation could also be observed in experiments related to systems like dusty plasmas, e-i plasmas, colloids, and condensed matter. There have been recent dusty plasma experiments where rotating electric fields of the kind used in this chapter has been applied over the entire system [166, 182]. However, to have the force in a limited region of the experiment, as desired for the spiral wave excitations can turn out to be quite challenging. We feel that one possible solution could be to insert a probe which bifurcates as a tuning fork at its other end. A potential difference can then be applied between the two prongs of the fork. The rest of the structure can be insulated. This fork can then be rotated mechanically in time. This will produce a electric field over a rectangular strip which spans a circular region with time and serving as REF as shown in Fig 5.12. For numerical ease, we had chosen a fixed circular patch region where the REF was finite all throughout time. However, we feel that the experimentalists will be in a better position to improvise and come up with an appropriate solution for this particular requirement.

6

Conclusion and future scope

6.1 Salient features of this thesis

In this thesis, we have carried out detailed simulation studies on linear and non-linear collective structures in a two-dimensional strongly coupled dusty plasmas. The collective structures provide an important insights into the dynamics and evolution of dusty plasmas. Due to longer response time (10 to 100's of milliseconds) and length (100's of micrometer) scales strongly coupled dusty (complex) plasmas provide a model system to study generic phenomena such as self-organization, transport, phase transitions, waves, structures and instabilities at the individual particle level. These phenomena are also common in the multidisciplinary field of science.

In this thesis, for the study of collective structures, we have carried out both fluid (continuum) and MD (kinetic) simulations. In the fluid simulation, we have considered dusty plasma as a visco-elastic fluid which is governed/modeled by the phenomenological Generalized-Hydrodynamics (GHD) model [16]. Visco-elastic fluid can have both fluid-like viscous as well as solid-like elastic traits, wherein it preserves the memory of its past configurations for some time. This memory develops in the dusty plasma with increased correlation among dust grains. Use of fluid model missed out the particle behavior of the medium. To take care of kinetic behavior of particles, we have carried out MD simulations. In the MD simulation, Yukawa inter-particle electrostatic interaction has been taken among dust species which mimics screening due to the presence of free electrons and ions among dust particles. Collective structures investigated in this thesis yield in the medium due to the presence of interaction among dust particles. In particular, the investigation is focused on the KdV soliton and multisoliton formation and their interaction. We have also investigated the excitation and dynamics of spiral waves (structures). These collective structure studies have relevance in the multidisciplinary field of science viz. ultracold plasmas, warm dense matter, regular liquids, charged colloids, polymers, electrolytes, condensed matter, and biological systems. These studies have been described in the various chapters of the thesis. Here in the subsequent section, we summarize important observations made in this thesis and also the future scope of this thesis.

In chapter 3, we have studied the KdV solitons in complex plasmas using molecular-dynamics simulations. we have applied an electric field perturbation of the experimental situation [45, 47, 48] to excite the solitonic structures. The collective response of the dust particles to such an applied electric field impulse gives an excitation of a compressible dust density pulse. This density structure propagates in one direction along with a train of negative perturbed rarefactive density oscillations (dispersive wave) in the opposite direction. We have also shown that by increasing the strength of electric field impulse, the amplitude of the solitonic structure increases and above a threshold, it split in the form of multiple solitons. Further, We have shown that by increasing the coupling parameter of the medium, the amplitude of the solitonic structures increases while their width decreases. We have also shown that with an increase in the neutral drag on the dust particles the amplitude of the solitonic structures decreases and its width decreases. We have carried out collisional interaction of these solitonic structures in many different configurations. As expected we have found that the phase shift is more in overtaking collision compared to head-on collision. Furthermore, it is observed that the phase shifts in the collisional interaction decrease with the increasing amplitude of the colliding solitonic structures.

In Chapter 4, We have studied a novel non-linear two-dimensional structure in dusty plasma using fluid simulations. This is essentially the observation of spiral wave excitation in dusty plasma medium. Spiral waves are ubiquitous structures found in a wide range of natural and laboratory scenario. In this chapter, the spatiotemporal development of spiral waves in the context of weak and strong coupling limits has been shown. While the weakly coupled medium has been represented by a simple charged fluid description, for strong coupling, a generalized hydrodynamic visco-elastic fluid [16] description has been employed. The medium has been driven by an external force in the form of a rotating electric field which is applied in a small circular region. It is shown that when the amplitude of force is small, the density perturbations in the medium are also small. In this case, the excitations do not develop as a spiral wave. Only when the amplitude of force is high so as to drive the density perturbations to nonlinear amplitudes does the spiral density wave formation occurs. We have found that the number of rings in the spiral pattern at a given time is proportional to the number of rotations made by the external forcing. Thus, if frequency of the driver is high then number of rings is also high. The radial propagation speed of the spiral is equal to the acoustic speed of the medium. The interplay between the acoustic speed of medium and frequency of forcing decides the spiral structure. In the simple charged dust fluid (that has no memory), with increasing shear viscosity η the source of vorticity diffuses out. On the other hand in visco-elastic fluids, an additional traverse shear wave (TSW) generated from the forcing region. Thus, in our studies the expansion of this wave increases with an increase in the strong coupling (the ratio of η and τ_m) of the medium because its velocity is equal to $\sqrt{\eta/\tau_m}$.

In chapter 5, the excitation of spiral waves in the context of driven two-dimensional dusty plasma (Yukawa system) has been demonstrated at the particle level using molecular-dynamics (MD) simulations. The spatiotemporal evolution of these spiral waves has been characterized as a function of the frequency and amplitude of the driving force and dust neutral collisions. The radial propagation of the spiral waves is governed by the dust lattice speed and the rotation gets decided by the forcing period. The interplay between the two decides the spiral wave structure. In order to obtain a distinctly clear spiral, a proper combination of the two is essential. The parametric dependence is consistent with the continuum study carried out in Chapter 4 wherein the dusty plasma has considered as a visco-elastic fluid.

Further, we have shown that there are additional features which emerge when the discrete particle effects are taken into account using MD simulations. For instance, when the amplitude of force is high the particles at the center get heated by acquiring random thermal velocity. This, in turn, affects the spacing of subsequent rings and collective spiral structure. Furthermore, a large amplitude forcing throws the particle out of the external forcing regime. The restoring force to bring the particles back at the center would, however, depends on the interparticle interaction. When κ is chosen high the shielding range is small and this restoring effect reduced. Thus, for high amplitude and high κ the central region where external forcing has been chosen to be finite becomes devoid of particles. The spiral then fails to form adequately. Another interesting feature that has been observed when the dust medium is in two-dimensional hexagonal crystalline state. In this case for high values of κ (for which the interparticle potential gets very weak) only a few neighboring particles participate in the interactions. The spiral waveform in such cases has a hexagonal front. This can be understood by realizing that for a hexagonal symmetric crystal (triangular lattice) the nearest neighbors separation along different directions are different. Therefore, there is an anisotropy in the radial propagation speed along the lattice axis and lattice diagonal direction and which leads to the formation of a hexagonal waveform.

6.2 Future scope

In the following, we provide some future possible studies that can be carried out from the extension of this thesis work:

- The possibility of reflection of the KdV soliton in the head-on collision can be studied. The ion flow on the propagation of KdV soliton can also be studied in the future.

- Analytical modeling of the spiral wave structure needs to be carried out.

- Investigation and study of coherent structures in three dimensions needs to be investigated.

- The presence of ion flow in dusty plasma medium is important in the experiments. Therefore, inclusion of the effect of ion drag in the simulations might change the collective structures and lead to much closer to experimental situations. One can perform such studies using molecular-dynamics (MD) or particle-in-cell (PIC) simulations.

- Experimental investigations of dusty plasmas in the presence of magnetic field are carried out in a number of laboratories [184–188]. In some cases the strength of magnetic field is chosen to be of the order 2.5 Tesla to magnetize the dusty plasma medium. Keeping this in view it would be of interest to pursue simulation and analytical studies in the context of magnetized dusty plasma medium.

Bibliography

[1] P. Hartmann, G. J. Kalman, Z. Donkó, and K. Kutasi. Equilibrium properties and phase diagram of two-dimensional yukawa systems. *Phys. Rev. E*, 72:026409, Aug 2005.

[2] S. Hamaguchi, R. T. Farouki, and D. H. E. Dubin. Triple point of yukawa systems. *Phys. Rev. E*, 56:4671–4682, Oct 1997.

[3] Bin Liu, J. Goree, and O. S. Vaulina. Test of the stokes-einstein relation in a two-dimensional yukawa liquid. *Phys. Rev. Lett.*, 96:015005, Jan 2006.

[4] Sanat Kumar Tiwari, Amita Das, Abhijit Sen, and Predhiman Kaw. Molecular dynamics simulations of soliton-like structures in a dusty plasma medium. *Physics of Plasmas*, 22(3), 2015.

[5] J. H. Chu and Lin I. Direct observation of coulomb crystals and liquids in strongly coupled rf dusty plasmas. *Phys. Rev. Lett.*, 72:4009–4012, Jun 1994.

[6] Goertz C. K. Dusty plasmas in the solar system. *Reviews of Geophysics*, 27(2):271–292.

[7] J Winter. Dust in fusion devices - experimental evidence, possible sources and consequences. *Plasma Physics and Controlled Fusion*, 40(6):1201, 1998.

[8] P.K. Shukla and A.A. Mamun. *Introduction to Dusty Plasma Physics*. Series in Plasma Physics. CRC Press, 2015.

[9] G. S. Selwyn, J. Singh, and R. S. Bennett. In situ laser diagnostic studies of plasmaâĂŘgenerated particulate contamination. *Journal of Vacuum Science & Technology A*, 7(4):2758–2765, 1989.

[10] Pere Roca i Cabarrocas, Patrick Gay, and Aomar Hadjadj. Experimental evidence for nanoparticle deposition in continuous argonâĂŞsilane plasmas: Effects of silicon nanoparticles on film properties. *Journal of Vacuum Science & Technology A*, 14(2):655–659, 1996.

[11] L Boufendi, M Ch Jouanny, E Kovacevic, J Berndt, and M Mikikian. Dusty plasma for nanotechnology. *Journal of Physics D: Applied Physics*, 44(17):174035, 2011.

[12] Gregor E. Morfill and Alexei V. Ivlev. Complex plasmas: An interdisciplinary research field. *Rev. Mod. Phys.*, 81:1353–1404, Oct 2009.

[13] A. Melzer, A. Homann, and A. Piel. Experimental investigation of the melting transition of the plasma crystal. *Phys. Rev. E*, 53:2757–2766, Mar 1996.

[14] H. Thomas, G. E. Morfill, V. Demmel, J. Goree, B. Feuerbacher, and D. Möhlmann. Plasma crystal: Coulomb crystallization in a dusty plasma. *Phys. Rev. Lett.*, 73:652–655, Aug 1994.

[15] D. Samsonov, S. K. Zhdanov, R. A. Quinn, S. I. Popel, and G. E. Morfill. Shock melting of a two-dimensional complex (dusty) plasma. *Phys. Rev. Lett.*, 92:255004, Jun 2004.

[16] P. K. Kaw and A. Sen. Low frequency modes in strongly coupled dusty plasmas. *Physics of Plasmas*, 5(10):3552–3559, 1998.

[17] P. K. Kaw. Collective modes in a strongly coupled dusty plasma. *Physics of Plasmas*, 8(5):1870–1878, 2001.

[18] A. Diaw and M. S. Murillo. Generalized hydrodynamics model for strongly coupled plasmas. *Phys. Rev. E*, 92:013107, Jul 2015.

[19] G. Kalman and K. I. Golden. Response function and plasmon dispersion for strongly coupled coulomb liquids. *Phys. Rev. A*, 41:5516–5527, May 1990.

[20] Kenneth I. Golden and Gabor J. Kalman. Quasilocalized charge approximation in strongly coupled plasma physics. *Physics of Plasmas*, 7(1):14–32, 2000.

[21] M. Rosenberg and G. Kalman. Dust acoustic waves in strongly coupled dusty plasmas. *Phys. Rev. E*, 56:7166–7173, Dec 1997.

[22] G. J. Kalman, P. Hartmann, Z. Donkó, and M. Rosenberg. Two-dimensional yukawa liquids: Correlation and dynamics. *Phys. Rev. Lett.*, 92:065001, Feb 2004.

[23] G. Kalman, M. Rosenberg, and H. E. DeWitt. Collective modes in strongly correlated yukawa liquids: Waves in dusty plasmas. *Phys. Rev. Lett.*, 84:6030–6033, Jun 2000.

[24] J. P. Boeuf. Characteristics of a dusty nonthermal plasma from a particle-in-cell monte carlo simulation. *Phys. Rev. A*, 46:7910–7922, Dec 1992.

[25] Giovanni Lapenta. Simulation of charging and shielding of dust particles in drifting plasmas. *Physics of Plasmas*, 6(5):1442–1447, 1999.

[26] Patrick Ludwig, Wojciech J Miloch, Hanno KÃďhlert, and Michael Bonitz. On the wake structure in streaming complex plasmas. *New Journal of Physics*, 14(5):053016, 2012.

[27] Heng Zhang, Xin Qi, Wen-Shan Duan, and Lei Yang. Envelope solitary waves exist and collide head-on without phase shift in a dusty plasma. *Scientific Reports*, 5:14239 EP –, Sep 2015. Article.

[28] K. Quest, M. Rosenberg, B. Kercher, and M. Dutreix. Simulations of the dust acoustic instability in a collisional plasma with warm dust. *Journal of Plasma Physics*, 82(6):905820602, 2016.

[29] K. Quest, M. Rosenberg, and B. Kercher. Simulations of the ionâĂŞdust streaming instability with non-maxwellian ions. *Journal of Plasma Physics*, 83(6):905830612, 2017.

[30] M. Rosenberg. Ion- and dust-acoustic instabilities in dusty plasmas. *Planetary and Space Science*, 41(3):229 – 233, 1993.

[31] S. M. Hosseini Jenab, I. Kourakis, and H. Abbasi. Fully kinetic simulation of ion acoustic and dust-ion acoustic waves. *Physics of Plasmas*, 18(7):073703, 2011.

[32] K. I. Golden, G. J. Kalman, and L. G. Silvestri. Is the Vlasov equation valid for Yukawa plasmas? *ArXiv e-prints*, June 2018.

[33] N.N. Rao, P.K. Shukla, and M.Y. Yu. Dust-acoustic waves in dusty plasmas. *Planetary and Space Science*, 38(4):543 – 546, 1990.

[34] A. Barkan, R. L. Merlino, and N. DâĂŹAngelo. Laboratory observation of the dustâĂŘacoustic wave mode. *Physics of Plasmas*, 2(10):3563–3565, 1995.

[35] Frank Melandso/. Lattice waves in dust plasma crystals. *Physics of Plasmas*, 3(11):3890–3901, 1996.

[36] B Farokhi, P.K Shukla, N.L Tsintsadze, and D.D Tskhakaya. Linear and nonlinear dust lattice waves in plasma crystals. *Physics Letters A*, 264(4):318 – 323, 1999.

[37] D. Samsonov, A. V. Ivlev, R. A. Quinn, G. Morfill, and S. Zhdanov. Dissipative longitudinal solitons in a two-dimensional strongly coupled complex (dusty) plasma. *Phys. Rev. Lett.*, 88:095004, Feb 2002.

[38] S. K. Zhdanov, D. Samsonov, and G. E. Morfill. Anisotropic plasma crystal solitons. *Phys. Rev. E*, 66:026411, Aug 2002.

[39] Popel S. I. and Yu M. Y. Ion acoustic solitons in impurity-containing plasmas. *Contributions to Plasma Physics*, 35(2):103–108.

[40] S. I. Popel, A. P. Golub', T. V. Losseva, A. V. Ivlev, S. A. Khrapak, and G. Morfill. Weakly dissipative dust-ion-acoustic solitons. *Phys. Rev. E*, 67:056402, May 2003.

[41] Y. Nakamura and A. Sarma. Observation of ion-acoustic solitary waves in a dusty plasma. *Physics of Plasmas*, 8(9):3921–3926, 2001.

[42] A. A. Mamun and P. K. Shukla. Cylindrical and spherical dust ionâĂŞacoustic solitary waves. *Physics of Plasmas*, 9(4):1468–1470, 2002.

[43] Ju-Kui Xue. Head-on collision of dust-acoustic solitary waves. *Phys. Rev. E*, 69:016403, Jan 2004.

[44] S. Jaiswal, P. Bandyopadhyay, and A. Sen. Theoretical study of head-on collision of dust acoustic solitary waves in a strongly coupled complex plasma. *Physics of Plasmas*, 21(5):053701, 2014.

[45] T. E. Sheridan, V. Nosenko, and J. Goree. Experimental study of nonlinear solitary waves in two-dimensional dusty plasma. *Physics of Plasmas*, 15(7):073703, 2008.

[46] K. Avinash, P. Zhu, V. Nosenko, and J. Goree. Nonlinear compressional waves in a two-dimensional yukawa lattice. *Phys. Rev. E*, 68:046402, Oct 2003.

[47] P. Bandyopadhyay, G. Prasad, A. Sen, and P. K. Kaw. Experimental study of nonlinear dust acoustic solitary waves in a dusty plasma. *Phys. Rev. Lett.*, 101:065006, Aug 2008.

[48] S. K. Sharma, A. Boruah, and H. Bailung. Head-on collision of dust-acoustic solitons in a strongly coupled dusty plasma. *Phys. Rev. E*, 89:013110, Jan 2014.

[49] B. M. Veeresha, S. K. Tiwari, A. Sen, P. K. Kaw, and A. Das. Nonlinear wave propagation in strongly coupled dusty plasmas. *Phys. Rev. E*, 81:036407, Mar 2010.

[50] P Bandyopadhyay, U Konopka, S A Khrapak, G E Morfill, and A Sen. Effect of polarization force on the propagation of dust acoustic solitary waves. *New Journal of Physics*, 12(7):073002, 2010.

[51] Sanat Kumar Tiwari, Amita Das, Predhiman Kaw, and Abhijit Sen. Observation of sharply peaked solitons in dusty plasma simulations. *New Journal of Physics*, 14(6):063008, 2012.

[52] Surabhi Jaiswal, P. Bandyopadhyay, and A. Sen. Experimental observation of precursor solitons in a flowing complex plasma. *Phys. Rev. E*, 93:041201, Apr 2016.

[53] S. Jaiswal, P. Bandyopadhyay, and A. Sen. Experimental investigation of flow induced dust acoustic shock waves in a complex plasma. *Physics of Plasmas*, 23(8):083701, 2016.

[54] V. V. Yaroshenko, H. M. Thomas, and G. E. Morfill. Dust density waves in a complex plasma layer. *Physics of Plasmas*, 14(8):082104, 2007.

[55] Robert L. Merlino. Dust-acoustic waves driven by an ion-dust streaming instability in laboratory discharge dusty plasma experiments. *Physics of Plasmas*, 16(12):124501, 2009.

[56] T. M. Flanagan and J. Goree. Development of nonlinearity in a growing self-excited dust-density wave. *Physics of Plasmas*, 18(1):013705, 2011.

[57] Heng Zhang, Wen-Shan Duan, Xin Qi, and Lei Yang. Head-on collision and overtaking collision between an envelope solitary wave and a kdv solitary wave in a dusty plasma. *Scientific Reports*, 6:21214, Feb 2016.

[58] F. MelandsÃÿ and P.K. Shukla. Theory of dust-acoustic shocks. *Planetary and Space Science*, 43(5):635 – 648, 1995.

[59] S. I. Popel, M. Y. Yu, and V. N. Tsytovich. Shock waves in plasmas containing variableâĂŘcharge impurities. *Physics of Plasmas*, 3(12):4313–4315, 1996.

[60] P. K. Shukla and A. A. Mamun. Dust-acoustic shocks in a strongly coupled dusty plasma. *IEEE Transactions on Plasma Science*, 29(2):221–225, Apr 2001.

[61] Sumita K. Sharma, A. Boruah, Y. Nakamura, and H. Bailung. Observation of dust acoustic shock wave in a strongly coupled dusty plasma. *Physics of Plasmas*, 23(5):053702, 2016.

[62] B. Eliasson and P. K. Shukla. Dust acoustic shock waves. *Phys. Rev. E*, 69:067401, Jun 2004.

[63] P K Shukla and A A Mamun. Solitons, shocks and vortices in dusty plasmas. *New Journal of Physics*, 5(1):17, 2003.

[64] Q.-Z. Luo, N. DâĂŹAngelo, and R. L. Merlino. Experimental study of shock formation in a dusty plasma. *Physics of Plasmas*, 6(9):3455–3458, 1999.

[65] D. Samsonov, G. Morfill, H. Thomas, T. Hagl, H. Rothermel, V. Fortov, A. Lipaev, V. Molotkov, A. Nefedov, O. Petrov, A. Ivanov, and S. Krikalev. Kinetic measurements of shock wave propagation in a three-dimensional complex (dusty) plasma. *Phys. Rev. E*, 67:036404, Mar 2003.

[66] V. E. Fortov, O. F. Petrov, V. I. Molotkov, M. Y. Poustylnik, V. M. Torchinsky, V. N. Naumkin, and A. G. Khrapak. Shock wave formation in a dc glow discharge dusty plasma. *Phys. Rev. E*, 71:036413, Mar 2005.

[67] J. Heinrich, S.-H. Kim, and R. L. Merlino. Laboratory observations of self-excited dust acoustic shocks. *Phys. Rev. Lett.*, 103:115002, Sep 2009.

[68] D. Samsonov, J. Goree, H. M. Thomas, and G. E. Morfill. Mach cone shocks in a two-dimensional yukawa solid using a complex plasma. *Phys. Rev. E*, 61:5557–5572, May 2000.

[69] Shukla P. K., Yu M. Y., and Bharuthram R. Linear and nonlinear dust drift waves. *Journal of Geophysical Research: Space Physics*, 96(A12):21343–21346.

[70] Akira Hasegawa and P.K. Shukla. Dust vortex modes in a nonuniform dusty plasma. *Physics Letters A*, 332(1):82 – 85, 2004.

[71] P K Shukla and A A Mamun. Solitons, shocks and vortices in dusty plasmas. *New Journal of Physics*, 5(1):17, 2003.

[72] A. Piel, V. Nosenko, and J. Goree. Experiments and molecular-dynamics simulation of elastic waves in a plasma crystal radiated from a small dipole source. *Phys. Rev. Lett.*, 89:085004, Aug 2002.

[73] M. R. Akdim and W. J. Goedheer. Modeling of self-excited dust vortices in complex plasmas under microgravity. *Phys. Rev. E*, 67:056405, May 2003.

[74] Mangilal Choudhary, S. Mukherjee, and P. Bandyopadhyay. Experimental observation of self excited co-rotating multiple vortices in a dusty plasma with inhomogeneous plasma background. *Physics of Plasmas*, 24(3):033703, 2017.

[75] Manjit Kaur, Sayak Bose, P. K. Chattopadhyay, D. Sharma, J. Ghosh, Y. C. Saxena, and Edward Thomas Jr. Generation of multiple toroidal dust vortices by a non-monotonic density gradient in a direct current glow discharge plasma. *Physics of Plasmas*, 22(9):093702, 2015.

[76] M. Klindworth, A. Melzer, A. Piel, and V. A. Schweigert. Laser-excited intershell rotation of finite coulomb clusters in a dusty plasma. *Phys. Rev. B*, 61:8404–8410, Mar 2000.

[77] U. Konopka, D. Samsonov, A. V. Ivlev, J. Goree, V. Steinberg, and G. E. Morfill. Rigid and differential plasma crystal rotation induced by magnetic fields. *Phys. Rev. E*, 61:1890–1898, Feb 2000.

[78] Yoshifumi Saitou and Osamu Ishihara. Dynamic circulation in a complex plasma. *Phys. Rev. Lett.*, 111:185003, Nov 2013.

[79] Predhiman K. Kaw, Kyoji Nishikawa, and Noriyoshi Sato. Rotation in collisional strongly coupled dusty plasmas in a magnetic field. *Physics of Plasmas*, 9(2):387–390, 2002.

[80] Vikram Singh Dharodi, Sanat Kumar Tiwari, and Amita Das. Visco-elastic fluid simulations of coherent structures in strongly coupled dusty plasma medium. *Physics of Plasmas*, 21(7), 2014.

[81] O. Havnes, T. Aslaksen, T. W. Hartquist, F. Li, F. MelandsÃÿ, G. E. Morfill, and T. Nitter. Probing the properties of planetary ring dust by the observation of mach cones. *Journal of Geophysical Research: Space Physics*, 100(A2):1731–1734.

[82] D. Samsonov, J. Goree, Z. W. Ma, A. Bhattacharjee, H. M. Thomas, and G. E. Morfill. Mach cones in a coulomb lattice and a dusty plasma. *Phys. Rev. Lett.*, 83:3649–3652, Nov 1999.

[83] A. Melzer, S. Nunomura, D. Samsonov, Z. W. Ma, and J. Goree. Laser-excited mach cones in a dusty plasma crystal. *Phys. Rev. E*, 62:4162–4176, Sep 2000.

[84] V. Nosenko, J. Goree, Z. W. Ma, and A. Piel. Observation of shear-wave mach cones in a 2d dusty-plasma crystal. *Phys. Rev. Lett.*, 88:135001, Mar 2002.

[85] S. Khrapak, D. Samsonov, G. Morfill, H. Thomas, V. Yaroshenko, H. Rothermel, T. Hagl, V. Fortov, A. Nefedov, V. Molotkov, O. Petrov, A. Lipaev, A. Ivanov, and Y. Baturin. Compressional waves in complex (dusty) plasmas under microgravity conditions. *Physics of Plasmas*, 10(1):1–4, 2003.

[86] Mierk Schwabe, Sergey K Zhdanov, Hubertus M Thomas, Alexei V Ivlev, Milenko Rubin-Zuzic, Gregor E Morfill, Vladimir I Molotkov, Andrey M Lipaev, Vladimir E Fortov, and Thomas Reiter. Nonlinear waves externally excited in a complex plasma under microgravity conditions. *New Journal of Physics*, 10(3):033037, 2008.

[87] A Usachev, A Zobnin, O Petrov, V Fortov, M H Thoma, H HÃűfner, M Fink, A Ivlev, and G Morfill. Externally excited planar dust acoustic shock waves in a strongly coupled dusty plasma under microgravity conditions. *New Journal of Physics*, 16(5):053028, 2014.

[88] M. Gedalin, T. C. Scott, and Y. B. Band. Optical solitary waves in the higher order nonlinear schrödinger equation. *Phys. Rev. Lett.*, 78:448–451, Jan 1997.

[89] Hermann A. Haus and William S. Wong. Solitons in optical communications. *Rev. Mod. Phys.*, 68:423–444, Apr 1996.

[90] Stephane Barland, Jorge R. Tredicce, Massimo Brambilla, Luigi A. Lugiato, Salvador Balle, Massimo Giudici, Tommaso Maggipinto, Lorenzo Spinelli,

Giovanna Tissoni, Thomas Knodl, Michael Miller, and Roland Jager. Cavity solitons as pixels in semiconductor microcavities. *Nature*, 419(6908):699–702, Oct 2002.

[91] A.L. New and R.D. Pingree. Large-amplitude internal soliton packets in the central bay of biscay. *Deep Sea Research Part A. Oceanographic Research Papers*, 37(3):513 – 524, 1990.

[92] N. J. Zabusky and M. D. Kruskal. Interaction of "solitons" in a collisionless plasma and the recurrence of initial states. *Phys. Rev. Lett.*, 15:240–243, Aug 1965.

[93] M Q Tran. Ion acoustic solitons in a plasma: A review of their experimental properties and related theories. *Physica Scripta*, 20(3-4):317, 1979.

[94] P. K. Shukla and B. Eliasson. Nonlinear dynamics of large-amplitude dust acoustic shocks and solitary pulses in dusty plasmas. *Phys. Rev. E*, 86:046402, Oct 2012.

[95] Steve Plimpton. Fast parallel algorithms for short-range molecular dynamics. *Journal of Computational Physics*, 117(1):1 – 19, 1995.

[96] M. Schwabe and D. B. Graves. Simulating the dynamics of complex plasmas. *Phys. Rev. E*, 88:023101, Aug 2013.

[97] Bin Liu and J. Goree. Determination of yield stress of 2d (yukawa) dusty plasma. *Physics of Plasmas*, 24(10):103702, 2017.

[98] BURKHARD DÃIJNWEG and WOLFGANG PAUL. Brownian dynamics simulations without gaussian random numbers. *International Journal of Modern Physics C*, 02(03):817–827, 1991.

[99] V. Nosenko and J. Goree. Shear flows and shear viscosity in a two-dimensional yukawa system (dusty plasma). *Phys. Rev. Lett.*, 93:155004, Oct 2004.

[100] I. Laut, C. Räth, L. Wörner, V. Nosenko, S. K. Zhdanov, J. Schablinski, D. Block, H. M. Thomas, and G. E. Morfill. Network analysis of three-dimensional complex plasma clusters in a rotating electric field. *Phys. Rev. E*, 89:023104, Feb 2014.

[101] Jiang-Xing Chen, Hong Zhang, and You-Quan Li. Drift of spiral waves controlled by a polarized electric field. *The Journal of Chemical Physics*, 124(1):014505, 2006.

[102] M. S. Murillo. Critical wave vectors for transverse modes in strongly coupled dusty plasmas. *Phys. Rev. Lett.*, 85:2514–2517, Sep 2000.

[103] Setsuo Ichimaru, Hiroshi Iyetomi, and Shigenori Tanaka. Statistical physics of dense plasmas: Thermodynamics, transport coefficients and dynamic correlations. *Physics Reports*, 149(2):91 – 205, 1987.

[104] Amita Das and Predhiman Kaw. Suppression of rayleigh taylor instability in strongly coupled plasmas. *Physics of Plasmas*, 21(6):062102, 2014.

[105] J. P. Boris, A. M. Landsberg, E. S. Oran, and J. H. Gardner. In *LCPFCT - A Flux-Corrected Transport Algorithm for Solving Generalized Continuity Equations. NRL Memorandum Report 93-7192*. 1993.

[106] William T. Vetterling, Saul A. Teukolsky, and William H. Press. *Numerical Recipes: Example Book (FORTRAN)*. Cambridge University Press, New York, NY, USA, 2nd edition, 1992.

[107] Hitendra K. Malik, Ravinder Kumar, Karl E. Lonngren, and Yasushi Nishida. Collision of ion acoustic solitary waves in a magnetized plasma: Effect of dust grains and trapped electrons. *Phys. Rev. E*, 92:063107, Dec 2015.

[108] Sita Sundar, Amita Das, Vikrant Saxena, Predhiman Kaw, and Abhijit Sen. Relativistic electromagnetic flat top solitons and their stability. *Physics of Plasmas*, 18(11):112112, 2011.

[109] S. Poornakala, A. Das, A. Sen, and P. K. Kaw. Laser envelope solitons in cold overdense plasmas. *Physics of Plasmas*, 9(5):1820–1823, 2002.

[110] P. K. Kaw, A. Sen, and T. Katsouleas. Nonlinear 1d laser pulse solitons in a plasma. *Phys. Rev. Lett.*, 68:3172–3175, May 1992.

[111] Zachariah Sinkala. Soliton/exciton transport in proteins. *Journal of Theoretical Biology*, 241(4):919 – 927, 2006.

[112] A. J. Heeger, S. Kivelson, J. R. Schrieffer, and W. P. Su. Solitons in conducting polymers. *Rev. Mod. Phys.*, 60:781–850, Jul 1988.

[113] S.I. Popel, S.I. Kopnin, I.N. Kosarev, and M.Y. Yu. Solitons in earthâĂŹs dusty mesosphere. *Advances in Space Research*, 37(2):414 – 419, 2006. Thermospheric-Ionospheric-Geospheric(TIGER)Symposium.

[114] P. G. Drazin. Solitons. In I. M. James, editor, *London Mathematical Society Lecture Note Series*, pages 1–62. Cambridge University Press, Oxford, 1983.

[115] J. X. Ma and Jinyuan Liu. Dust-acoustic soliton in a dusty plasma. *Physics of Plasmas*, 4(2):253–255, 1997.

[116] R. Heidemann, S. Zhdanov, R. Sütterlin, H. M. Thomas, and G. E. Morfill. Dissipative dark soliton in a complex plasma. *Phys. Rev. Lett.*, 102:135002, Mar 2009.

[117] T. K. Baluku, M. A. Hellberg, I. Kourakis, and N. S. Saini. Dust ion acoustic solitons in a plasma with kappa-distributed electrons. *Physics of Plasmas*, 17(5):053702, 2010.

[118] D. Farina and S. V. Bulanov. Relativistic electromagnetic solitons in the electron-ion plasma. *Phys. Rev. Lett.*, 86:5289–5292, Jun 2001.

[119] J.F. Miramar Blazqez. Application of solitons to the study of laser propagation into a thermonuclear plasma in inertial confinement fusion. *Laser and Particle Beams*, 20(1):153–157, 001 2002.

[120] Amita Das, Vikram Dharodi, and Sanat Tiwari. Collective dynamics in strongly coupled dusty plasma medium. *Journal of Plasma Physics*, 80(6):855–861, 12 2014.

[121] P. Harvey, C. Durniak, D. Samsonov, and G. Morfill. Soliton interaction in a complex plasma. *Phys. Rev. E*, 81:057401, May 2010.

[122] A. Boruah, S. K. Sharma, Y. Nakamura, and H. Bailung. Observation of dust acoustic multi-solitons in a strongly coupled dusty plasma. *Physics of Plasmas*, 23(9), 2016.

[123] U. Konopka, G. E. Morfill, and L. Ratke. Measurement of the interaction potential of microspheres in the sheath of a rf discharge. *Phys. Rev. Lett.*, 84:891–894, Jan 2000.

[124] Z DonkÃş, G J Kalman, and P Hartmann. Dynamical correlations and collective excitations of yukawa liquids. *Journal of Physics: Condensed Matter*, 20(41):413101, 2008.

[125] ShÅńichi NosÃľ. A molecular dynamics method for simulations in the canonical ensemble. *Molecular Physics*, 52(2):255–268, 1984.

[126] William G. Hoover. Canonical dynamics: Equilibrium phase-space distributions. *Phys. Rev. A*, 31:1695–1697, Mar 1985.

[127] Harvey Segur. The korteweg-de vries equation and water waves. solutions of the equation. part 1. *Journal of Fluid Mechanics*, 59(4):721–736, 03 2006.

[128] David W. Aossey, Steven R. Skinner, Jamie L. Cooney, James E. Williams, Matthew T. Gavin, David R. Andersen, and Karl E. Lonngren. Properties of soliton-soliton collisions. *Phys. Rev. A*, 45:2606–2610, Feb 1992.

[129] Frank Verheest, Manfred A. Hellberg, and Willy A. Hereman. Head-on collisions of electrostatic solitons in nonthermal plasmas. *Phys. Rev. E*, 86:036402, Sep 2012.

[130] James P. Keener and John J. Tyson. Spiral waves in the belousov-zhabotinskii reaction. *Physica D: Nonlinear Phenomena*, 21(2-3):307–324, 1986.

[131] Dwight Barkley. Euclidean symmetry and the dynamics of rotating spiral waves. *Phys. Rev. Lett.*, 72:164–167, Jan 1994.

[132] M. Bär and M. Eiswirth. Turbulence due to spiral breakup in a continuous excitable medium. *Phys. Rev. E*, 48:R1635–R1637, Sep 1993.

[133] T. Frisch, S. Rica, P. Coullet, and J. M. Gilli. Spiral waves in liquid crystal. *Phys. Rev. Lett.*, 72:1471–1474, Mar 1994.

[134] Alain Karma. Electrical alternans and spiral wave breakup in cardiac tissue. *Chaos: An Interdisciplinary Journal of Nonlinear Science*, 4(3):461–472, 1994.

[135] Jorge M. Davidenko, Arcady V. Pertsov, Remy Salomonsz, William Baxter, and Jose Jalife. Stationary and drifting spiral waves of excitation in isolated cardiac muscle. *Nature*, 355(6358):349–351, Jan 1992.

[136] Ligang Li, Xinhao Liao, Kit H. Chan, and Keke Zhang. On nonlinear multiarmed spiral waves in slowly rotating fluid systems. *Physics of Fluids*, 22(1):011701, 2010.

[137] D. M. Elmegreen. A near-infrared atlas of spiral galaxies. *The Astrophysical Journal Supplement Series*, 47:229–233, nov 1981.

[138] Volker Springel and Lars Hernquist. Formation of a spiral galaxy in a major merger. *The Astrophysical Journal Letters*, 622(1):L9, 2005.

[139] Erik A. Martens, Carlo R. Laing, and Steven H. Strogatz. Solvable model of spiral wave chimeras. *Phys. Rev. Lett.*, 104:044101, Jan 2010.

[140] Shin-ichiro Shima and Yoshiki Kuramoto. Rotating spiral waves with phase-randomized core in nonlocally coupled oscillators. *Phys. Rev. E*, 69:036213, Mar 2004.

[141] K. Kruse, J. F. Joanny, F. Jülicher, J. Prost, and K. Sekimoto. Asters, vortices, and rotating spirals in active gels of polar filaments. *Phys. Rev. Lett.*, 92:078101, Feb 2004.

[142] S. Clar, K. Schenk, and F. Schwabl. Phase transitions in a forest-fire model. *Phys. Rev. E*, 55:2174–2183, Mar 1997.

[143] Gui-Quan Sun, Zhen Jin, Quan-Xing Liu, and Li Li. Chaos induced by breakup of waves in a spatial epidemic model with nonlinear incidence rate. *Journal of Statistical Mechanics: Theory and Experiment*, 2008(08):P08011, 2008.

[144] Xiaoying Huang, Weifeng Xu, Jianmin Liang, Kentaroh Takagaki, Xin Gao, and Jian young Wu. Spiral wave dynamics in neocortex. *Neuron*, 68(5):978 – 990, 2010.

[145] Vincent Hakim and Alain Karma. Spiral wave meander in excitable media: The large core limit. *Phys. Rev. Lett.*, 79:665–668, Jul 1997.

[146] Richard FitzHugh. Impulses and physiological states in theoretical models of nerve membrane. *Biophysical Journal*, 1(6):445 – 466, 1961.

[147] J. Nagumo, S. Arimoto, and S. Yoshizawa. An active pulse transmission line simulating nerve axon. *Proceedings of the IRE*, 50(10):2061–2070, Oct 1962.

[148] Dwight Barkley, Mark Kness, and Laurette S. Tuckerman. Spiral-wave dynamics in a simple model of excitable media: The transition from simple to compound rotation. *Phys. Rev. A*, 42:2489–2492, Aug 1990.

[149] A.M. Pertsov, E.A. Ermakova, and A.V. Panfilov. Rotating spiral waves in a modified fitz-hugh-nagumo model. *Physica D: Nonlinear Phenomena*, 14(1):117 – 124, 1984.

[150] N.N. Rao, P.K. Shukla, and M.Y. Yu. Dust-acoustic waves in dusty plasmas. *Planetary and Space Science*, 38(4):543 – 546, 1990.

[151] C. Thompson, A. Barkan, N. DâĂŹAngelo, and R. L. Merlino. Dust acoustic waves in a direct current glow discharge. *Physics of Plasmas*, 4(7):2331–2335, 1997.

[152] E. Thomas and R. L. Merlino. Dust particle motion in the vicinity of dust acoustic waves. *IEEE Transactions on Plasma Science*, 29(2):152–157, Apr 2001.

[153] J. B. Pieper and J. Goree. Dispersion of plasma dust acoustic waves in the strong-coupling regime. *Phys. Rev. Lett.*, 77:3137–3140, Oct 1996.

[154] M. Rosenberg and G. Kalman. Dust acoustic waves in strongly coupled dusty plasmas. *Phys. Rev. E*, 56:7166–7173, Dec 1997.

[155] A. Barkan, R. L. Merlino, and N. DâĂŹAngelo. Laboratory observation of the dustâĂŘacoustic wave mode. *Physics of Plasmas*, 2(10):3563–3565, 1995.

[156] J. Pramanik, G. Prasad, A. Sen, and P. K. Kaw. Experimental observations of transverse shear waves in strongly coupled dusty plasmas. *Phys. Rev. Lett.*, 88:175001, Apr 2002.

[157] Amita Das, Vikram Dharodi, and Sanat Tiwari. Collective dynamics in strongly coupled dusty plasma medium. *Journal of Plasma Physics*, 80(6):855âĂŞ861, 2014.

[158] S. Nunomura, D. Samsonov, and J. Goree. Transverse waves in a two-dimensional screened-coulomb crystal (dusty plasma). *Phys. Rev. Lett.*, 84:5141–5144, May 2000.

[159] Sandeep Kumar, Sanat Kumar Tiwari, and Amita Das. Observation of the korteweg-de vries soliton in molecular dynamics simulations of a dusty plasma medium. *Physics of Plasmas*, 24(3):033711, 2017.

[160] Sanat Kumar Tiwari, Amita Das, Predhiman Kaw, and Abhijit Sen. Observation of sharply peaked solitons in dusty plasma simulations. *New Journal of Physics*, 14(6):063008, 2012.

[161] D. Samsonov, S. K. Zhdanov, R. A. Quinn, S. I. Popel, and G. E. Morfill. Shock melting of a two-dimensional complex (dusty) plasma. *Phys. Rev. Lett.*, 92:255004, Jun 2004.

[162] R. Bharuthram and P.K. Shukla. Large amplitude ion-acoustic solitons in a dusty plasma. *Planetary and Space Science*, 40(7):973 – 977, 1992.

[163] Mierk Schwabe, Sergey Zhdanov, Christoph Räth, David B. Graves, Hubertus M. Thomas, and Gregor E. Morfill. Collective effects in vortex movements in complex plasmas. *Phys. Rev. Lett.*, 112:115002, Mar 2014.

[164] E. M. Hollmann, F. Anderegg, and C. F. Driscoll. Confinement and manipulation of non-neutral plasmas using rotating wall electric fields. *Physics of Plasmas*, 7(7):2776–2789, 2000.

[165] J. R. Danielson and C. M. Surko. Radial compression and torque-balanced steady states of single-component plasmas in penning-malmberg traps. *Physics of Plasmas*, 13(5):055706, 2006.

[166] L. Worner, V. Nosenko, A. V. Ivlev, S. K. Zhdanov, H. M. Thomas, G. E. Morfill, M. Kroll, J. Schablinski, and D. Block. Effect of rotating electric field on 3d complex (dusty) plasma. *Physics of Plasmas*, 18(6):063706, 2011.

[167] John J. Tyson and James P. Keener. Singular perturbation theory of traveling waves in excitable media (a review). *Physica D: Nonlinear Phenomena*, 32(3):327 – 361, 1988.

[168] A. V. Holden, M. Markus, and Hans G. Othmer, editors. *Nonlinear Wave Processes in Excitable Media*, volume 244 of *NATO ASI series, Series B, Physics*, 1991.

[169] Vladimir S. Zykov and Eberhard Bodenschatz. Wave propagation in inhomogeneous excitable media. *Annual Review of Condensed Matter Physics*, 9(1):435–461, 2018.

[170] V. Perez-Muñuzuri, R. Aliev, B. Vasiev, V. Perez-Villar, and V. I. Krinsky. Super-spiral structures in an excitable medium. *Nature*, 353:740, Oct 1991.

[171] Gil Bub, Alvin Shrier, and Leon Glass. Spiral wave generation in heterogeneous excitable media. *Phys. Rev. Lett.*, 88:058101, Jan 2002.

[172] Ligang Li, Xinhao Liao, Kit H. Chan, and Keke Zhang. On nonlinear multiarmed spiral waves in slowly rotating fluid systems. *Physics of Fluids*, 22(1):011701, 2010.

[173] Sandeep Kumar, Bhavesh Patel, and Amita Das. Spiral waves in driven dusty plasma medium: Generalized hydrodynamic fluid description. *Physics of Plasmas*, 25(4):043701, 2018.

[174] T. Palberg, W. Mönch, F. Bitzer, R. Piazza, and T. Bellini. Freezing transition for colloids with adjustable charge: A test of charge renormalization. *Phys. Rev. Lett.*, 74:4555–4558, May 1995.

[175] Takamichi Terao and Tsuneyoshi Nakayama. Crystallization in quasi-two-dimensional colloidal systems at an air-water interface. *Phys. Rev. E*, 60:7157–7162, Dec 1999.

[176] Yan Levin. Electrostatic correlations: from plasma to biology. *Reports on Progress in Physics*, 65(11):1577, 2002.

[177] Alpha A. Lee, Carla S. Perez-Martinez, Alexander M. Smith, and Susan Perkin. Scaling analysis of the screening length in concentrated electrolytes. *Phys. Rev. Lett.*, 119:026002, Jul 2017.

[178] M. Lyon, S. D. Bergeson, and M. S. Murillo. Limit of strong ion coupling due to electron shielding. *Phys. Rev. E*, 87:033101, Mar 2013.

[179] C. E. Simien, Y. C. Chen, P. Gupta, S. Laha, Y. N. Martinez, P. G. Mickelson, S. B. Nagel, and T. C. Killian. Using absorption imaging to study ion dynamics in an ultracold neutral plasma. *Phys. Rev. Lett.*, 92:143001, Apr 2004.

[180] M. Tribeche and A. Merriche. Nonextensive dust-acoustic solitary waves. *Physics of Plasmas*, 18(3):034502, 2011.

[181] Srimanta Maity, Amita Das, Sandeep Kumar, and Sanat Kumar Tiwari. Interplay of single particle and collective response in molecular dynamics simulation of dusty plasma system. *Physics of Plasmas*, 25(4):043705, 2018.

[182] V. Nosenko, A. V. Ivlev, S. K. Zhdanov, M. Fink, and G. E. Morfill. Rotating electric fields in complex (dusty) plasmas. *Physics of Plasmas*, 16(8):083708, 2009.

[183] Sergey A. Khrapak and Hubertus M. Thomas. Fluid approach to evaluate sound velocity in yukawa systems and complex plasmas. *Phys. Rev. E*, 91:033110, Mar 2015.

[184] H. Kählert, J. Carstensen, M. Bonitz, H. Löwen, F. Greiner, and A. Piel. Magnetizing a complex plasma without a magnetic field. *Phys. Rev. Lett.*, 109:155003, Oct 2012.

[185] Hanno Kählert, André Melzer, Marian Puttscher, Torben Ott, and Michael Bonitz. Magnetic field effects and waves in complex plasmas. *The European Physical Journal D*, 72(5):83, 2018.

[186] Edward Thomas Jr, Uwe Konopka, Robert L Merlino, and Marlene Rosenberg. Initial measurements of two-and three-dimensional ordering, waves, and plasma filamentation in the magnetized dusty plasma experiment. *Physics of Plasmas*, 23(5):055701, 2016.

[187] M Puttscher, A Melzer, U Konopka, S LeBlanc, B Lynch, and E Thomas Jr. Vertical oscillations of dust particles in a strongly magnetized plasma sheath induced by horizontal laser manipulation. *Physics of Plasmas*, 24(1):013701, 2017.

[188] Noriyoshi Sato, Giichiro Uchida, Toshiro Kaneko, Shinya Shimizu, and Satoru Iizuka. Dynamics of fine particles in magnetized plasmas. *Physics of Plasmas*, 8(5):1786–1790, 2001.